Theses and Dissertations

2005-08-12

An Acoustical Analysis of Domes Coupled to Rooms, with Special Application to the Darussholah Mosque, in East Java, Indonesia

Sentagi Sesotya Utami
Brigham Young University - Provo

AN ACOUSTICAL ANALYSIS OF DOMES COUPLED TO ROOMS,

WITH SPECIAL APPLICATION TO

THE DARUSSHOLAH MOSQUE,

IN EAST JAVA, INDONESIA

by

Sentagi S. Utami

A thesis submitted to the faculty of

Brigham Young University

in partial fulfilment of the requirements for the degree of

Master of Science

Department of Physics and Astronomy

Brigham Young University

August 2005

BRIGHAM YOUNG UNIVERSITY

GRADUATE COMMITTEE APPROVAL

of a thesis submitted by

Sentagi S. Utami

This thesis has been read by each member of the following graduate committee and by majority vote has been found to be satisfactory.

Date	Timothy W. Leishman, Chair

Date	Scott D. Sommerfeldt

Date	Jonathan D. Blotter

BRIGHAM YOUNG UNIVERSITY

As chair of the candidate's graduate committee, I have read the thesis of Sentagi S. Utami in its final form and have found that (1) its format, citations, and bibliographical style are consistent and acceptable and fulfil university and department style requirements; (2) its illustrative materials including figures, tables, and charts are in place; and (3) the final manuscript is satisfactory to the graduate committee and is ready for submission to the university library.

_____   _____
Date   Timothy W. Leishman
                                      Chair, Graduate Committee

Accepted for the Department

                                      _____
                                      Ross L. Spencer
                                      Graduate Coordinator

Accepted for the College

                                      _____
                                      G. Rex Bryce
                                      Associate Dean, College of Physical
                                      and Mathematical Sciences

ABSTRACT

AN ACOUSTICAL ANALYSIS OF DOMES COUPLED TO ROOMS,

WITH SPECIAL APPLICATION TO

THE DARUSSHOLAH MOSQUE,

IN EAST JAVA, INDONESIA

Sentagi S. Utami

Department of Physics and Astronomy

Master of Science

Concave surfaces are often considered to be detrimental or precarious in room acoustics, especially because of the impact they have on the distribution of sound energy. However, it is often difficult to avoid such surfaces in buildings with specific architectural functions. A primary example of this involves mosques, which are sacred places of worship for Muslims. In keeping with the Islamic architectural style, most mosques incorporate a symbolic centralized domed ceiling as part of their roof structures. These domes are open on the bottom and coupled to the acoustic spaces below. In many cases, the lower spaces may be idealized as rectangular enclosures. Owing to the

distinctness and ubiquity of this basic architectural form, a thorough, fundamental analysis of such environments would be useful to the architectural acoustics community. In this study, predictions from EASE^{TM} computer models were compared to the results derived from physical scale model measurements. The scale model measurement techniques involved evaluation of impulse responses in a 1:12 scale model of Darussholah mosque, in East Java, Indonesia. A miniature human voice source was created to carry out the impulse response measurements. It was carefully evaluated to ensure that it produced adequate frequency response and directivity comparable to an actual human voice. Acoustical parameters were derived from the impulse responses. Statistical analysis using ANOVA and *t*-tests were used to compare results from the measurements with variations of domed ceiling configurations and other aspects of the measurement setting. Conclusions were based on these comparisons and on auralization listening tests in order to ascertain the elements that produced the most significant impact on the mosque acoustics. The analysis helps establish criteria for good acoustics in mosques and other buildings with domed ceilings.

ACKNOWLEDGMENTS

I would like to express my greatest gratitude to the following individuals and groups for their assistance, support, and contributions throughout this research:

- Dr. Leishman, Dr. Sommerfeldt, and Dr. Blotter for serving on my committee, and their helpful advisement, especially for their extensive help in my final days.

- BYU Department of Physics and Astronomy for the financial support provided for this research.

- Ryan Chester for the great assistance and team working, from the beginning until the end of this research.

- Wesley Lifferth, Jared Ellsworth, Richard Watkins, and my husband, Winny, for their supervision and assistance in building the scale model.

- Ben Faber, Brian Monson, Gordon Dix, Heather Smith, Sarah Rollins, and Micah Shepherd, for teaching me how to use the equipment and EASE ^{TM} software and also their contribution for MATLAB$^{®}$ codes.

- Hannah Pritchett and Agus Purwanto for helping in the technical writing process, which without, I would have been in trouble.

- All of the members in the ARG, for their help especially in the listening test and help while preparing the scale modeling measurement in the semi-

anechoic chamber and conducting the measurements in the anechoic chamber.

- Gadjahmada University, Department of Physics Engineering, where I teach, for giving me the opportunity to study abroad.

- In memorial, K. H. Yusuf Muhammad, the owner of *Pondok Pesantren* Darussholah, East Java, Indonesia.

- My friends in ATQONA architectural consulting: Bowo, Irawan, Farah, Dedi and in memorial Aang..

- My dearest husband, Winny, my children, Atiya and Daffa, for their patience and infinite love while supporting me during my school.

- My parents and family, for their prayers in my behalf.

Table of Contents

List of Tables

List of Figures

xvii

CHAPTER 1
INTRODUCTION

Mosques are important public spaces used by millions of Muslims around the world for a variety of worship activities. Because of their international ubiquity and various modes of use, their acoustical properties should be well understood and regularly optimized. Analysis of their acoustics should also be an important, well-documented subject in technical architectural acoustics. However, little in-depth attention has been given to this vital topic in the past. This thesis aims to address this deficiency by introducing an analysis of key acoustical characteristics of mosques, particularly those associated with domes over room volumes with larger plan areas.

Because of these domed ceiling elements, mosques would be expected to exhibit various acoustical anomalies. However, this architectural configuration is not unique to mosques in Islamic architectural style. It is also common to other religious edifices (e.g., Byzantine-era chapels), government buildings, planetariums, etc. The Islamic architecture style for mosques with a domed ceiling was influenced by the Ottoman architecture style.

Researchers from Europe have conducted several limited studies on the acoustical performances of existing buildings with domed structures. A preliminary study to plan renovation on Bjergsted Concert Hall in Stavangar, Norway, found that the existing dome shaped room created uneven sound energy distribution and focusing effects in the audience area.[1] The CAHRISMA project[2] and Papageorgiou[3] both proposed the computer modeling method to study rooms with curved shaped walls, including a domed ceiling. The cases studied in the CAHRISMA project were mosques and a cathedral in Turkey. A group of researchers in Spain explored the acoustics of the cathedral-mosque of

Cordoba.[4] Researchers from Jordan[5], Kuwait[6] and Saudi Arabia[7] have also performed similar studies for the acoustics of mosques. Auralization or measurements were performed to compare the acoustical characteristics of several mosques with the same basic geometry. The goals of these studies were to propose mosques designs that could produce satisfactory acoustical performance.

This thesis addresses challenges of the general architectural mosque configuration in relation to mosques and in particular: a case study of the Darussholah mosque in Jember (East Java), Indonesia. It explores the acoustical impact of its principal dome with various dome shapes and configurations.

This chapter provides an overview of mosques, including their key architectural features and uses. It also details the motivations, objectives, and scope of the research project.

1.1 Key Characteristics of Mosques

Mosques are uniquely important buildings in every Muslim community. They usually have a certain size and location in relation to the community. In general, they may be classified as large state mosques, major landmark structures, community center complexes, and small local neighborhood mosques.[8] While their uses are clearly varied, they also have several consistent characteristics.

1.1.1 Worship Considerations and Their Influence on Spatial Arrangement

The distinct worship activities inside mosques include prayer, public speaking, preaching, lecturing, and *Qur'an* recitations. The activities are performed by people either individually or in conjunction with others. The activities may be categorized into

one of two primary worship modes: prayer mode or preaching mode. In prayer mode, all mosque users are either standing, bowing, or prostrating, always on the same floor level, and aligned in rows parallel to the *Qibla'* wall (front wall), with the *imam* (speaker) facing away from listeners. In preaching mode, the listeners are sitting on the floor in rows parallel to the Qibla' wall, while the imam is standing on a four-step high platform (*minbar*) facing the listeners.

The worship activities generally require adequate speech audibility and intelligibility. The leader or imam generally stands in front of the gathering, near the *mihrab*, a distinct area provided for him. General mosque orientation is based on the position of the mihrab, which is intended to face the Qibla' (a cubical building at Mecca, Saudi Arabia).

Prayer from the imam is to address the gathering from his position. For certain prayers such as *Jumma* (Friday) prayers, the imam addresses the gathering with preaching, or *khutba*, from the minbar, which in general is considered to be high enough for the gathering's visibility (see Fig. 1.1).
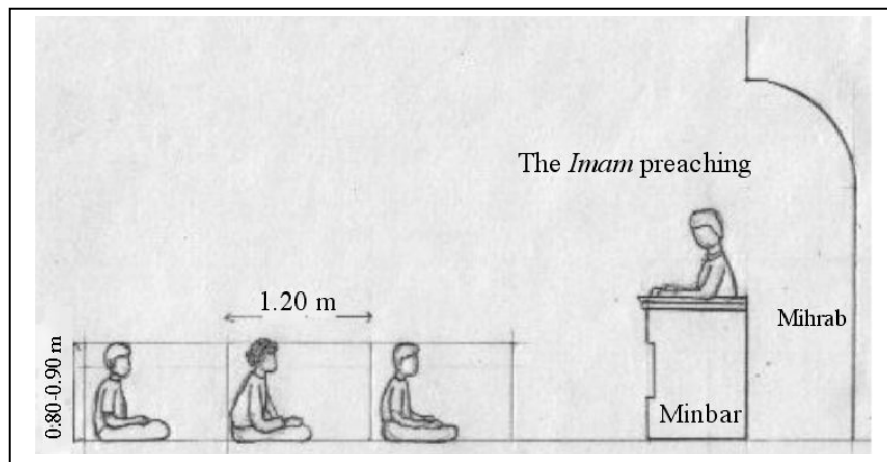
Figure 1.1. Preaching inside the prayer hall.

The congregational capacity of the mosque is usually determined by the floor area divided by the area required per worshipper to perform various prayers motions[7]. This is approximately 0.80 x 1.2 = 0.96 m^2 (Fig. 1.2).
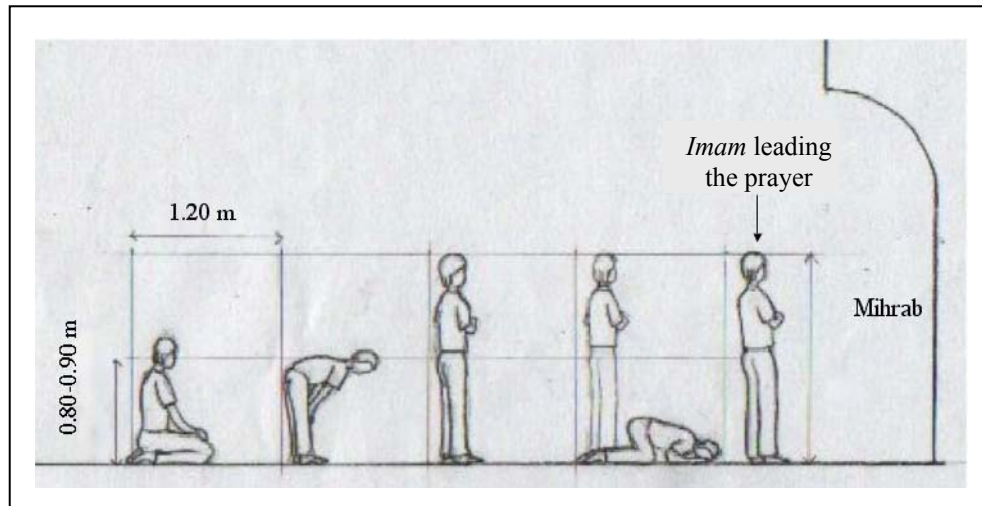
Figure 1.2. Praying inside the prayer hall, the imam is leading the prayer followed by the worshippers.

1.1.2   Specific Characteristics of the Darussholah Mosque

The Darussholah mosque may be classified by its size and location as a large mosque. As of the time of the writing of this thesis, it is still under construction. The mosque is situated on a corner of Muhammad Yamin Street located in Jember, a city in East Java, Indonesia. This mosque was intended to become a public landmark of the city. Its design was mainly based on worship activities. The area on the second floor is divided into three regions: the circulation area, leader (imam) area, and group praying/worshipping/gathering area. The circulation area is distinguished from the praying areas by slightly different floor elevations. This helps provide demarcation of the more sacred praying area. The design process of the Darussholah mosque was started in 1999 by IVADA consulting architecture in Yogyakarta, Indonesia. This company name is now being changed to ATQONA.

There are two main floor levels in the mosque. The ground floor has an area 30 m x 30 m and is planned to be used as a multipurpose room for preaching and teaching activities. The second floor is the main sanctuary area of the mosque. It also has an area of 30 m x 30 m and may be considered a semi-enclosed room. Many of its exterior walls are partially open to the outside. This floor was the object in this research. Its use was for the worship activities described above.

Mosques in different parts of the Islamic world are built using different construction systems and building materials. The choice of building methods is influenced by many factors. Some countries in the same continent have typical construction systems and architectural styles. Large mosques in Java are commonly constructed with reinforced concrete skeletal structures and bricks to form the partition walls. This was the approach used for the Darussholah mosque. They usually have a dome as part of the roof structure that spans a wider space while eliminating the intermediate columns. Columns are generally arranged on grids.

Most parts of the interior of the Darussholah mosque were intended to be finished with acoustically reflective materials such as painted plaster and tile (both marble and ceramic). However, the floor area was to be covered with heavy carpet. The ceilings, including the dome, will be finished with painted plaster and ornamentation. Arches made from concrete and finished with painted plaster will be used as joint elements between the columns to strengthen the construction and to provide interior decorative elements.

1.1.3 Important Elements in the Mosque for the Acoustical Study

Certain architectural elements of the mosque are very important in this acoustical study. The two most important elements in the praying area are the mihra*b* and the domed ceiling.

1.1.3.1 Mihrab

The mihrab must be well designed in order to passively carry the voice of the leader to the gathering. In general, mihrabs are designed to have a half-hemispherical ceiling attached to a half cylindrical wall section. The mihrab shape and size in the Darussholah mosque was adapted and simplified into a design model as shown in Fig. 1.3. It is also shown that the source is placed in a certain position inside the mihrab.
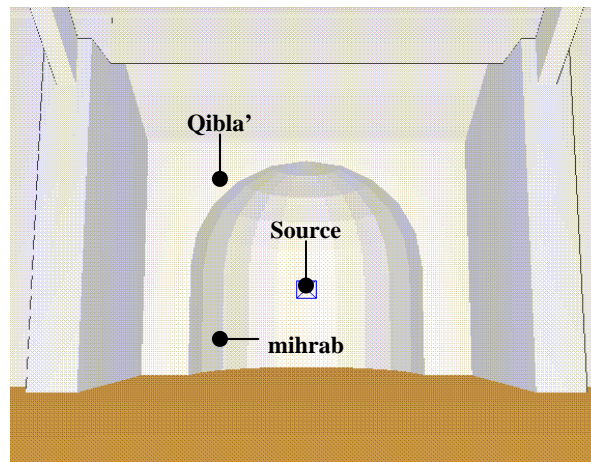
Figure 1.3. Area for the imam leading the prayer facing the mihrab.

1.1.3.2 Dome

For the Darussholah mosque, there is a main dome within the roof structure with a 12 m diameter and 4 smaller domes, each with 2.5 m diameters. In the analysis of this thesis, the smaller domes are ignored. The related objective of the research is to evaluate the influence of the main dome, which encompasses the largest portion of the praying

area ceiling. Another reason for eliminating the smaller domes is that only a main dome would be considered symbolic of the Islamic architectural style for most mosques.

There are actually several dome designs commonly used for mosques. Each type might be expected to create a unique acoustical condition for the room coupled to it. Figures 1.4 (a) shows the dome style used in the Darussholah mosque. A hemispherical dome [Fig.1.4 (b)] is also commonly found in several countries around the world.

(a)

(b)
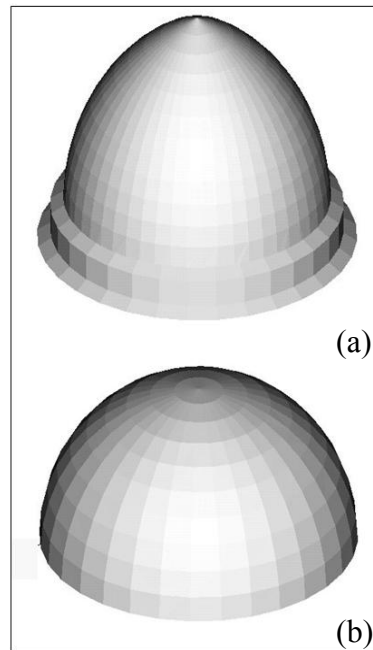
Figure 1.4. Type of domes investigated in the research.

1.2   Motivation of Research

A lot of the research on mosque acoustics conducted in the past involved existing mosques, both occupied and unoccupied. The construction incorporated a flat roof on a rectangular prayer hall instead of a domed ceiling. There are basic design elements of mosques in Saudi Arabia.[9] The applications of the results were thus limited to a particular prototype. Other studies of mosques with domed ceilings did not propose a generalized

design to model a mosque with a domed ceiling. According, detailed acoustical research of mosques with domed ceilings has never been conducted.

This research is intended to contribute a general acoustical analysis method to simulate and predict the quality of sound in rectangular rooms coupled to domes, particularly mosques. Unfortunately, the difficulty of translating acoustical requirements into architectural designs, specific room shapes, and choices of acoustical materials is compounded by the fact that only a few architects, engineers, or builders have a good understanding of how acoustical quality is affected by these factors.[10] This problem highlights the importance of knowledgeable considerations of acoustical hazards during the design process.

A three-pronged approach (analytical, numerical modeling, and acoustical scale modeling) would greatly increase understanding of mosque acoustics. By simulating and comparing results from measurements and calculations using these methods, we can better validate modeling results and develop an understanding that helps us design similarly shaped rooms in addition to mosques. This research could then be useful for many applications around the world.

1.3 Objectives

The primary goal of the research is to explore the physical characteristics and problems of domed ceilings coupled to an acoustical space below, with special application to mosques. In order to perform a thorough acoustical analysis of the issues, the investigation involved the three-pronged approach mentioned above: analytical, computer modeling (EASE[TM]), and experimental (via scale modeling). While using computer modeling, simplifications were often incorporated in order to get the software

- 8 -

tools to work for the given room shape and dimensions. An analytical study helped to check the validity of such assumptions. Results from computer and scale modeling were complementary. The combined use of scale modeling and computer modeling provides much better insight and prediction capability than the use of either alone. The scale modeling approach was also intended as a secondary goal to be a pilot study for the BYU Acoustics Research Group.

Speech intelligibility is the main concern in the acoustical performance of a mosque. The acoustical analysis was therefore derived from three parameters common used in speech intelligibility analysis: RASTI, C_{50}, and %AL_{cons}.[11]

The spatial distribution of sound energy and speech intelligibility was observed after adjusting three architectural and acoustical properties: (1) the configuration of the dome structure, (2) the sound absorption of the materials lining the inside of the models, and (3) the measurements set-up.

Several general limitations were applied to the research approach:

- The configurations of the dome structure in the computer model were limited for two different shapes of the dome (hemispherical and onion shaped domes). They were combined with three different ring structures used as the base of the dome. In the scale modelling, only the hemispherical dome was used with the alternate ring structures.

- Only one source position was considered in computer and scale modeling during the impulse response measurements. Another position was explored in the analytical study.

- The number of uniformly spaced receiver positions was 36 for the computer model and 20 positions for the scale model.

- The important acoustical details of the actual mosque were focused on in the models. Unfortunately, several architectural details and additional shapes were slightly different due to limitations on the construction process of the scale modeling, although similarities between models in both computer and scale modeling were kept consistent.

1.4   Plan of Development

The next two chapters discuss geometrical acoustics theory pertinent to the analysis of mosque acoustics and then present a review of several parameters related to speech intelligibility. Chapter 4 discusses details of the computer modeling efforts. Chapter 5 discusses the physical scale modeling work. Finally, Chapter 6 provides conclusions and recommendations for future work.

CHAPTER 2
GEOMETRICAL ROOM ACOUSTICS

Geometrical room acoustics is a simplified way to describe the acoustical properties of rooms that are relatively large and irregular in shape.[12] Its use is permitted if the dimensions of the room and its bounding surfaces are large compared with the wavelength of sound. In this case, the sound waves see the room surfaces as infinite planes that create specular reflections. All the computational approaches in this research used for modeling the mosque were based on this geometrical room acoustics method.

Ray tracing and image source methods are two classical geometrical methods used for simulation of sounds in such rooms. The ray tracing method is well suited to study the propagation of high-frequency sound waves and their reflections from large surfaces. The Darussholah mosque consists of many large surfaces with dimensions that generally satisfy the required assumptions. The backgrounds of this method and the image-source method are discussed briefly in this chapter. A discussion of a hybrid method is also given, as it is now the method most generally used in computer-modeling packages.

2.1   Ray Tracing Method

The ray tracing method uses a large number of sound rays, which originate from a certain point and are emitted in various directions. They are meant to represent a small portion of a spherical wave with a vanishing aperture. The rays are traced around the room, losing energy as they impinge upon room boundaries. The lost energy results from boundary and air absorption. In order to obtain a calculation result of reflection paths related to a specific receiver position, a minimum number of rays (N) is required: [13]

$$N \geq \frac{8\,\pi c^2}{A} t^2,$$

where t is the propagation time, c is the speed of sound in air, and A is the total surface area of the room. In the early stage of its development, the ray tracing method emphasized visual inspection of reflection distribution.[14] It was then further developed to calculate an impulse response.[15] Recently, the ray-tracing method has been adopted for use with a circular cones technique and the use of triangular pyramids, in order to calculate an impulse response.[16]

2.2 Image Source Method

In an enclosed space, signals radiated from a source will encounter acoustically reflective surfaces. The reflection could be seen as a signal radiated from a virtual source. This virtual source is a mirror of the actual source, which means it is placed behind the surface with a distance $d' = d$, where d is the perpendicular distance between the source and the surface (see Fig. 2.1). The reflection will then interact with other reflecting surfaces, creating additional reflections by mirroring the source and/or virtual source with respect to other plane surfaces.
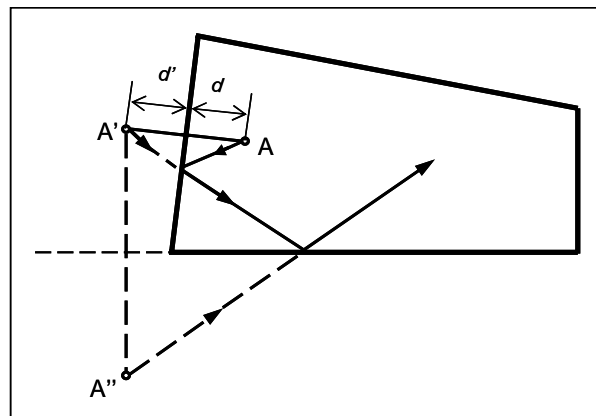
Figure 2.1. Image sources of first and second order. A = source, A'= first order image source, and A''= second order image source.

In general, the number of surfaces a reflection has encountered is the order of reflection. The total number of images of order N up to i_n is obtained by adding all of the images that were generated while the sound travelled in the enclosure[12], i.e.,

$$N(i_n) = N \frac{(N-1)^{i_n} - 1}{N - 2} \qquad (2.2)$$

Rindell[17] proposed a formula to approximate the number of image sources within a radius of ct in a rectangular box-shaped room:

$$N_{refl} = \frac{4\pi c^3}{3V} t^3, \qquad (2.3)$$

where V is the room volume (m^3).

2.3 Hybrid Method in Computer Modeling

Disadvantages were found by Vorlander in the validity and application of the law of specular reflection, both in terms of ray tracing and the method of image sources.[18, 19] He found reasonable results from the acoustical analysis in only three of fourteen models used in his round-robin research. Apparently, all three models used hybrid methods. This has led to the development of hybrid procedures in order to combine the advantages of ray tracing and image sources (see Rindell[13] and Howarth and Lam[20]). The idea of the combined method is to have an efficient way to find image sources with high probabilities of validity by tracing rays from the source and noting the surfaces they hit. Each path detected in this way is associated with a particular sequence of valid image sources, which are identified by backtracking the path of a sound particle, then testing it to determine whether it gives a contribution at the chosen receiver position. Once the valid images have been found, the energy impulse response can be formed by adding the

contributions of all image sources and using the energy reflection coefficients of the room boundaries involved.

A secondary source method has proven to be efficient at choosing the early and late reflections. This method is currently being used in the ODEON program.[21] In general, the early reflections are calculated by combining the image source method and the ray-tracing method. The late reflections are calculated using a ray-trace process, which generates diffuse secondary sources. In this process the rays are sent from the source position, detecting image sources up to a certain reflection order, then detecting secondary sources on the surfaces of the room at the collision points.

The image sources which lie within a certain distance of the receiver are checked strictly to determine whether they give a contribution at the receiver. Image sources lying farther away are treated statistically to generate a realistic reverberant decay which approximates the true one.[22] As determined by this method, the last early reflection from one image source may arrive at a receiver position after the first late reflection from a second image source; there will be an overlap. This will lead to the energy response curve, which is the reverse-integrated impulse response.[23] Reverberation time can be estimated from this curve. Other acoustical properties of the room can be derived from other integrations of the impulse response.

The computer modeling package used in this research was EASE[TM]. The hybrid method used in EASE is basically the same as the first hybrid method described above, involving the building of an image tree. Detailed discussion of the algorithm is available in H.M. Smith's thesis.[24]

2.4   Geometrical Acoustics of Domes (Concavely Curved Surfaces)

Domed ceilings are encountered as concavely curved surfaces in rooms. In general, these surfaces are considered detrimental to a room's acoustics since they have the tendency to impede the uniform distribution of sound energy or to concentrate the sound energy near a certain point. Curved walls and domed ceilings can be approximated as spherical or cylindrical segments. Accordingly, the laws of geometrical optics for rays reflected at a concave or convex mirror can be applied to the problem (see Fig. 2.2).
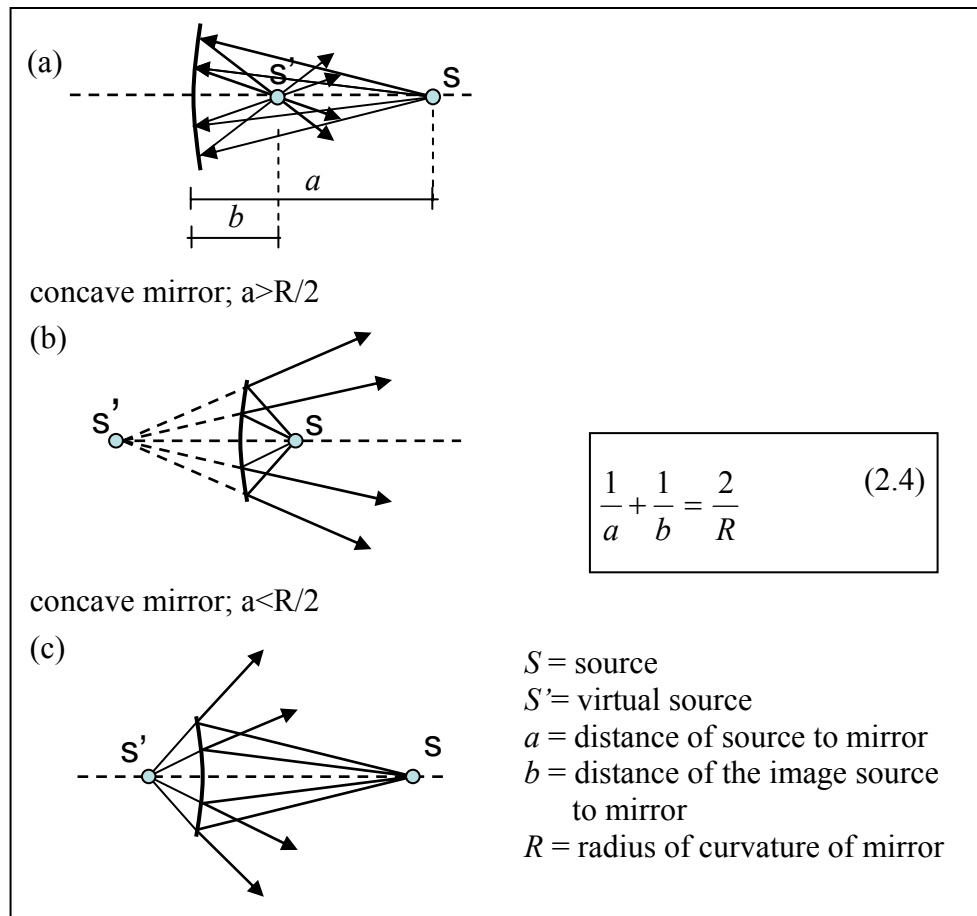
Figure 2.2. Reflection from concave and convex mirrors. (a) Reflection from a concave mirror with a>R/2, (b) reflection from a concave mirror with a<R/2, and (c) reflection from a convex mirror.

A few practical conclusions can be drawn for a domed surface, when being characterized as a concave mirror [see Fig. 2.3 (a)] with a completed full circle radius R. The impinging sound energy may be concentrated in certain regions or distributed over a

wide angular range, depending on the position of the source and the receiver. For a spherical concave surface with a large aperture, these reflected sounds can form an envelope, which is known as a caustic. The reflected rays that are not collected at a point will create a caustic form [see Fig. 2.3 (a)]. Near the axis, the caustic reaches the focal point at the distance $b=R/2$ when $a{\to}\infty$. A focusing effect is considered the main concern of a spherical concave curve surface such as a dome, which in practice is avoided since it can present serious acoustical problems.

Another sound distribution effect is the whispering gallery effect. It often occurs when the reflecting surface geometry has more of an elliptical shape. Because of the two foci [see Fig. 2.3 (b)] the sound will be collected at the receiving point.
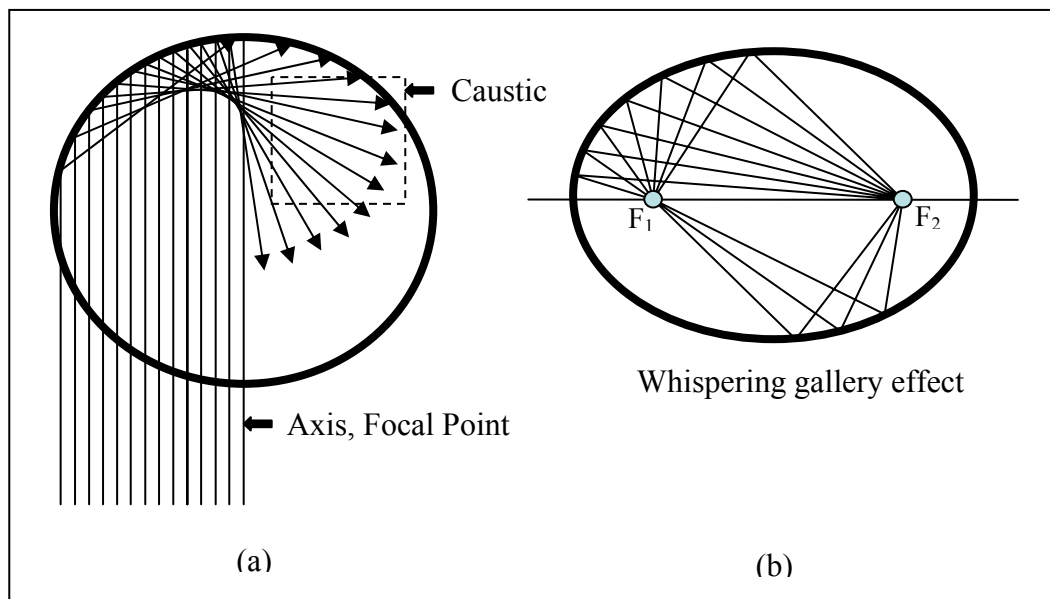
Figure 2.3. **(a) Focusing point effect (b) Whispering gallery effect**[12], F_1= focal point 1, and F_2= focal point 2.

The dimensions of a reflector, which in this case is the concave dome surface, must be seen in relation to the distances a_1 and a_2, the distance of the source and the receiver to the dome surface, respectively. A useful parameter is the characteristic distance $a*$ defined by the relation:

$$a^* = \frac{2a_1 a_2}{a_1 + a_2} \qquad (2.5)$$

An additional term used to approximate the reflection from a cylinder with radius of curvature R is: [25]

$$L_r = -10\log\left|1 + \frac{a^*}{R\cos\theta}\right| \qquad (2.6)$$

By knowing the approximate reflection from a curvature surface, the sound attenuation caused by the diffraction on this surface can be defined from Eq. (2.6) above, since $1 - L_r = L_a$, is the approximate absorption of the curvature surface. In a cylinder with a concave curve, the energy is concentrated by the reflection, and a focusing effect appears if $R = -a* / \cos\theta$.

In the acoustical computer models, it is necessary to subdivide a curved surface into a number of flat planar surfaces. In a concave surface, particularly in domes, what might create a problem is that each flat plane surface may contribute a reflection. As a consequence, the total reflections from the flat plane surfaces that create the curve surface will increase with the number of sub-surfaces. For such a simulation in computer modeling, Kuttruff concluded that it is preferable to compute the exact sound paths without approximating the curved boundary with flat plane surfaces,[26] since such an approximation inevitably leads to significant errors, especially near the focal region of the curved surfaces. Papageorgiau[3] verified this assumption through an analytical and numerical study, comparing results from a particular model with a curved roof. It was found that using the exact curved surfaces, as opposed to the flat surface approximation, we can represent a more accurate and efficient solution.

The idea to model an exact curved surface was not applicable in this research since EASE^{TM} describes the geometry of a curved surface by a number of flat plane surfaces. The problems that might occur by using this approximation method can be greatly reduced if the diffraction attenuation (equation 2.6) is introduced in the model. H. M. Smith (Ref. 27) studied the details of the EASE^{TM} technique and algorithm to compensate for this problem discussed above.

It is important to determine a sufficient number of flat plane surfaces to model the curved surfaces. Unfortunately, a conclusive method to determine this sufficient number is not yet available, particularly for concaved domes. Papageorgiau[3] found through his model that increasing the number of plane sections to represent the curved walls decreases the efficiency of the model without any real benefit to the accuracy.

CHAPTER 3
METHODS FOR PREDICTON OF SPEECH INTELLIGIBILITY

Based on the main activities held inside mosques, the main purpose of their existence is speech communication. Therefore, the acoustical design should be aimed at achieving a very high degree of speech intelligibility for all listeners, particularly inside the prayer hall. Intelligibility of direct, reinforced, or reproduced speech denotes the degree to which a normal listener can understand speech content. In general, an Imam that leads prayers and delivers speeches inside mosques is a male. We might consider three different presentation levels for male speech signals: soft (approximately 55dB SPL), normal (approximately 65-70dB SPL) and loud (approximately 75dB SPL).[12] These are measured at a distance of 1m from the speaker and at the frontal direction, denoted by 0°. The Imam is traditionally expected to speak at the loud level.

For a given talker-to-listener distance, speech intelligibility is chiefly degraded by two phenomena: noise and reverberation.[27] The three main approaches to predict speech intelligibility in rooms are based on consideration of these acoustical phenomena.[28, 11] The simplest approach is based on steady-state signal-to-noise concepts. The Articulation Index (AI) is a well known measure of this type. The second approach was introduced by Lochner and Burger, which is the concept of useful to detrimental reflection ratio.[29] The useful energy was a weighted sum of the energy arriving in the first 0.095 seconds after the arrival of the direct sound. This weighting procedure proposed by Lochner and Burger is quite complicated and requires the identification of individual reflections in the impulse response. The detrimental energy includes that arriving later than 0.095 seconds, plus the background noise energy in the room. Such a measure is essentially an early-to-

late sound ratio, with the background sound energy added to the late-arriving sound. The third approach involves measurement of the Speech Transmission Index (STI). It is derived from the modulation transfer functions and background noise levels. A simpler variant of the STI has also been developed, which is known as RASTI (Rapid STI).[30] The following sections provide more details about these important methods.

3.1   Articulation Index

The Articulation Index has been shown to be a valid predictor of speech intelligibility under a wide variety of conditions involving noise masking and speech waveform distortion.[31] The calculation procedure has also been standardized in the ANSI Standard S3.5-1969 and can be described as follows. First, 12 dB is added to the long-time average signal-to-noise ratio in each standard octave band from 125 Hz to 8 kHz. Each modified signal-to-noise ratio is then multiplied by a weighting factor. The weighting factor represents the amount of information that is important in each octave band for speech intelligibility.[32] Weighted ratios are summed to produce an AI value between 0 and 1. The added 12dB is intended to represent the difference between long-time average speech levels and the peak levels.

An AI value of 0 represents completely unintelligible speech, whereas a value of 1 represents perfectly intelligible speech. An AI of 0.3 or below is considered unsatisfactory, 0.3 to 0.5 is considered satisfactory, 0.5 to 0.7 is considered good, and greater than 0.7 is considered very good to excellent.

3.2 Clarity of Speech (C_{50})

The early-to-late energy ratio, $C_{50,}$ has been used as an indicator of the effects of room acoustics on speech clarity.[33] It is determined from the impulse response and defined as the ratio of the sound energy arriving at the reception measuring position over the first 50 ms to the sound energy arriving after 50 ms:

$$C_{50} = 10\log_{10}\left\{\frac{\int_0^{0.05} p^2(t)dt}{\int_{0.05}^{\infty} p^2(t)dt}\right\} \approx 10\log_{10}\left(\frac{\sum_{n=1}^{N_1} p_n^2}{\sum_{n=N_1+1}^{N_2} p_n^2}\right), \qquad (3.1)$$

where $p(t)$ is the instantaneous pressure in the room impulse response and t is time. The second formulation is for sampled data, where n is the sample number starting with n = 1 when the direct sound arrives. The value N_1 is the sample number 50 ms after n = 1, i.e., $N_1 = 0.05$ x f_s, where f_s is the sampling frequency. The value N_2 is the total number of samples used in the impulse response.

Thiele proposed a related but less used objective criterion called the degree of definition D or D_{50}.[34] It is given in % and defined by the following expressions: [35]

$$E_{50} = \int_0^{0.05} p^2(t)dt$$

$$E_{\infty} = \int_{0.05}^{\infty} p^2(t)dt$$

$$D_{50} = \frac{E_{50}}{E_{\infty}}$$

It is related to C_{50} as follows:

$$C_{50} = 10\log\left(\frac{D_{50}}{1-D_{\infty}}\right)$$

Intelligibility of syllables of at least 85% is achieved if D = $D_{50} \geq 0.5$, or 50%. However, C_{50} is apparently a better measure because it is linearly related to subjective assessments of the clarity of speech sounds.[36]

3.3   Articulation Loss of Consonants (%AL$_{cons}$)

Peutz proposed an articulation loss concept with the idea that subjective intelligibility could be based on the percentage of correctly understood consonants in special monosyllabic nonsense words.[37] The articulation loss varies with the square of the source-to-listener distance. The relationship holds until a certain distance is reached, which Peutz called the critical distance, or the intelligibility distance, beyond which the articulation loss remains constant. This distance is about 3.2 times greater than the traditional critical distance, namely, the distance at which direct and reverberant fields from a source in a room are equal. Peutz's formula for percentage articulation loss of consonants (%AL$_{cons)}$ is [38]

$$\% AL_{cons} = \frac{200 D^2 T_{60}{}^2}{V} \, , \tag{3.2}$$

where D is the source-to-listener distance in meters, T is the reverberation time of the room for each octave band in seconds, and V is the room volume in m^3.

3.4   Speech Transmission Index

The Speech Transmission Index (STI) is based on the reduction of the signal modulation between a source and receiver at octave center frequencies from 125 to 8000 Hz. This section explains the process pf computing the STI and a more practical variant, the rapid speech transmission index (RASTI).

3.4.1 The Modulation Transfer Function

When an acoustic signal propagates in an enclosure, the time-dependent intensity envelope of the received signal is in general a smoothed version of the original envelope. In quantifying speech intelligibility using the modulation transfer function (MTF), the function of interest is the temporal envelope of running speech. The temporal speech envelope must have a reasonably stable shape so that the intensity envelope produced at the speaker's position is still present at the listener's position. In order to preserve the intensity envelope at any audio frequency for the squared impulse signal, the envelope can be sine-wave modulated. The basic principle of the MTF approach may then be described mathematically as follows:[39]

$$\text{Input Intensity:} \quad I_i(t) = \overline{I}_i(1 + \cos 2\pi F t), \text{ For a range of F values} \tag{3.2}$$

$$\text{Output Intensity:} \quad I_o(t) = \overline{I}_o\{1 + m\cos[2\pi F t + \theta]\} \tag{3.3}$$

where theta (θ) indicates the phase response, m is the amplitude response of the transmission system or the modulation index, and F is the modulation frequency. This modulation index (m) is then converted into attenuation in dB by $MT = 20\log m$. The modulation transfer function is the modulation transfer, MT, as a function of modulation frequency, F. This means that the MTF is a reduction factor of the modulation index as a function of frequency.[40] Schroeder[41] introduced the relation between the MTF and the impulse response. One of the examples of the impulse response was the impulse response of an auditorium with purely exponential reverberation and no discrete echoes, where in the impulse response could be described as

$$h(t) = e^{-t/\tau}s(t), \tag{3.4}$$

where $s(t)$ is a sample function from a stationary white-noise process. The definition of complex modulation transfer function (CMTF) can be described mathematically as follows:

$$m(\omega) = \int_0^\infty h^2(t) e^{-i\omega t} dt \bigg/ \int_0^\infty h^2(t) dt \qquad (3.5)$$

Plugging Eq. (3.4) into Eq. (3.5) and replacing $\tau/2$ with $T_{60}/13.8$ for strictly exponential sound decay, one obtains

$$m(\omega) = 1/(1 + i\omega T_{60}/13.8), \qquad (3.6)$$

and

$$|m(\omega)| = \left[1 + (\omega T_{60}/13.8)^2 \right]^{-1/2} \qquad (3.7)$$

where T_{60} is the reverberation time for a 60dB decay. The CMTF was created to express the way in which the modulation index m is changed by the transient behaviour of the room.[12] Interfering noise results in an additional modulation reduction factor, which depends on the signal-to-noise ratio:

$$m_{noise} = \left(1 + 10^{(-S/N)/10} \right)^{-1} \qquad (3.8)$$

Some practical considerations should be addressed when using the MTF exclusively for predicting speech intelligibility:

1. The source should have directional characteristics comparable to those of a talker.

2. The microphone setup should ideally account for specific features of binaural listening; an omnidirectional microphone may be used for practicality in some situations.

3.4.2 STI Algorithm

The modulation reduction factor $m(\omega)$ where $\omega = 2\pi F$, as a function of modulation frequency F, is derived from a comparison of the intensity modulations at the input and output of the system and is generally affected not only by reverberation [Eq.(3.7)], but also by ambient noise [Eq. (3.8)]. It is defined mathematically as follows:

$$m(F) = \underbrace{\frac{1}{\sqrt{1 + \left[2\pi F \dfrac{T_{60}}{13.8}\right]^2}}}_{\text{Reverberation Effect}} \cdot \underbrace{\frac{1}{1 + 10^{(-S/N)/10}}}_{\text{Noise Effect}} \tag{3.9}$$

where T is the reverberation time in seconds, F is the modulation frequency, and S/N is the signal-noise ratio. The MTF of a sound transmission system for speech intelligibility, roughly, has a range of modulation frequencies from 0.5 to 16 Hz in 1/3-octave intervals.[42]

The speech transmission index is a single index representing the effect of a transmission system on speech intelligibility. It is derived from a transformation of such a set of data quantifying a family of MTF curves. One curve is used for each octave band of the speech noise carrier and each curve is defined by 14 points on the modulation frequency scale, comprising 7 x 14 = 98 modulation index values. Each of the 98 $m(F)$ values are then converted into apparent signal-to-noise ratio $(S/N)_{app}$:

$$(S/N)_{app} = 10\log\left[\frac{m(F)}{1 - m(F)}\right] , \tag{2.10}$$

where $(S/N)_{app}$ is the apparent signal-to-noise ratio in dB, and m is the modulation reduction factor. A weighted average of the 98 $(S/N)_{app}$ values thus obtained results in the STI, after applying appropriate normalizations, where values of $(S/N)_{app}$ are truncated

when exceeding the range of ± 15 dB. Thus, if $(S/N)_{app} > 15$, it is defined as 15 dB and, similarly, if $(S/N)_{app} < -15$, it is defined as -15 dB. All 14 values of $(S/N)_{app}$ derived from one octave-band are simply averaged. The result is the octave-band-specific $(S/N)_{app}$ ratio defined as $(S/N)_{app,k}$, where the index k refers to the seven octave bands considered. Finally, the two last mathematical derivations are:

$$\overline{(S/N)_{app}} = \sum_{k=1}^{7} w_k (S/N)_{app,k} \tag{3.11}$$

and

$$STI = \left[\overline{(S/N)_{app}} + 15\right]/30 \tag{3.12}$$

where w_k are octave-band-specific weighting factors. Their values are 0.13, 0.14, 0.11, 0.12, 0.19, 0.17, and 0.14, corresponding to the seven octave bands with center frequencies from 125 Hz to 8 kHz, respectively.[43]

3.5   Rapid Speech Transmission Index (RASTI)

The RASTI approach is a more rapid procedure based on STI and is used for fast computational evaluations of auditorium conditions. This approach is acceptable since in a great number of practical situations the detailed analysis grid of STI is unnecessary. The mathematical expression used to calculate RASTI is the same as for calculating STI, but restricted to only two octave bands: 500 Hz, with four modulation frequencies (1, 2, 4, and 8Hz); and 2 kHz, with 5 modulation frequencies (0.7, 1.4, 2.8, 5.6, and 11.2 Hz).[44] Therefore, the average apparent signal-to-noise ratio for RASTI is,

$$\overline{(S/N)_{app}} = \sum_{k=1}^{2} w_k (S/N)_{app,k} \tag{3.13}$$

Finally, RASTI is defined by,

$$RASTI = \left[\overline{(S/N)}_{app} + 15\right]/30 \tag{3.14}$$

Details of the calculation in MATLAB® are provided in Appendix A.

CHAPTER 4
ANALYSIS USING COMPUTER MODELS AND NUMERICAL CALCULATION

This chapter addresses the acoustics of rooms with domed ceilings from the standpoint of computer models and numerical analysis. Models were adapted to the mosque described in Chapter 1. This chapter begins with a discussion of the modeling process and various modeling configurations.

The computer models allowed investigation several areas of interest. By generalizing the analysis, a description of the acoustical characteristics of the mosque models can be obtained. Observation of the dome ceiling configurations is the main interest in this study. In this observation, analytical studies using the propagation of these sound rays were also done to verify the results. Observations of the number of particles used for the simulations and the number of flat plane sections used to create the domed surfaces were also made. Two source orientations were also studied to model activities inside the mosque. Different model configurations were used to study the effects of absorptive materials inside these models. Reverberation time estimates through numerical calculations using the Sabine and Eyring equations are also important since some acoustical characteristics of a room may be predicted directly from reverberation time values.

4.1   Process for Room Data Input and Description of the Models

The original design of the mosque for input into EASE^{TM} was drawn in Autodesk Architectural Desktop 2004 with the AEC object [Fig. 4.1 (a)]. The advantage of using

this package is that it enables one to produce a file, which is small and compatible, to expedite the drawing process. Although the drawing process was faster, it actually failed to provide the single layer faces/planes that are needed in EASE^{TM}, since it automatically generated solid masses. By exporting the drawings into an AutoCAD 2000 *dwg* file, the problem was solved. This process automatically explodes the solid masses and changes the faces of the solid masses into editable planes. After this file was saved into *dxf* format, it was successfully imported into EASE^{TM} as room data [Fig. 4.1 (b)].
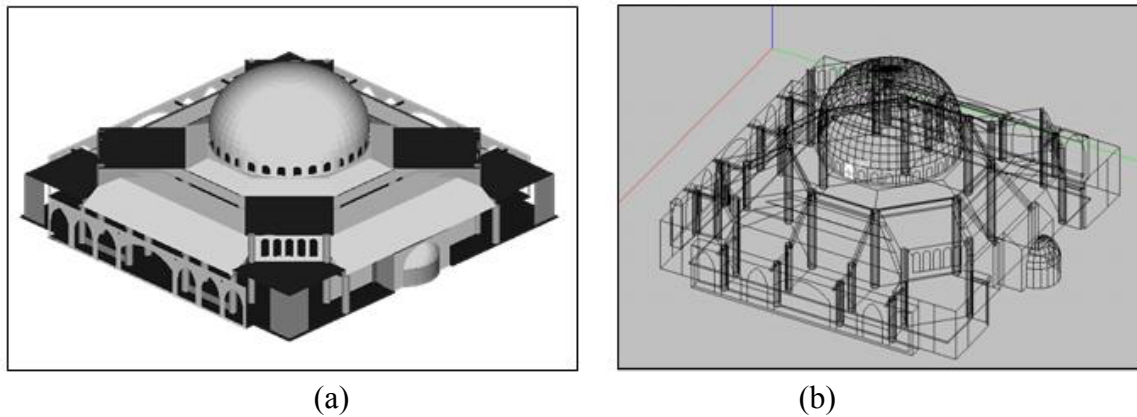
(a)   (b)
Figure 4.1. (a) AutoCAD *dwg* file   (b) EASE 4.1 project data file.

While the room data were assigned, simplification of the original AutoCAD drawing was done for several reasons, including the following:

1. Limitations of the number of faces in the model due to time constraints and computer capabilities.

2. Finding the optimum model, which is the most reduced model that still gives appropriate results.

The room data input process also involved entering appropriate absorption and scattering coefficients of boundary materials. A variety of combinations using two different domes (see Fig. 1.4) and three base structures for the domes or the ring structures (Fig. 4.2) gave six different principal models (See Fig. 4.3 and Table 4.1)
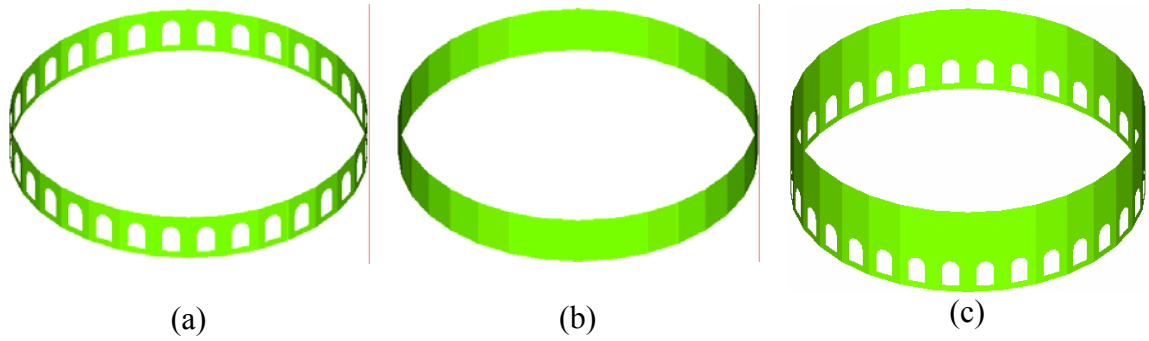
(a)   (b)   (c)

Figure 4.2. Three different ring structures: (a) Ring L (with windows), (b) Ring M (without windows), (c) Ring N (Ring L and M stacked parallel).
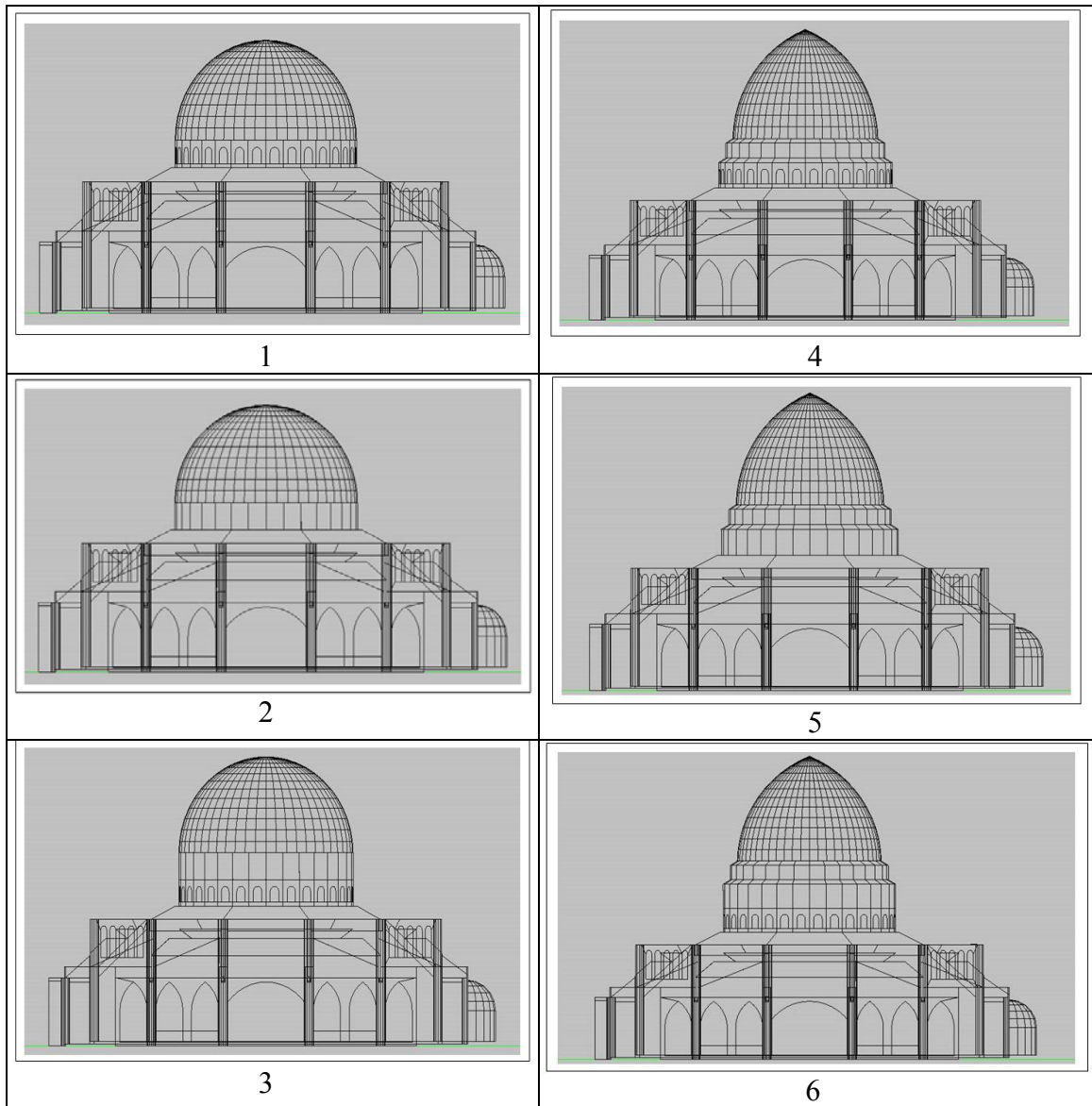
Figure 4.3. Principle models in the computer modeling.

Table 4.1. Description of the models created in the computer modeling.

Models	Worship modes	Type of Dome	Ring Structure	Dome Material	Sections	Description	Drawing (Figure)
1a	preaching	Dome A	Ring L	BASWA-phon	520	Spherical Dome, Ring structure with windows	4.3 (1)
1b	praying						
2a	preaching	Dome A	Ring M	BASWA-phon	520	Spherical Dome, Ring structure without windows	4.3 (2)
2b	praying						
3a	preaching	Dome A	Ring N	BASWA-phon	520	Spherical Dome, Ring L & Ring N	4.3 (3)
3b	praying						
4a	preaching	Dome B	Ring L	BASWA-phon	520	Onion shaped dome, Ring structure with windows	4.3 (4)
4b	praying						
5a	preaching	Dome B	Ring M	BASWA-phon	520	Onion shaped dome, Ring structure with windows	4.3 (5)
5b	praying						
6a	preaching	Dome B	Ring N	BASWA-phon	520	Onion shaped dome, Ring L & Ring N	4.3 (6)
6b	praying						
7	praying	Dome A	Ring L	BASWA-phon	320	Model 1 with different number of sections	N/A
8	praying	Dome A	Ring M	BASWA-phon	320	Model 2 with different number of sections	N/A
9	praying	Dome A	Ring N	BASWA-phon	320	Model 3 with different number of sections	N/A
11	praying	Dome A	Ring L	concrete	520	Model 1 with different dome material	4.3 (1)
12	praying	Dome A	Ring M	concrete	520	Model 2 with different dome material	4.3 (2)
13	praying	Dome A	Ring N	concrete	520	Model 3 with different dome material	4.3 (3)
14	praying	Dome B	Ring L	concrete	520	Model 3 with different dome material	4.3 (4)
15	praying	Dome B	Ring M	concrete	520	Model 3 with different dome material	4.3 (5)
16	praying	Dome B	Ring N	concrete	520	Model 3 with different dome material	4.3 (6)

The simulated audience area is the prayer hall with the addition of 36 seats that represent the positions of receivers (see Fig. 4.4) on one half of the hall. The prayer hall is assumed to be symmetrical. Seats in EASE^{TM} are point receivers, as if microphones

were placed at an actual room position for acoustical measurements. Their settings are immaterial. The body movements in prayers generally can be classified as having two different heights of ear level, that is, at a standing or sitting height. The heights of the seats are 80 cm, approximately the height of a person's ears in a seated position on the praying area floor. This is based on the average height for an Indonesian male, which is approximately 165 cm. The use of the numerous seats in EASE[TM] gives the ability to do detailed observations of the acoustical characteristics over space. This is applied to the seated position in order to address preaching inside mosques, where speech intelligibility is a particularly important matter.

The distributed audience area height is 152 cm from the prayer hall floor, corresponding to the height of a person's ears in a standing position. By having two different measurement heights (distributed audience area and fixed seats), the speech intelligibility for key worship activities in mosques can be observed.
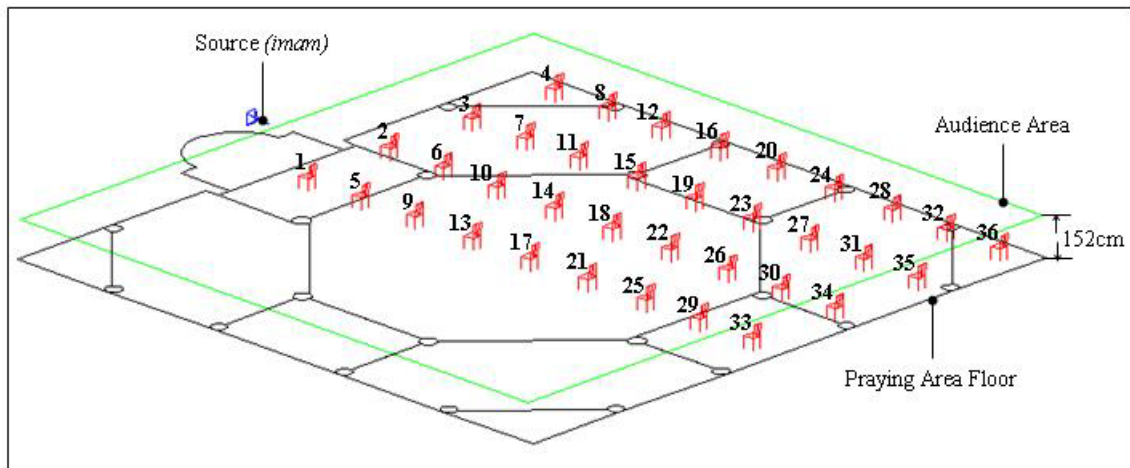
Figure 4.4. Seats' positions, seats' numbers and audience area.

Figure 4.5 shows the interior of the models from two different positions. Seat 33 is the receiver position at the back end of the prayer hall, facing straight toward the mihrab. Seat 17 is beneath the center of the dome, which in Fig. 4.5 is looking toward the side

walls, showing the open boundaries represented by black surfaces. All of the models are made with carpeting and in an unoccupied condition.
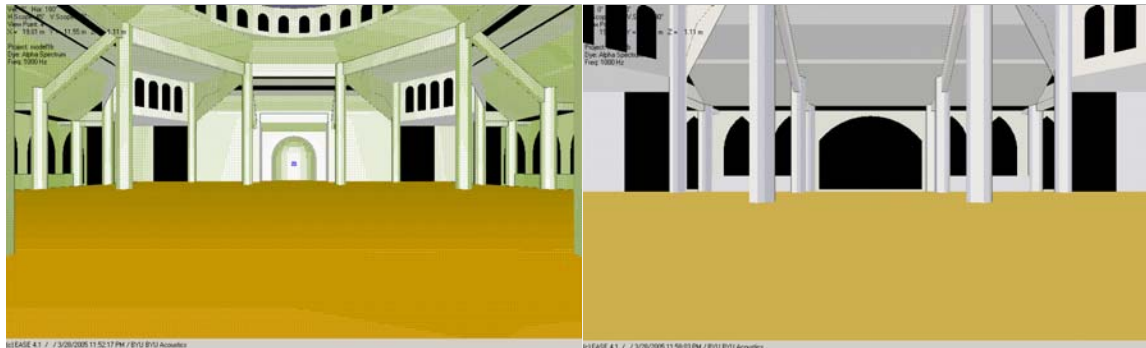
Figure 4.5. View in the model (a) from seat 33 facing the front (b) from seat 17 facing the side.

In EASE^{TM}, the acoustical parameters (calculated according to ISO standard 3382) are mapped using the AURA mapping module onto the audience area or individual listener seats (see Fig. 4.4) by simulating the echogram.[45] Another useful tools is AURA response, which is used for Auralization. AURA is an abbreviation for Analysis Utility for Room Acoustics. The module is based on the CAESAR algorithm developed by Aachen University.

4.2   Statistical Methods Used in the Research

The parameters being discussed here are %AL$_{cons}$, C$_{50}$ and RASTI. It is important to note that the C$_{50}$ and %AL$_{cons}$ parameters used for the analysis in this research are for the 1000 Hz octave band only. The visualizations of the AURA mappings provide the ability to evaluate how the values are distributed throughout the audience area.

Statistical analysis using samples of parameter values measured at certain seats provided a straightforward comparison of results from the various models. All statistical tests work in a similar way in testing a null hypothesis H$_0$, which is a hypothesis that is presumed true until statistical evidence in the form of a hypothesis test indicates

otherwise. The alternate hypothesis H_a, on the other hand, is an interesting result, which is generally the result that the researcher is trying to demonstrate and is the opposite condition of H_0. The result of the statistical test determines whether one will reject H_0 (accept H_a) or not reject H_0 (not accept H_a). There is always a level of significance $\propto$ (alpha), associated in the statistical tests, which is used to evaluate p-values. The p-values are used to reject H_0 if they are small compared to the level of significance or to accept H_0 if they are sufficiently large.

A level of significance is always needed in every statistical test. It is represented by *alpha* ($\propto$), which is actually the level we choose that determines the risk we are willing to take of being wrong. In this research, $\propto = 0.05$ was chosen for all statistical tests. Setting the alpha level at 0.05 means that this research is willing to accept the risk of 5% of the test run being wrong. This is related to the p-value in that, if $p < 0.05$, we reject the H_0 and if $p > 0.05$, we do not reject the H_0. The p-values can be found in binomial or standard normal distribution tables (e.g., t-distribution, z-distribution, χ^2-distribution, F-distribution)[46] using this confidence level. This is explained further in the discussion of each statistical test used in the research. Furthermore, it can be assumed that we have 95% confidence in the evidence provided by the samples. The reason for choosing a 95% confidence level (from $\propto = 0.05$ and $1-\propto$) is because many research fields seem to be content with this confidence level. In one case, the p-values can be used to decide whether the test had insufficient sample sizes.

There are three statistical tests used in this research:

- Paired t-test, based on a t-distribution.

- Analysis of Variance (ANOVA), based on an F-normal distribution.

- Bonferroni *t*-test, based on a *t*-distribution.

For comparison between pair-wise models, a simple *match pair t*-test was used (for pair-wise models, a population is assigned with two different treatments that created two populations). The reason for using this test instead of the *two-sample t*-test is because we are observing results at the same receiver positions in our acoustical measurements and seeing whether different treatments created different results. This method was not intended to observe whether the two groups came from the same population as addressed by the two-sample *t*-test. In this test, we make the following hypothesis:

- H_0: there are no differences between the pair-wise means (averages).
- H_a: there are differences between the pair-wise means (averages).

Another parameter in the *t*-test that can be used to derive the conclusion, besides the *p*-value analysis, is the comparison between *t*-statistic (*t*-stat) with the *t*-critical. The *t*-critical is a number that represents the size of the mean difference required for the alpha level selected with the associated degrees of freedom (*df*). The *t*-statistic is a number that represents the actual size of the difference between the two test means. Assume that $\alpha = 0.05$. If *t*-stat > t-critical, there is a 95% chance that the means come from different populations and the null hypothesis should be rejected.

The statistical analysis for testing the multiple models used the ANOVA test. It evaluates the sample variance to see whether there are differences in the population means (averages). In this test, we make the following hypothesis:

- H_0: there are no differences in the population means (averages).
- H_a: there are differences in the population means (averages).

The ANOVA test calculates the *F*-statistic from comparison of multiple samples. From this *F*-statistic we find the *p*-value from the standard normal *F*-distribution at the 95% confidence level. The *F*-distributions depend on two degrees of freedom (*df*). If H_0 is not rejected, that is by *F*-statistic < *F*-critical and p > *alpha*, it could be concluded that the population means are indistinguishable on the basis of the data given.[47] On the other hand, if H_0 is rejected (*F*-statistic > *F*-critical and p < *alpha*) this could mean all of the samples means are different or only that it indicates that there is a significant difference between at least one pair of the sample means. It does not indicate what pair or pairs are significantly different. In this case, a multiple comparison procedure (MCP) needs to be done in order to find which one differs from the rest. In other words, the MCP is not used to make decisions, but to identify the differences of system performances.[48]

Among several MCPs available, the Bonferroni *t*-test was chosen because it determines an overall confidence bound, instead of having separate confidence levels for each comparison.[49] It is the safest MCP because of wide robustness on sample sizes and test scenarios.

4.3 Observation of Differences due to Absorption Materials (The Dome and Ring Structure)

The materials applied in the model can be classified into seven types.

Table 4.2. List of absorption coefficients for materials used in the computer models (Ref. EASE[TM]).

Materials	Absorption coefficient (α) in octave bands						
	125Hz	250Hz	500Hz	1 kHz	2 kHz	4 kHz	8 kHz
Concrete smooth plastered painted	0.01	0.01	0.02	0.02	0.02	0.05	0.06
Absorber (opened boundaries)	1	1	1	1	1	1	1
Carpet (commercial grade carpet)	0.03	0.05	0.09	0.23	0.38	0.54	0.71
Painted brick wall	0.01	0.01	0.02	0.02	0.02	0.03	0.03
BASWAphon® [50]	0.57	0.82	0.77	0.65	0.63	0.49	0.43
Tile floor	0.02	0.03	0.03	0.03	0.03	0.02	0.02
Glazed tile	0.01	0.01	0.01	0.01	0.02	0.02	0.02

Details of the materials and their absorption coefficients are provided in Table 4.2. In the computer models, scattering coefficient were generally applied by adding 10% scattering coefficients at all surfaces based on the default setting in EASE^{TM}. There are plenty of open boundaries and windows in the models, including those in the ring structure. In the computer models, a perfect absorbing material (perfect absorber) with $\alpha = 1$, was assigned to these boundaries.

BASWAphon$^{®}$ is a recently patented system produced by BASWA Schall-und Wärmedämmstoffe AG. The system consists of pre-coated semi-rigid insulation panels, which are first glued to the ceiling; they are finely textured, so that after a final coating, the surface takes on the appearance of a smooth plaster.[51] The ingredients of BASWAphon$^{®}$ involve a proprietary emulsion of spherical mineral particles, which form a micro-porous membrane. The micro-porous membrane offers a tortuous path to incident sound waves and, if backed with mineral wool, provides significant mid-high frequency absorption (see Table 4.2).

All of the principal models (models 1-6) had BASWAphon$^{®}$ for the dome surface material. These models are compared to models with concrete plastered domes (models 11-16). Table 4.3 is the paired *t*-test result for all parameters using 6 pairs of models. The *p*-values are defined from the standard normal *t*-distribution table using the *t-statistic'* values, with *df* = 35 and 95% confidence level ($\alpha = 0.05$). All of them are zeroes except one, which means that the probability of the difference in the test means/averages coming from these pair groups in the same population is zero. The results provide evidence that the dome treatment material (RPG BASWAphon$^{®}$) did produce a significant difference in the speech intelligibility parameters in model 1 through 6 for the 36 seats positions. It is

also shown that in all cases the t-stat > t-critical, that is, the actual mean difference is larger then the required one for $\alpha = 0.05$.

Table 4.3. Paired t-test on models 1 through 6 and 11 through 16.

Paired t-test for: RASTI, C_{50}, %AL$_{cons}$	t-stat	p-observed	t-critical	Conclusion
RASTI model 1 and 11	15.0590	0.0000	2.028	Reject H_o
RASTI model 2 and 12	18.822	0.0000	$\alpha = 0.05$	Reject H_o
RASTI model 3 and 13	16.291	0.0000	$df = 35$	Reject H_o
RASTI model 4 and 14	14.362	0.0000		Reject H_o
RASTI model 5 and 15	7.472	0.0000		Reject H_o
RASTI model 6 and 16	8.945	0.0000		Reject H_o
C50 model 1 and 11	6.564	0.0000		Reject H_o
C50 model 2 and 12	7.325	0.0000		Reject H_o
C50 model 3 and 13	4.711	0.0000		Reject H_o
C50 model 4 and 14	5.297	0.0000		Reject H_o
C50 model 5 and 15	5.3	0.0000		Reject H_o
C50 model 6 and 16	6.640	0.0000		Reject H_o
%AL$_{cons}$ model 1 and 11	-2.106	0.0424		Reject H_o
%AL$_{cons}$ model 2 and 12	-3.577	0.0000		Reject H_o
%AL$_{cons}$ model 3 and 13	-9.838	0.0000		Reject H_o
%AL$_{cons}$ model 4 and 14	-11.222	0.0000		Reject H_o
%AL$_{cons}$ model 5 and 15	-11.408	0.0000		Reject H_o
%AL$_{cons}$ model 6 and 16	-9.523	0.0000		Reject H_o

The effect of the BASWAphon material inside the model can be seen from the aggregate absorption plots in Fig. 4.6 and compared with concrete (Fig. 4.7). The BASWAphon contributed significant absorption inside the model. It can also be assumed that less sound reflection might occur in the domed ceiling region due to this absorption. This means fewer echoes might occur in this region since the intensity of the focusing effect was reduced by the BASWAphon absorption. Applying this total absorption into Sabine's reverberation equation produces less reverberation inside the model with the BASWAphon material.
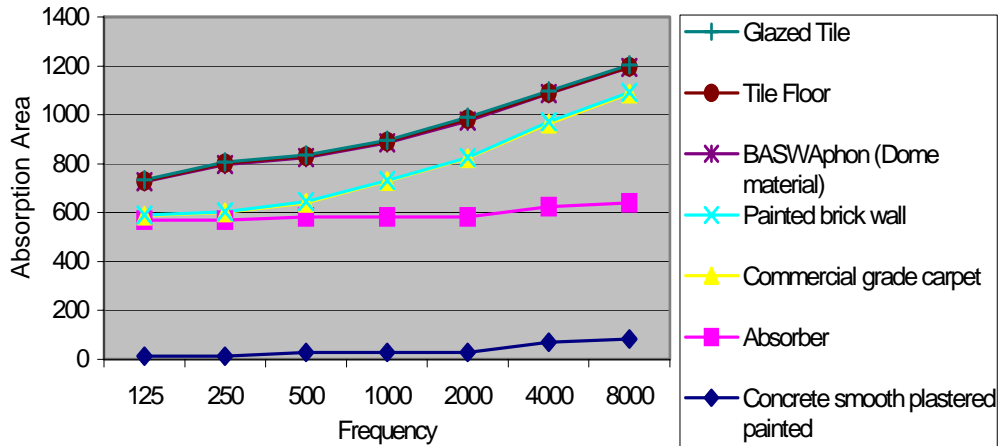
Figure 4.6. Cumulative absorption curves for model 1.
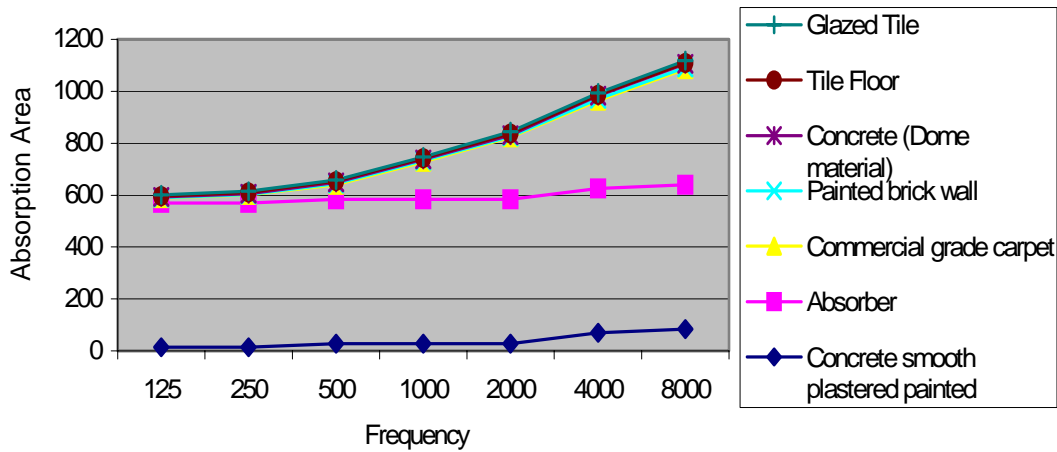
Figure 4.7. Cumulative absorption curves for model 11.

Using the speech parameters, we can determine whether this treatment improved the speech performances inside the room as shown in Fig. 4.8 (for RASTI), around 50% of the seats in model 1 have very good intelligibility (RASTI from 0.60 to 0.75) and only 25% for model 11. For the C_{50} (Fig. 4.9), the percentage on having a good clarity ($C_{50} \geq$ 50dB) is almost the same for model 1 (30 %) and model 11 (25%). Finally, for % AL_{cons} (Fig 4.10) there are 25% of the seats that have a poor intelligibility ($Al_{cons} > 11\%$) in model 11 and only 12% for model 1. From these comparisons, it is apparent that the dome treatment applied in model 1 provided better speech intelligibility.
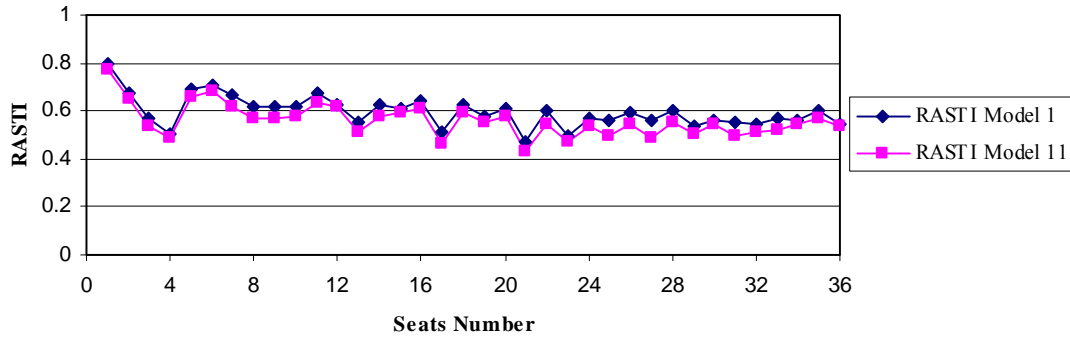
Figure 4.8. RASTI on seats for model 1 (BASWAphon dome) and model 11 (concrete dome).
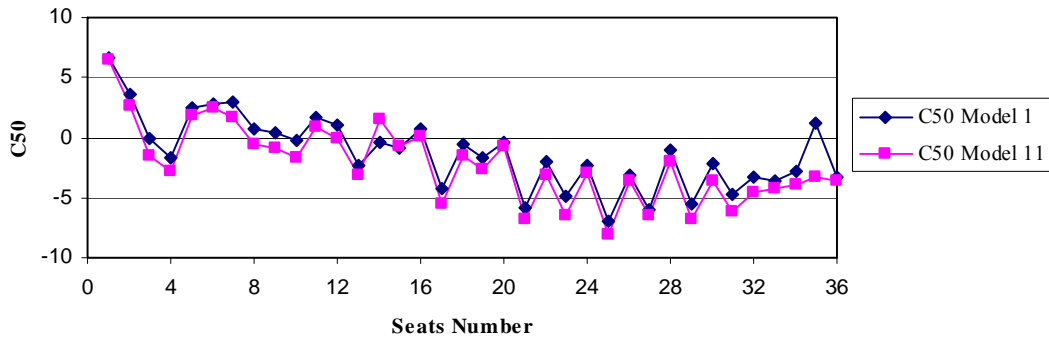
Figure 4.9. C$_{50}$ of seats for model 1 (BASWAphon dome) and model 11 (concrete dome).
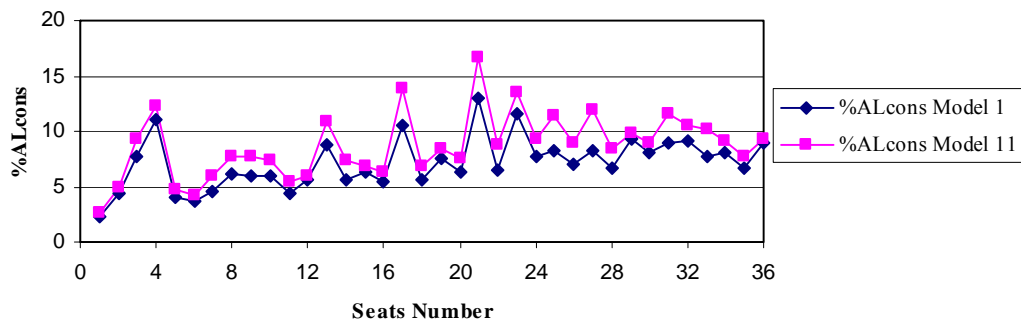
Figure 4.10. %AL$_{cons}$ of seats for model 1 (BASWAphon dome) and model 11 (concrete dome).

In order to assure that the discrepancies of the speech parameters are due to the different dome material, an energy time curve of the impulse responses of certain seats in these models are compared in Fig. 4.11. Stronger reflections are shown at 20 until 35 seconds of the energy time curve of the model with a concrete dome for seat 1. Longer reflection tail that reached above 30 seconds of the energy time curve of the model with a concrete dome is shown for seat 2.

| Model 1b (BASWAphon) seat number 1 | Model 1b (BASWAphon) seat number 2 |
| Model 11b (concrete) seat number 1 | Model 11b (concrete) seat number 2 |
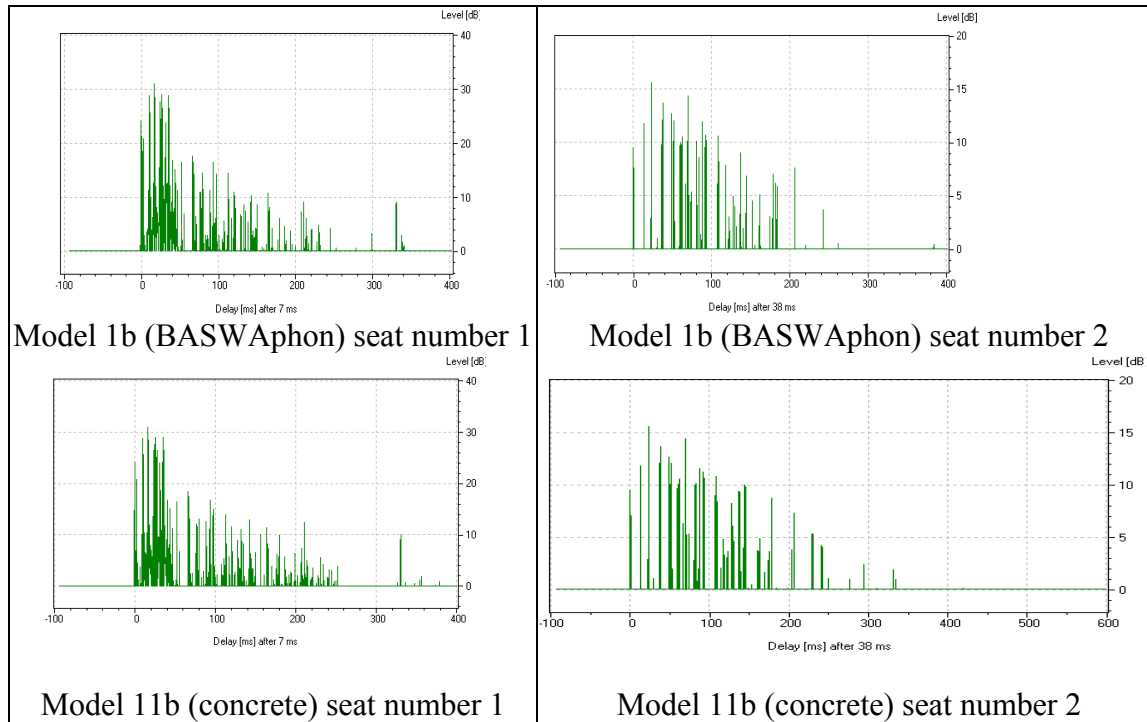
Figure 4.11. Energy time curve of model 1b and model 11b.

Observation of the differences of the ceiling structure is provided in section 4.4 (page 44). Figure 4.12 shows the effect of the windows on the ring structure to the total sound absorption inside model 1.

Cumulative absorption curves for model 1

	125	250	500	1000	2000	4000	8000
Glazed Tile	4.0319	4.0319	4.0319	4.0319	8.0638	8.0638	8.0638
Tile Floor	3.5718	5.3577	5.3577	5.3577	5.3577	3.5718	3.5718
BASWAphon	134.96	194.16	182.32	153.91	149.17	116.02	101.82
Painted Brick	2.0208	2.0208	4.0416	4.0416	4.0416	6.0624	6.0624
Carpet	18.858	31.431	56.575	144.58	238.87	339.45	446.31
Absorber	555.57	555.57	555.57	555.57	555.57	555.57	555.57
Concrete	13.903	13.903	27.807	27.807	27.807	69.517	83.42

Figure 4.12. Aggregate plot of the absorption area for model 1.

Cumulative absorption curves for model 2

	125	250	500	1000	2000	4000	8000
Glazed Tile	4.0319	4.0319	4.0319	4.0319	8.0638	8.0638	8.0638
Tile Floor	3.5716	5.3574	5.3574	5.3574	5.3574	3.5716	3.5716
BASWAphon	136.05	195.72	183.78	155.14	150.37	116.95	102.63
Painted Brick	2.0208	2.0208	4.0416	4.0416	4.0416	6.0624	6.0624
Carpet	18.858	31.431	56.575	144.58	238.87	339.45	446.31
Absorber	534.79	534.79	534.79	534.79	534.79	534.79	534.79
Concrete	14.071	14.071	28.141	28.141	28.141	70.354	84.424

Figure 4.13. Aggregate plot of the absorption area for model 2.

The total area of the windows on the ring structure in model 1 is not large enough to create significant overall differences with model 2 in cumulative absorption.

Figure 4.14. Energy time curve comparison of model 1b to model 2b.
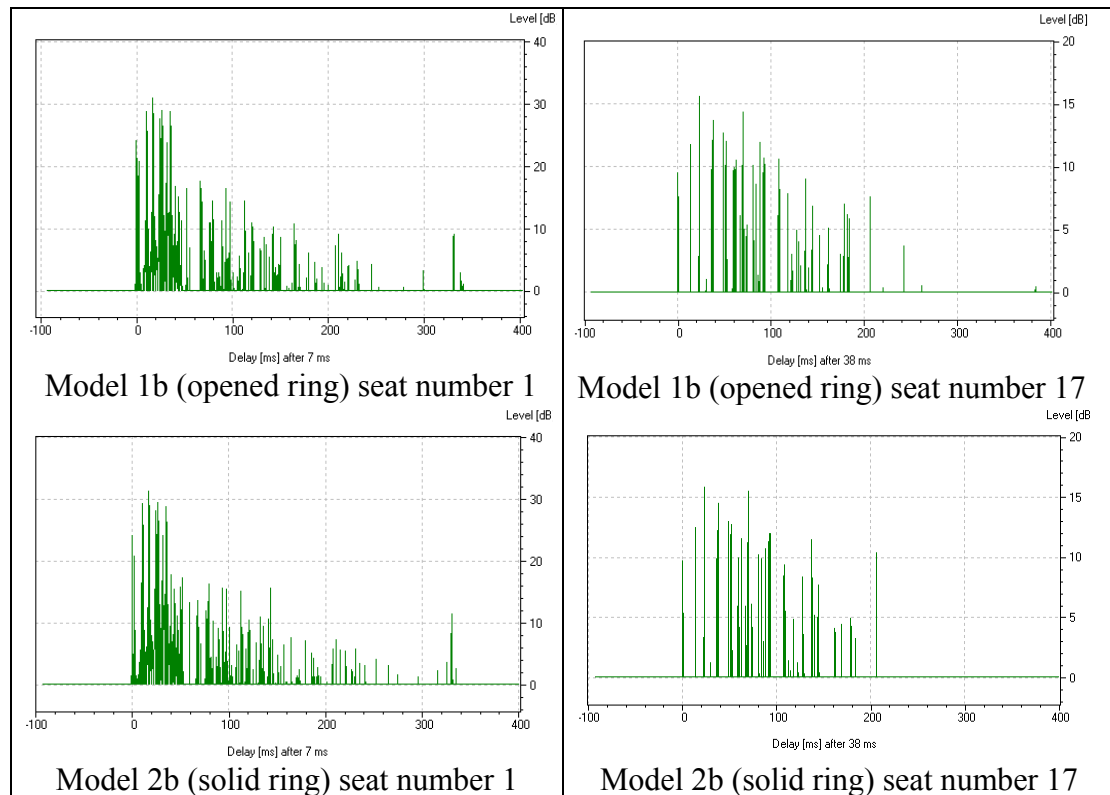
Model 2 with the solid ring has stronger reflections which then lead to the conclusion that this solid ring did create different results in the acoustics of the room, although it did not show up in the speech parameters.

4.4   Calculation of Reverberation Time

Reverberation time is a quantity introduced by W.C. Sabine about a century ago to characterize the duration of sound decay in a room. It is defined as the time required for the sound level to decay by 60 dB from its initial steady state value. Its typical formulation is[52]

$$T_{60} = 0.161 \frac{V}{S\overline{\alpha}} \quad , \tag{4.1}$$

where V is the room volume in cubic meters S is the surface area of the room in square meters, and $\overline{\alpha}$ is the average absorption coefficient.

This is a standard formula for predicting reverberation time of rooms that are relatively reverberant (i.e., with $\overline{\alpha} < 0.2$) and free from pronounced focusing effects. It is intended to be used for sound fields where all directions of sound propagation contribute equal sound intensities, not only in steady state conditions, but also at each moment during the decay of a sound field. The Eyring-Norris reverberation formula[53] was derived by assuming the intensity of sound in a room, during growth, steady state, or decay, is given by summing up the contributions of radiant sound energy from all possible image sources. Its formulation is

$$T_{60} = -0.161 \frac{V}{S \ln(1 - \overline{\alpha})} \quad , \tag{4.2}$$

Air absorption is taken into account by introducing $4mV$ in the formula, where m is the air absorption in the air. It is defined by [53]

$$m = 5.5 \times 10^{-4} \left(50/h\right)\left(f/1000\right)^{1.7}$$

where h is the air humidity, and f is the frequency. This term can usually be neglected for small rooms. With this term, Eq. 4.2 becomes

$$T_{60} = -0.161 \frac{V}{S\ln\left(1-\overline{\alpha}\right)-4mV} \quad . \tag{4.3}$$

Equation 4.1 and 4.2 converge for very reverberant rooms with small values of $\overline{\alpha}$ (i.e., $-\ln(1-\overline{\alpha})$ is nearly equal to $\overline{\alpha}$). We can then write the equation involving air absorption in the simplified form

$$T_{60} = 0.161 \frac{V}{S\overline{\alpha}+4mV} \quad . \tag{4.4}$$

The EASE[TM] computer modeling provided reverberation time values using both the Sabine and Eyring formulas. Reverberation time is an important factor in speech intelligibility inside a large room such as the mosque.
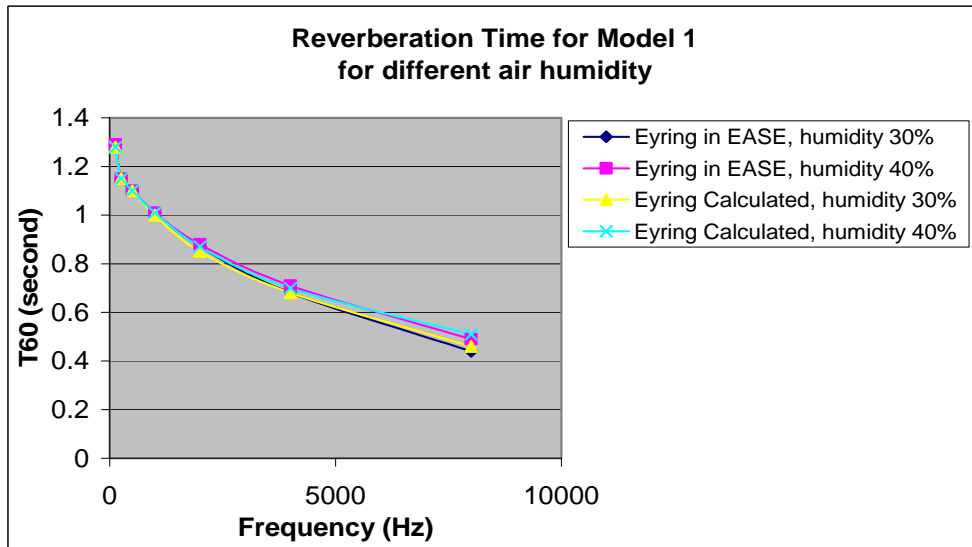
Figure 4.15.   Chart of reverberation time in model 1, comparing values for 30% and 40% air humidity using results from EASE[TM] and numerical calculations.

In order to ensure accuracy, the results from EASE[TM] were compared to other numerical calculations. The effects of different air humidity were evaluated using Eyring's formula

through EASE^{TM} and other numerical calculations as shown in Fig. 4.15. It shows that the T_{60} values for 30% and 40% humidity start to deviate by more than 0.02 seconds at 8 kHz, which is not significant since the acoustical parameters are not evaluated above 8 kHz octave band.

4.5 Observations for Different Ceiling Structures (Dome and Ring Structures)

There are two main points of interest in this investigation related to the ceiling structures, each consisting of different domes and ring structures:

- Comparison of models with a spherical dome (dome A) to models with an onion-shaped dome (dome B): model 1 compared to model 4, model 2 to model 5, and model 3 to model 6.

- Comparison of models with the same dome but with different ring structures: comparison of model 1 to model 2 to model 3, and comparison of model 4 to model 5 to model 6.

4.5.1 Results for Praying Mode (Source Facing Mihrab)

The first discussion concerns the praying mode (see Fig. 1.2). The ANOVA test is used in the comparison of these six different models (1b through 6b). The investigation can be addressed in the same statistical test by using the multiple comparison technique (refer to Section 4.3). The results of the ANOVA tests for each parameter are shown in Table 4.4. For all parameters, F-stat < F-critical and $p > 0.05$ (nearly 1).

Table 4.4. ANOVA test of RASTI, C_{50}, %AL$_{cons}$ for models 1b through 6b.

ANOVA Test	F-stat	p-observed	F-critical	Conclusion
ANOVA RASTI	0.2126	0.9569	2.257067	Does not rejectH$_o$
ANOVA C_{50}	0.0212	0.9998	$\alpha = 0.05$	Does not rejectH$_o$
ANOVA %AL$_{cons}$	0.3242	0.8981	$df_1 = 5$	Does not rejectH$_o$
			$df_2 = 210$	

Therefore, the results failed to reject the null hypothesis that there are no differences on means, based on the data given.

Although the H_0 were rejected, the $t_{\text{Bonferroni}}$ -tests (Table 4.5 through 4.7) were still done in order to determine which paired model had the largest difference. The $t_{\text{Bonferonni}}$ defined in the tables below are in principle the same as t-critical in the paired t-tests. The negative values of the t-statistics are negligible and only the magnitudes are important. Related to the normal t-distribution curve, these negative t-statistics are evaluated with the negative side of the normal curve. Using the $t_{\text{Bonferroni}}$-test, some of the paired models have a larger t-stat than others, which means there are larger differences for these paired samples than for others.

Table 4.5.   Bonferroni t-test for RASTI models 1b through 6b.

For RASTI	$t_{\text{Bonferroni}}$ = **2.633**	1	2	3	4	5
	2	0.777				
	3	0.842	0.065			
	4	0.583	-0.194	-0.259		
	5	0.842	0.065	0	0.259	
	6	0.777	0	0.065	0.194	-0.065

Table 4.6.   Bonferroni t-test for C_{50} model 1b through 6b.

For C_{50} (at 1 kHz octave band)	$t_{\text{Bonferroni}}$ = **2.633**	1	2	3	4	5
	2	0.06				
	3	-0.045	-0.104			
	4	-0.059	-0.118	-0.014		
	5	-0.235	-0.295	-0.191	-0.177	
	6	0.015	-0.045	0.059	0.073	0.25

Table 4.7.   Bonferroni t-test for $\%AL_{\text{cons}}$ model 1b through 6b.

For $\%AL_{\text{cons}}$ (at 1 kHz octave band)	$t_{\text{Bonferroni}}$ = **2.633**	1	2	3	4	5
	2	-0.852				
	3	-0.914	-0.062			
	4	-0.311	0.541	0.603		
	5	-0.966	-0.114	-0.052	-0.655	
	6	-0.901	-0.049	0.013	0.59	0.065

For RASTI and %AL$_{cons}$, model 1b had the largest $t_{Bonferroni}$-statistics but not large enough to conclude that there are differences in the population means for these paired models.

The parameter mappings in Figures 4.16 and 4.17 can also be used to verify the analysis in this section. Generally, it is difficult to see significant differences between the mappings for any of the parameters. This also holds for the subjective interpretation. The RASTI values toward the back of the prayer hall are slightly better for models 4, 5 and 6 than those in the models with a spherical dome (models 1, 2 and 3). Variations in the ring structure only show some effects on models 5 and 6, especially at the back of the prayer hall. The front side of the prayer hall seems to be unaffected by the ceiling changes. The onion-shaped dome seems to have a narrower spread area for the good values, particularly in the region underneath the dome.

0.00– 0.30	Unsatisfactory intelligibility
0.30 – 0.45	Poor intelligibility
0.45 – 0.60	Good intelligibility
0.60 – 0.75	Very good intelligibility
0.75 – 1.00	Excellent intelligibility[54]
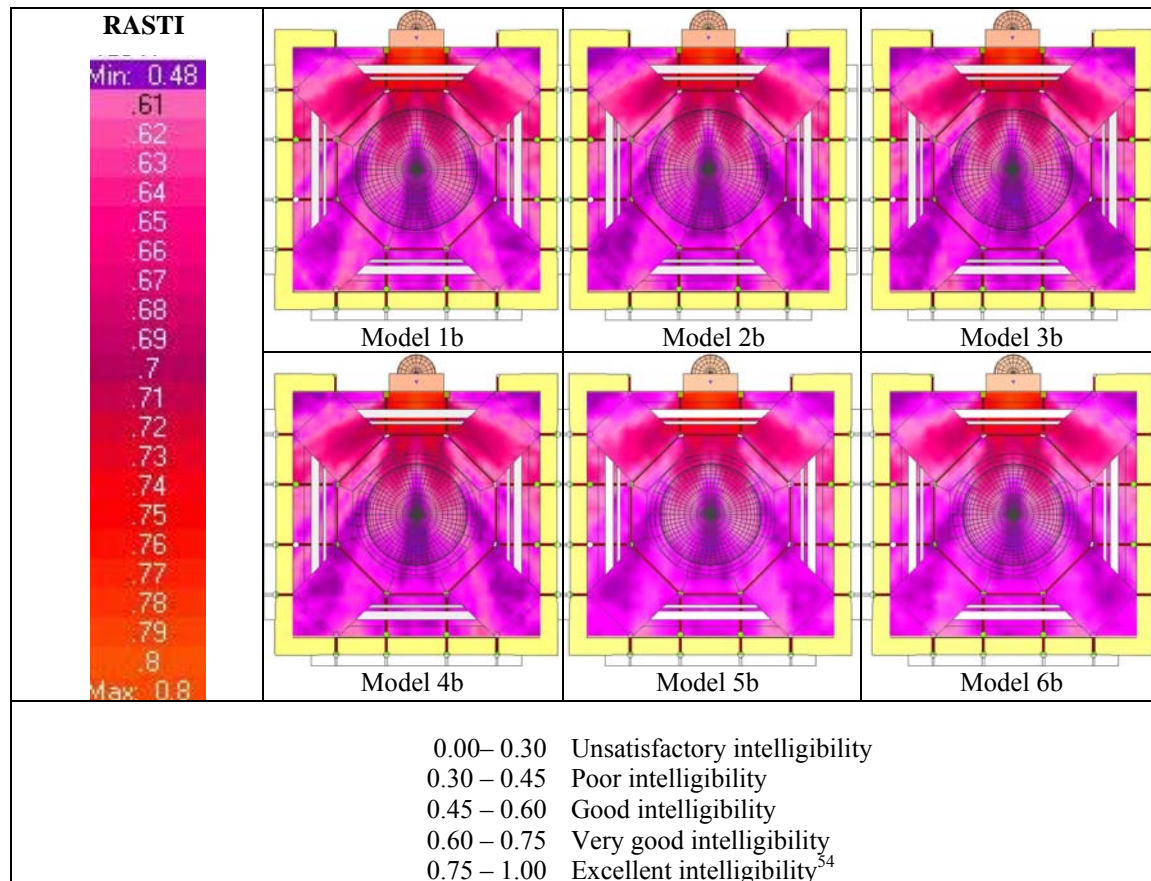
Figure 4.16. RASTI mapping of the prayer hall for praying.

C50 ≥ 0dB, good speech clarity[54]

< 3 %	ideal intelligibility
3% - 8%	very good intelligibility
8% -11%	good intelligibility
>11%	poor intelligibility
>20%	worthless intelligibility[54]
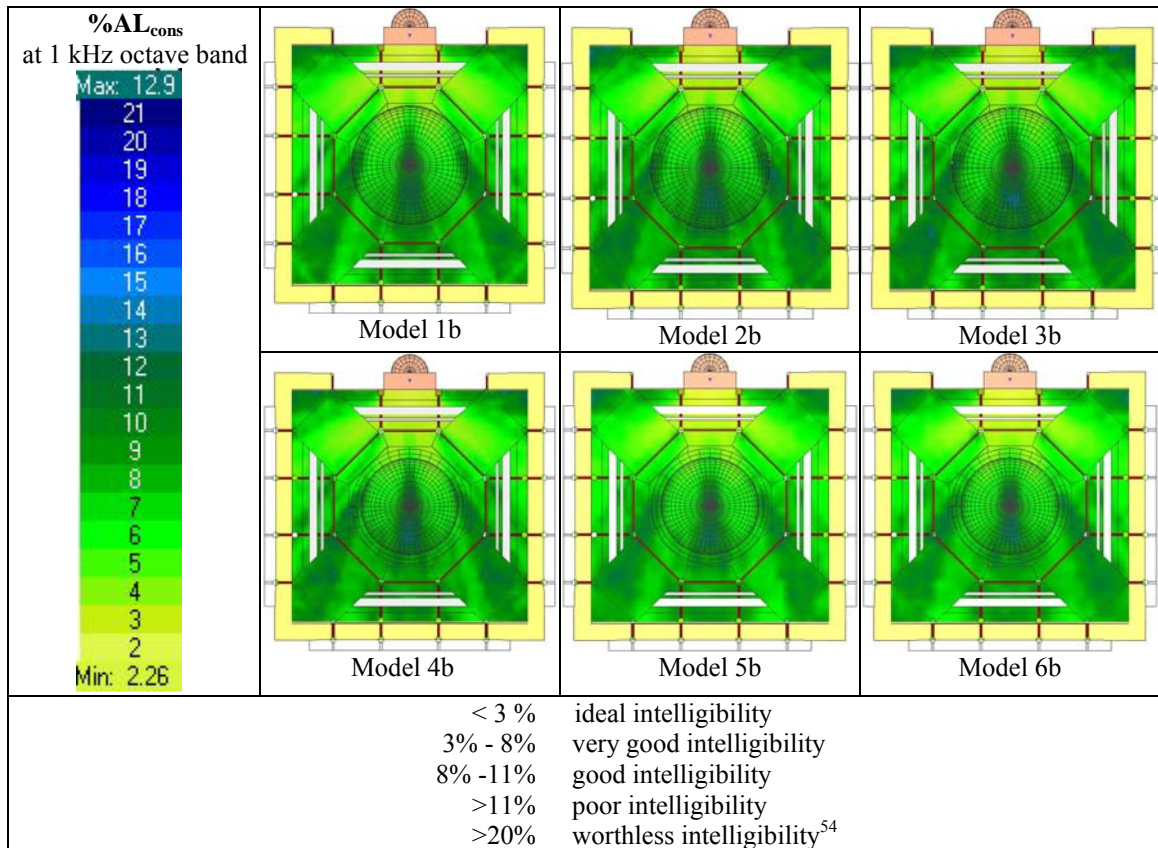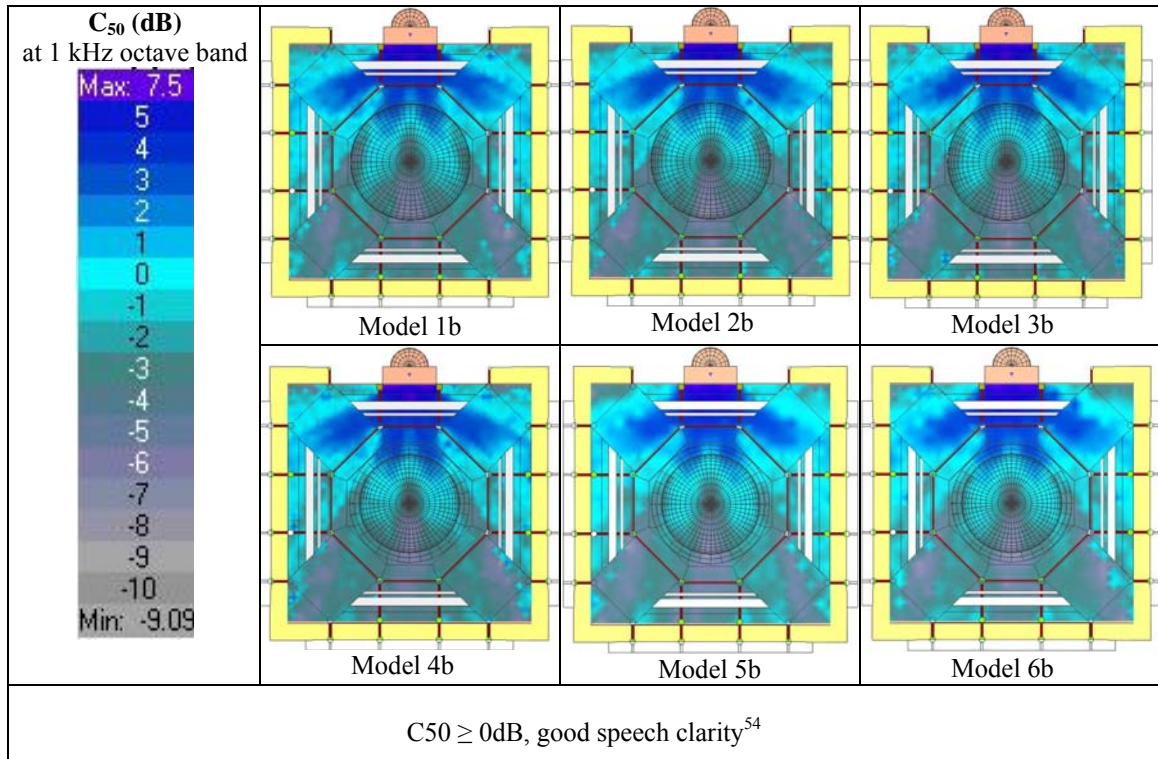
Figure 4.17. C$_{50}$ and %AL$_{cons}$ mappings of the prayer hall for praying modes.

4.5.2 Results for Preaching Mode (Source Facing the Audience)

The results of the ANOVA tests for each parameter and the preaching mode are shown in Table 4.8.

Table 4.8. ANOVA test of RASTI, C_{50}, (1 kHz) and %AL_{cons} (1 kHz) for model 1a to 6a.

Test	*F*-statistic	*p*-observed	*F*-critical	Conclusion
ANOVA RASTI	0.1880	0.9669	2.257067	Does not rejectH_o
ANOVA C_{50}	0.0267	0.9997	$\alpha = 0.05$ $df_1 = 5$	Does not rejectH_o
ANOVA %AL_{cons}	0.2762	0.9258	$df_2 = 210$	Does not rejectH_o

Once again, this source orientation failed to reject the null hypothesis for all models. The same result also holds in the *t*-Bonferroni test (Tables 4.9 through 4.11), where comparisons of model 1 to other models are seen to have the largest differences among all paired comparisons. This is shown by larger t-values, particularly for the RASTI parameter.

Table 4.9. Bonferroni *t*-test for RASTI model 1a through 6a.

For RASTI at 1 kHz octave band	$T_{Bonferroni}$ = **2.633**	1	2	3	4	5
	2	0.828				
	3	0.707	-0.121			
	4	0.707	-0.121	0		
	5	0.707	-0.121	0	0	
	6	0.421	-0.408	-0.287	-0.287	-0.287

Table 4.10. Bonferroni *t*-test for C_{50} model 1a through 6a.

For C_{50} at 1 kHz octave band	*t* $_{Bonferroni}$ = **2.633**	1	2	3	4	5
	2	-0.036				
	3	-0.023	0.013			
	4	-0.182	-0.146	-0.159		
	5	0	0.036	0.023	0.182	
	6	-0.276	-0.241	-0.253	-0.094	-0.276

Table 4.11. Bonferroni *t*-test for %AL_{cons} model 1a through 6a.

For %AL_{cons} at 1 kHz octave band	*t* $_{Bonferroni}$ = **2.633**	1	2	3	4	5
	2	-1.024				
	3	-0.944	0.081			
	4	-0.547	0.487	0.397		
	5	-0.611	0.414	0.333	-0.064	
	6	-0.427	0.597	0.516	0.119	0.183

The parameter mapping used for this observation is only the RASTI (see Fig. 4.18).
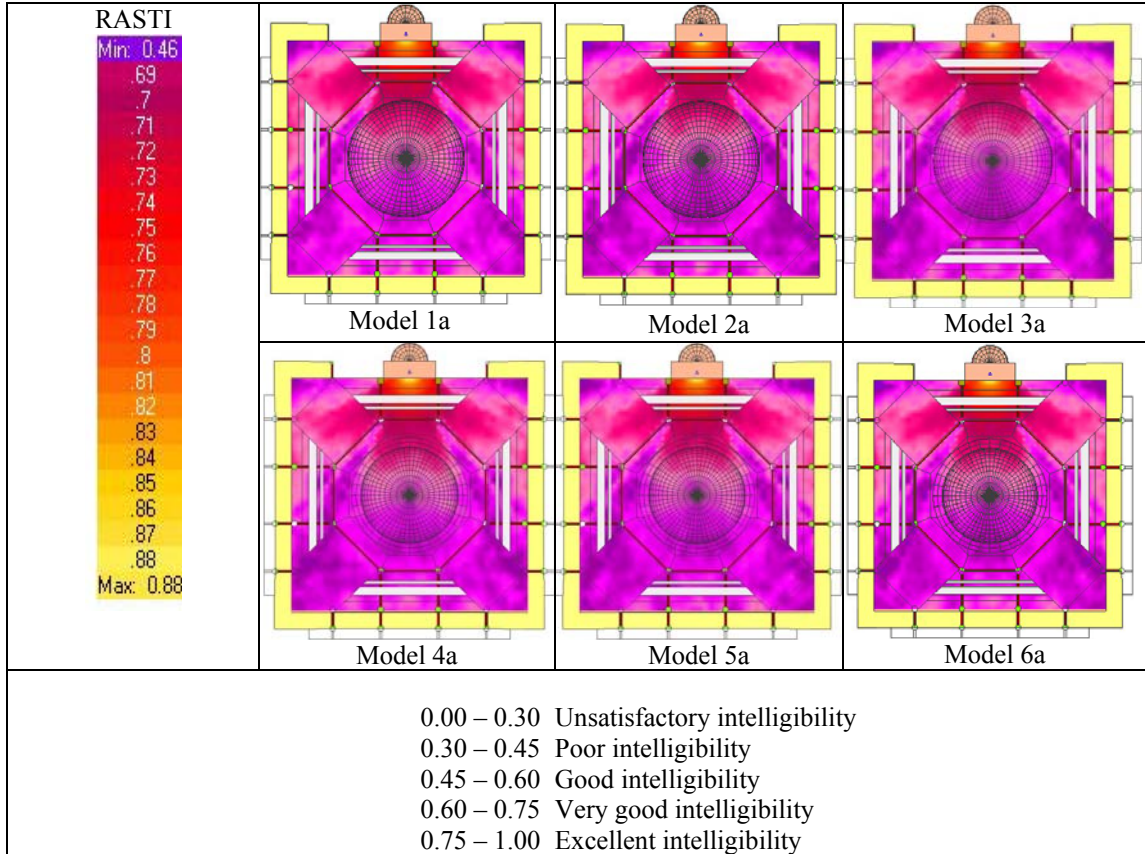
Figure 4.18. RASTI mapping of the prayer hall for preaching.

The reason is because the results for praying also hold in the preaching orientation, where all the parameters have a similar mapping pattern, and therefore one parameter can be used to depict the patterns of the other parameter mappings.

4.5.3   Analysis Based on EASE^{TM} Results

The front side of the prayer hall does not seem to be affected by the ceiling structure. In this area, the direct sound is more dominant than the reflected sound. The narrower area of good intelligibility underneath the dome seems to relate to the sound pressure levels that occur in this area. This statement is justified in part by the geometrical acoustics analysis of reflected sound intensity underneath the dome, presented in the following section. All the p-values in the F-test are nearly unity,

verifying that there is strong evidence provided by the data. Furthermore, it is also appropriate to assume that the test is significant, with α = 0.05, to produce a conclusion, which is that the variation of the ceiling structures on these models did not create significant differences in the speech intelligibility.

While significant differences did not appear in the speech intelligibility parameters, energy time curves show that there are differences in the results produced by the models (see Figs. 4.19 and 4.20).
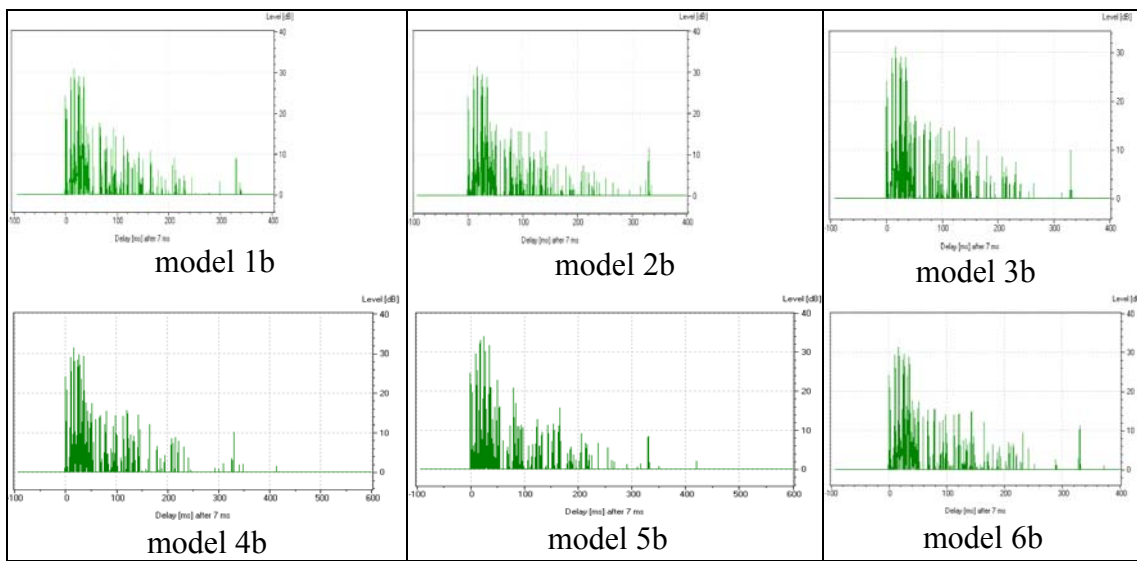
Figure 4.19. Comparison of models 1b through 6b at seat 1 using the energy time curves.
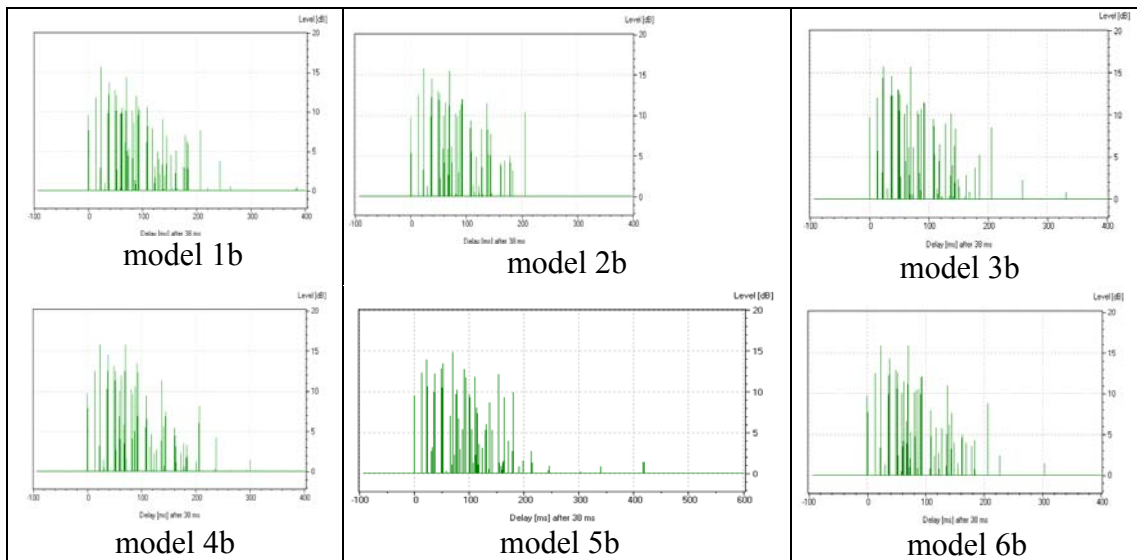
Figure 4.20. Comparison of models 1b through 6b at seat 17 using the energy time curves.

The differences due to dome shapes are more dominant throughout the time interval than those due to the ring configurations for the same dome shape.

4.5.4   Analysis Based on Sound Ray Reflections by Concave Domed Ceiling

It is not very promising to apply methods of wave theory to find answers to practical questions in room acoustics, especially for rooms that are quite large and have irregular shapes, such as the mosque. The calculation of the associated normal mode and eigenvalues in such cases is quite difficult and must generally be conducted using numerical methods. Therefore, geometrical room acoustics was used instead to study the acoustical effects of a domed ceiling element in the room.

The following analysis is used as an addition to the former analysis to see the effect of different ceiling structures, the main interest being the area beneath the dome. Cremer[55] provided a practical method to observe the sound distribution effect in such rooms by using several variable relationships as discussed below. His method is graphically explained in Fig. 4.21. In order to use this method, the analysis was conducted by placing the source at a standing position height with reference to the floor, at the center of the dome. The dome reflects the original ray bundle according to the concaved mirror formula in Eq.(4.5) [also see Eq.(2.4)],

$$\frac{1}{h} + \frac{1}{h'} = \frac{2}{r} \, ,$$

(4.5)

where h is the distance between the source and the dome or plane surface, h' is the distance between the image point and the dome or plane surface, and r is the radius of curvature of the dome. Both h and h' are on the axis of the dome. The relationship between diameters of the reflected ray bundle is given by

$$d' = \frac{d}{2}\left(\frac{h - h'}{h'}\right) , \qquad (4.6)$$

The diameter at the ceiling plane covered by the original ray bundle is d/2. The condition

for the dome reflection to be weaker than the flat ceiling reflection in the receiver plane is

$$\frac{d'}{d} = \frac{1}{2}\left(\frac{h}{h'} - 1\right) > 1 . \qquad (4.7)$$

This condition is met if the center of curvature lies higher above the floor than the

halfway point to the ceiling [Eq. (4.8)]:

$$r < \frac{h}{2} . \qquad (4.8)$$
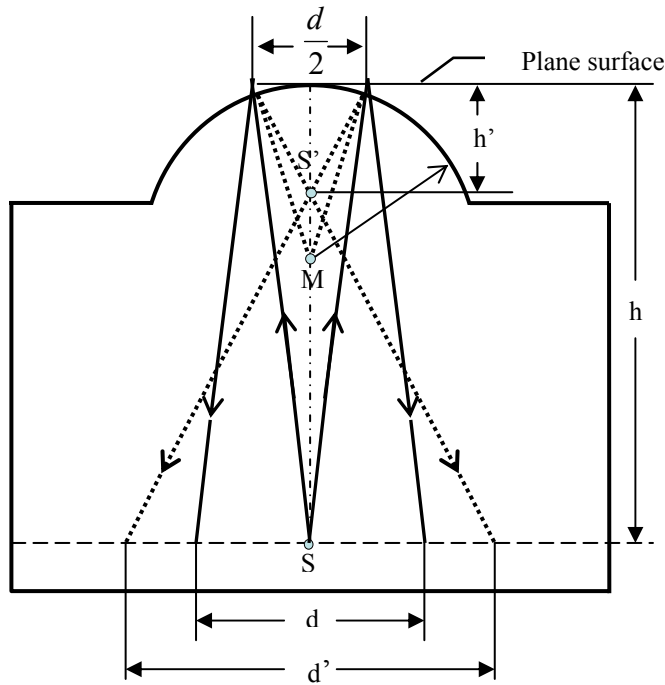
Figure 4.21. Ray bundle reflections on dome ceiling.

This method was used to depict the ray bundle reflections of the two different

domes modeled in EASE^{TM} in order to understand the influence of having different

vertical dimensions of height and its spherical concave surface radius. Both model 1 and

model 2 have the same ceiling structure heights. These models and model 3 have ceiling

structures with smooth spherical concave domes but with two different altitudes.
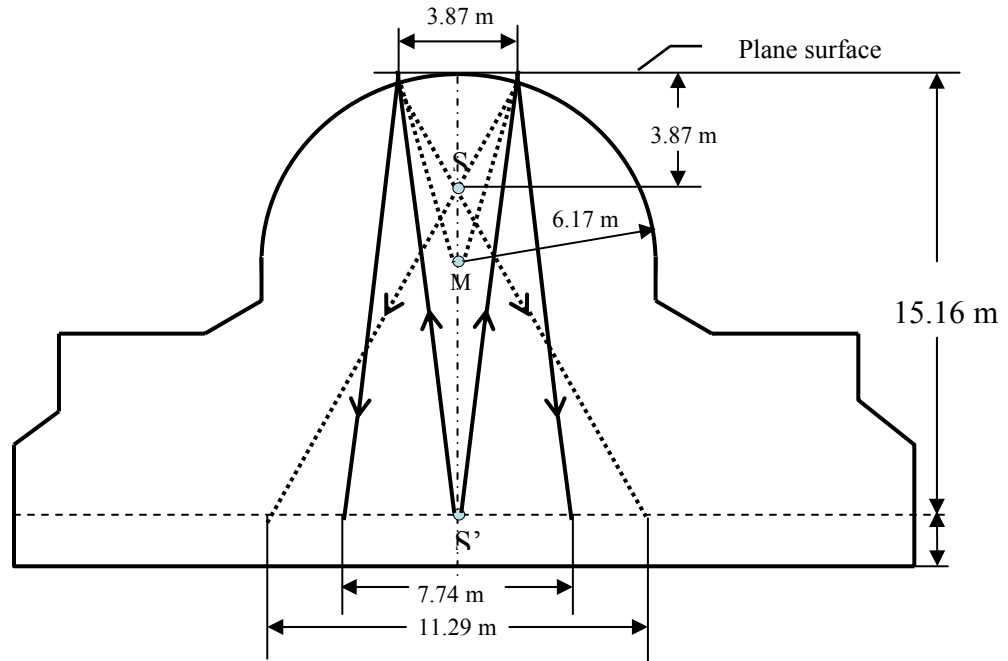
Figure 4.22. Geometrical analysis of models 1 (or model 2).
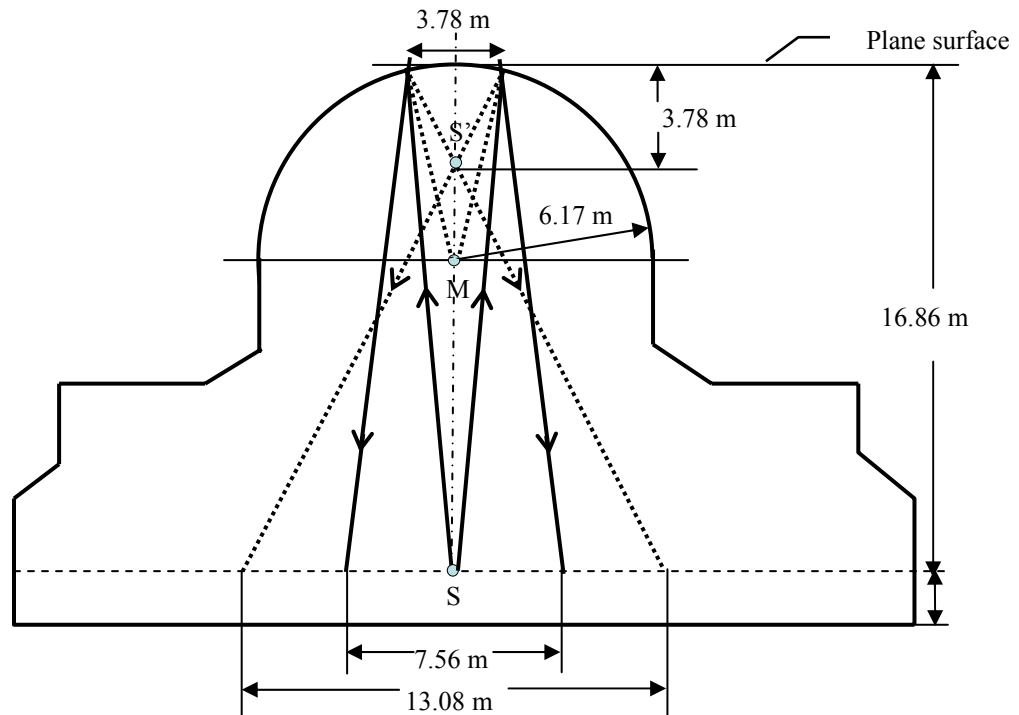
Figure 4.23. Geometrical analysis of model 3.

In Fig. 4.22 and Fig. 4.23, $r < h/2$. Therefore the dome reflection is more divergent than the reflections from the plane surface ($d' > d$), which means the dome reflection is weaker in intensity then the reflections from a plane surface. If $r > h/2$, then the dome reflection is more concentrated. In addition, in order to have equally distributed reflecting rays in the audience, the radius of the curvature needs to exceed $2h$, so it will also exceed the parabolic limit.

Table 4.12 is the analytical study for comparing the diameter of the dome reflections in model 1 (or model 2) and model 3 using Eqs. (4.6) through (4.8). By having a larger h in model 3, the ratio between the diameters of dome reflections with the diameters of plane surface reflections is larger.

As long as in the curvature surface (the two dimensional section of the dome) there is neither a source nor receiver point occurring, then focusing should be limited. Figure 4.24 shows that in the area beneath the dome, the onion shaped dome created more concentrated reflection rays than the spherical dome. Therefore, several reflections had the potential to create a pronounced focusing effect.

Table 4.12 Analytical comparison between model 1 (or model 2) and model 3

Model 1 or 2 (see Fig. 4.22)	**Model 3** (see Fig. 4.23)
$h = 15.16$ m, $r = 6.17$ m $$\frac{1}{h} + \frac{1}{h'} = \frac{2}{r}$$ $$\frac{1}{15.16} + \frac{1}{h'} = \frac{2}{6.17} \Rightarrow h' = 3.87$$ $$d' = \frac{d}{2}\left(\frac{h-h'}{h'}\right)$$ $$\frac{d'}{d} = \frac{1}{2}\left(\frac{15.16}{3.87} - 1\right) = \frac{11.29}{7.74} = 1.46 > 1$$	$h = 16.86$ m, $r = 6.17$ m $$\frac{1}{h} + \frac{1}{h'} = \frac{2}{r}$$ $$\frac{1}{16.86} + \frac{1}{h'} = \frac{2}{6.17} \Rightarrow h' = 3.776$$ $$d' = \frac{d}{2}\left(\frac{h-h'}{h'}\right)$$ $$\frac{d'}{d} = \frac{1}{2}\left(\frac{16.86}{3.78} - 1\right) = \frac{13.08}{7.56} = 1.73 > 1$$
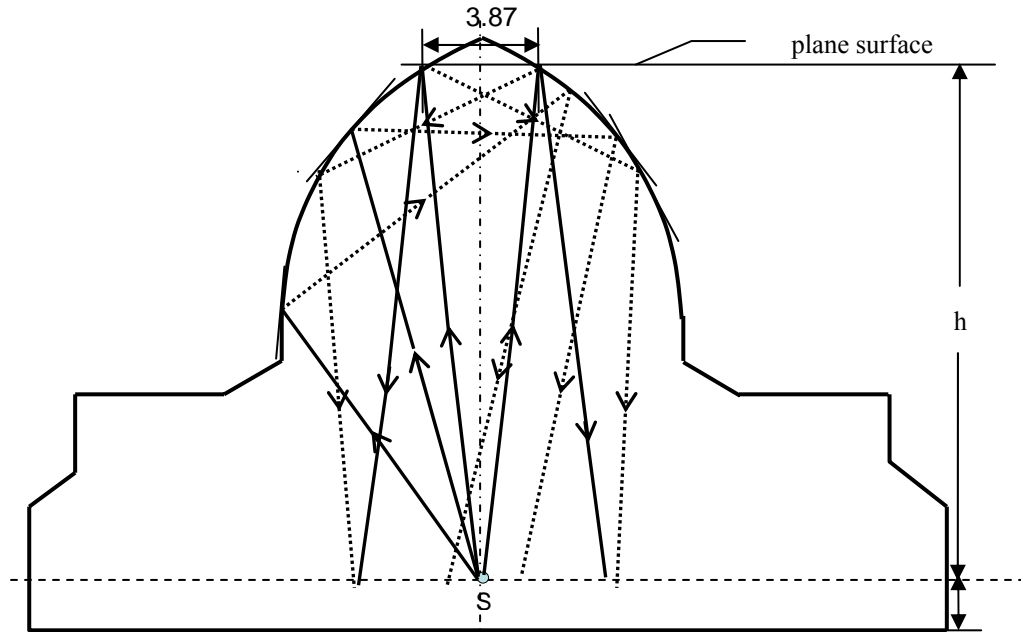
Figure 4.24. Geometrical analysis of model 4 (model 1 with an onion-shaped dome).

4.5.5 Analysis Based on The Intensity of the Ray Bundles

The effect of the curved surfaces (domes) can be studied quantitatively using the following equations: [12]

$$I_o = \frac{A}{|a + x|^n} \, , \tag{4.9}$$

$$I_r = \frac{B}{|b - x|^n} \, , \tag{4.10}$$

$$\frac{I_o}{I_r} = \left| \frac{1 + \dfrac{x}{a}}{1 - \dfrac{x}{b}} \right|^n \, , \tag{4.11}$$

where: I_o = Intensity of the incident bundle reflected at the mirror
I_r = Intensity of the reflected bundle
x = radius of the mirror (meters)
a = distance between the source and the mirror (meters)
b = distance between the image and the mirror (meters)
n = coefficient, 2 for the spherical mirror including dome
Both A and B are constants representing the intensity of the ray bundles.

It is based on the ratio of the intensity of the incident ray bundle at a mirror with the intensity of the reflected ray bundles. The ratio of both intensities $A/B = [a/b]^n$ at x = 0, where both intensities must be equal.

Using the equations above, Table 4.13 shows the results for the intensity ratio of model 1 and model 3. It is shown that a model with a smaller a or h (see Fig. 4.22) has more intensity in the reflected bundles. This also agrees with the sound ray analysis in Table 4.12, where that particular model created a smaller d', which is the reflected sound ray diameter. The ratio of the intensity ratio between model 1 and 3 is 1.19, which means both intensity ratios are nearly the same. The analytical studies on both the sound ray reflections and intensity ratios further suggests that the ceiling structure variations in models 1 through 6 did not create dramatic differences inside the mosque.

Table 4.13. Intensity Ratio of model 1 (or model 2) and model 3.

Model 1 (see Fig. 4.17)	**Model 3** (see Fig. 4.18)
$a = h = 15.16$ m $b = h' = 3.87$ m $x = r = 6.17$ m	$a = h = 16.86$ m $b = h' = 3.78$ m $x = r = 6.17$ m
$$\frac{I_r}{I_o} = \left\| \frac{1+\dfrac{x}{a}}{1-\dfrac{x}{b}} \right\|^n = \left\| \frac{1+\dfrac{6.17}{15.16}}{1-\dfrac{6.17}{3.87}} \right\|^2$$	$$\frac{I_r}{I_o} = \left\| \frac{1+\dfrac{x}{a}}{1-\dfrac{x}{b}} \right\|^n = \left\| \frac{1+\dfrac{6.17}{16.86}}{1-\dfrac{6.17}{3.87}} \right\|^2$$
$$= \frac{1.407}{-0.5943} = 5.605$$	$$= \frac{1.366}{-0.632} = 4.671$$
$$\frac{I_{r1}}{I_{o1}} : \frac{I_{r3}}{I_{o3}} = \frac{5.605}{4.671} = 1.19$$	

4.6 Observation of Differences due to Different Numbers of Particles in the EASE^{TM} models

The number of particles is an expression for the number of radiated rays in EASE^{TM}. It is expected that the higher the number of particles, the more accurate the simulation. Unfortunately, the calculation time also becomes longer. One might question

why the models show no significant differences in the speech intelligibility parameters for the different ceiling structures. Both the preaching and praying modes showed negligible differences in the parameters. One possibility is that the simulation might need many more sound rays impinging on the dome in order to generate sufficient reflections.

We address this possibility only for the praying modes since it is the most frequent activity in the mosque. A paired t-test based on the difference of sample means is used to compare results from the models with two different numbers of particles: 100,000 and 500,000. The parameters in all other observations were generated using 100,000 particles. These numbers of particles can be assumed as different treatments. Therefore, the generalized H_0 is that any difference observed among the treatment conditions occurs by chance and does not reflect a true difference. Models 1 through 6 were used in this observation. Table 4.14 provides evidence that there are no differences in the speech parameters generated by the model due to different numbers of particles except perhaps for the $\%AL_{cons}$ parameter in model 4.

Table 4.14. Paired t-test of RASTI, C_{50} and $\%AL_{cons}$ for difference in number of particles.

RASTI	Model	t-statistic	p-observed	t-critical	Conclusion
	1	0.541	0.5191	2.028	Does not reject H_0
	2	-1.01	0.3194	$\alpha = 0.05$	Does not reject H_0
	3	-0.253	0.8014	$df = 35$	Does not reject H_0
	4	1.864	0.0707		Does not reject H_0
	5	0.458	0.6497		Does not reject H_0
	6	0.572	0.5711		Does not reject H_0
C_{50} at 1 kHz octave band	1	0.1	0.920		Does not reject H_0
	2	-0.035	0.9723		Does not reject H_0
	3	-0.848	0.4024		Does not reject H_0
	4	1.291	0.2050		Does not reject H_0
	5	0.348	0.7301		Does not reject H_0
	6	0.666	0.5096		Does not reject H_0
$\% AL_{cons}$ at 1 kHz octave band	1	-0.160	0.8737		Does not reject H_0
	2	-0.244	0.8083		Does not reject H_0
	3	0.111	0.9124		Does not reject H_0
	4	-2.723	0.01		Reject H_0
	5	1.29	0.2055		Does not reject H_0
	6	0.016	0.9876		Does not reject H_0
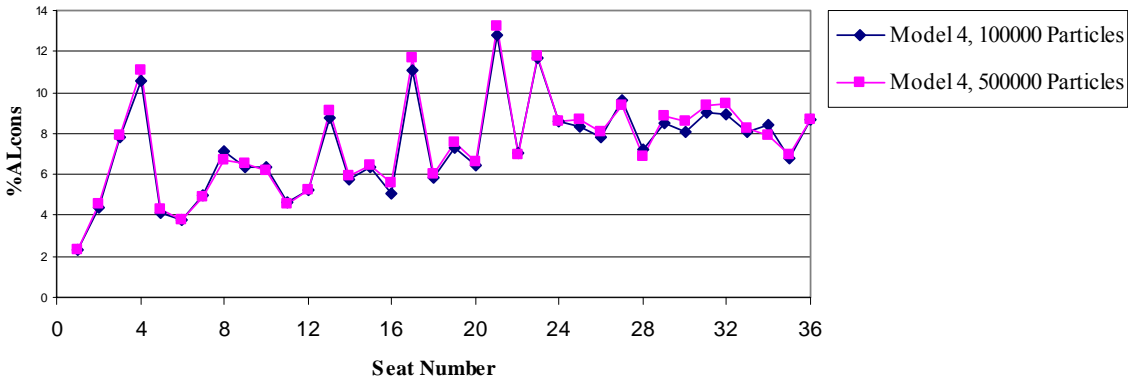
Figure 4.25. %AL$_{cons}$ of model 4 with different number of particles.

Figure 4.25 shows that there are more than 13 pair seats that deviated significantly and contributed to reject the null hypothesis in %AL$_{cons}$ of model 4. Nevertheless, it is still clear that there is no evidence to reject the hypothesis for no difference in the mean of the speech parameter values due to different numbers of particles in the simulation.

4.7   Observation for Different Source Orientation

Praying and preaching inside a mosque are two activities conducted at separate times when the imam is standing at the same position, close to the mihrab, but with 180° differences in his orientation. A single comparison using the parameter mappings was done on model 1a (preaching activity) to model 1b (praying activity), shown in Fig. 4.26. From the mappings, speech intelligibility is shown to differ for the two modes. The difference might be associated with the parameters throughout the whole prayer hall (i.e., globally) and not so much with a spatial variation over the receiver positions (seats).

- 58 -

RASTI Model 1a	C_{50} Model 1a	%AL_{cons} Model 1a
RASTI Model 1b	C_{50} Model 1b	%AL_{cons} Model 1b
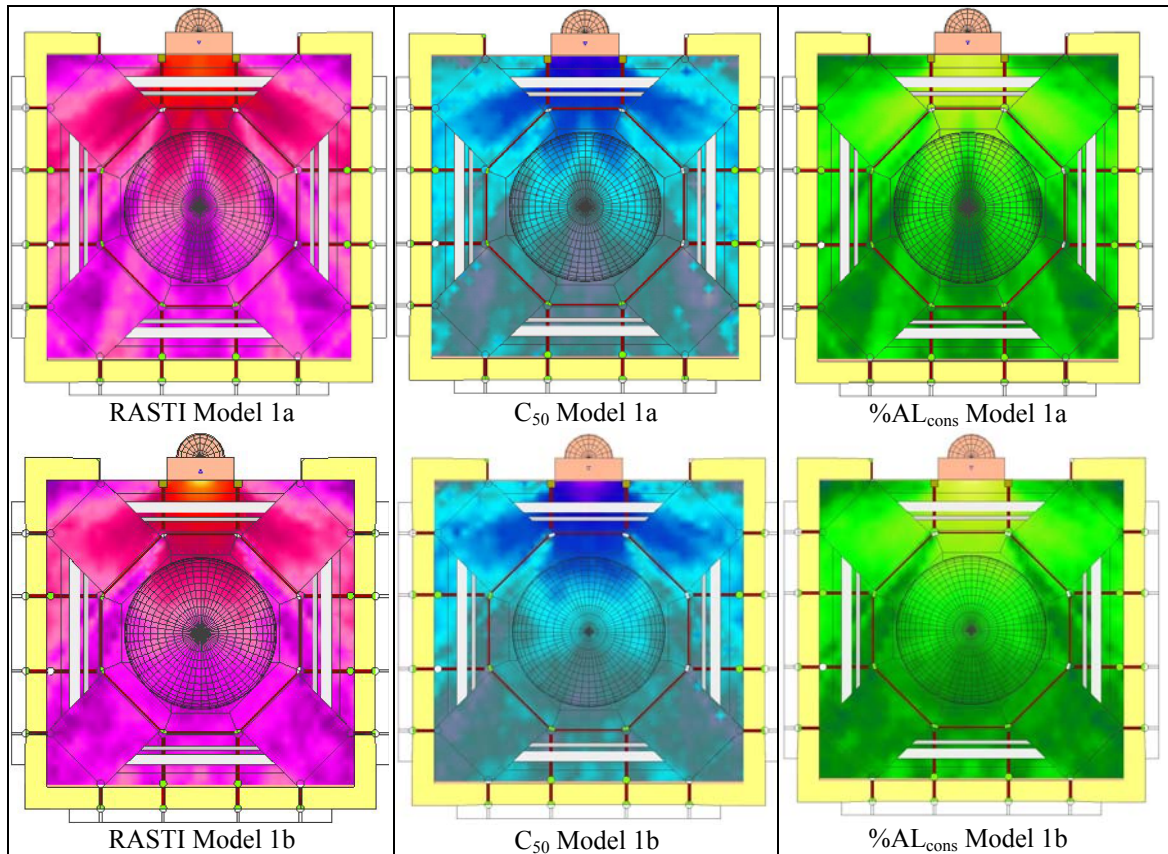
Figure 4.26. RASTI, C_{50} and %AL_{cons} mappings for model 1a and model 1b.

This assertion is verified through the paired *t*-test for each parameter on model 1a compared to model 1b with the null hypothesis (H_0) that there are no differences (refer to Table 4.15).

Table 4.15 Paired *t*-test of model 1a and model 1b for RASTI, C_{50}, and %AL_{cons}

Parameter	t-statistic	p-observed	t-critical	Conclusion
RASTI	0.584	0.5631	2.028	Does not reject H_0
C_{50}	-2.745	0.0095	*df* = 35	Reject H_0
%AL_{cons}	-0.485	0.6306	α = 0.05	Does not reject H_0

It is only the *t*-test for C_{50} that rejects the H_0, which means this is the only evidence that shows differences for the two modes. The preaching mode was expected to have better speech intelligibility because the source is facing the receiving positions. In the praying mode there are two conditions that might lead to less speech intelligibility. One is the possibility that a lower level is heard by the receiver, since the direct signal is coming

from the back of the source. Another is the presence of the mihrab, which acts as the first boundary impinged upon by the direct sound from the front of the source. All of the parameters might have rejected the H_0 and proved that there are differences due to source orientation as compared to the praying area mapping if more seat positions were being observed. Most seats of model 1a (80%) have a better speech clarity than seats in model 1b (see Fig. 4.28). There are 6 seats in the first 2 rows that have nearly the same $\%AL_{cons}$ (see Fig. 4.29). This is also seen in the RASTI data (Fig. 4.27).
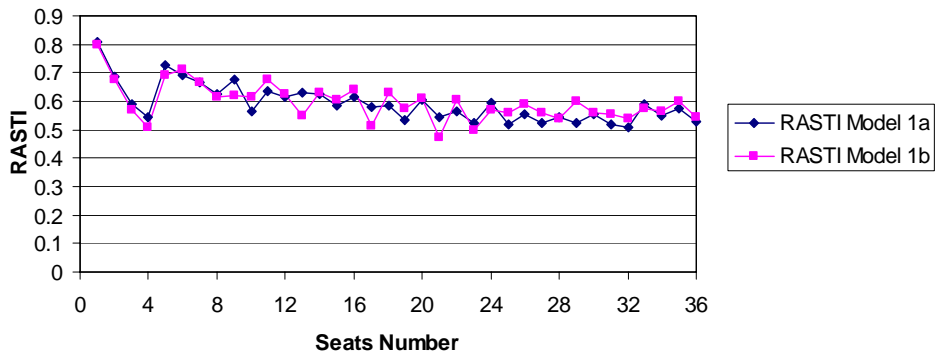
Figure 4.27. RASTI of model 1a and model 1b.
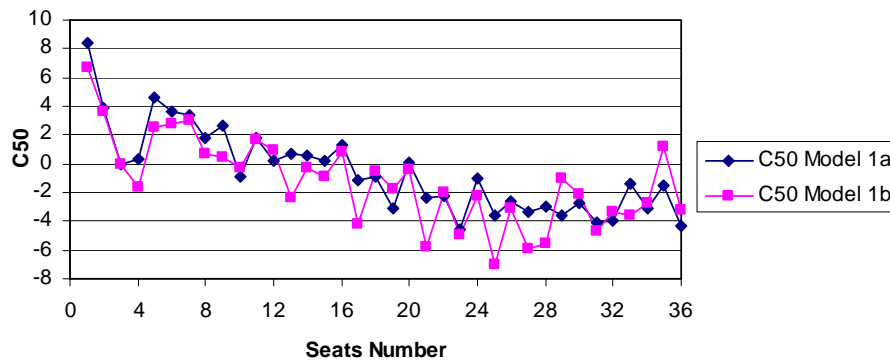
Figure 4.28. C_{50} of Model 1a and Model 1b.
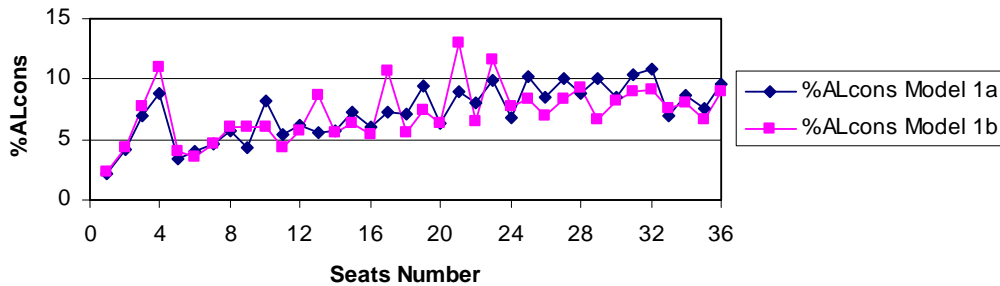
Figure 4.29. $\%AL_{cons}$ of Model 1a and Model 1b.
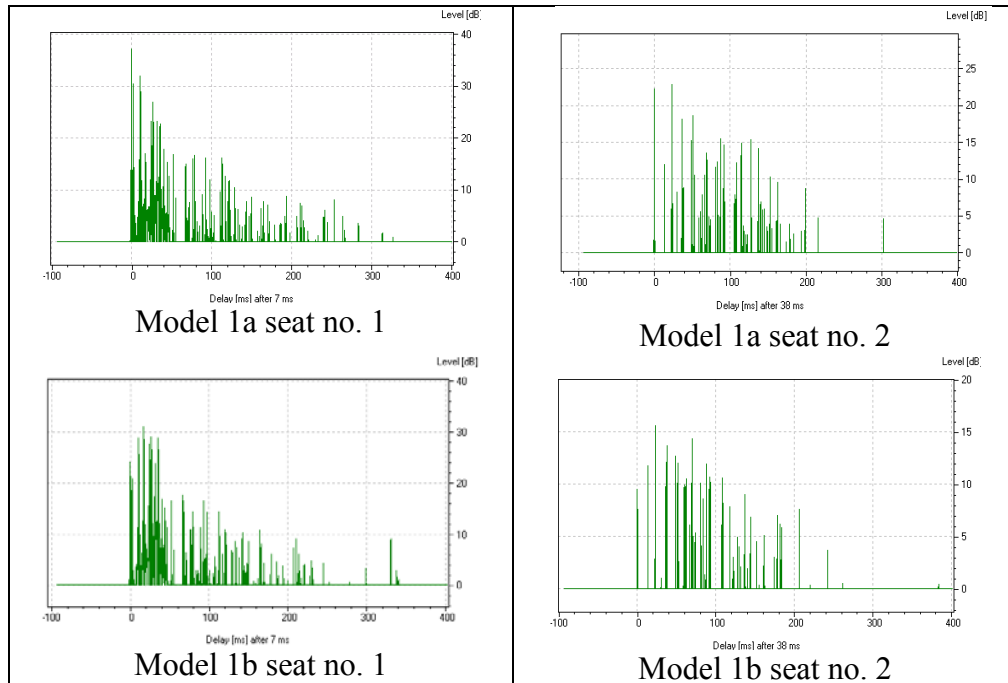
Figure 4.30. Comparison of model 1a to model 1b (different source orientations) using energy time curves

Using energy time curve comparisons, it is shown that different source orientations did created different reflections. The direct sounds are also shown to be different, which is stronger for the source facing the receiver (preaching mode) as would be expected. Some stronger reflections created by the mihrab are also found from model 1b. This means that the mihrab did have an important role in the production of sound reflections inside the room.

4.8   Observation of Differences due to Different Numbers of Planes

EASE^{TM} and other computer modeling packages do not provide the ability to model smooth curved surfaces. Instead, one must model such surfaces as a number of plane sections. In order to see whether different numbers of planes in the domes give different results, three additional models with spherical domes were simulated using 320 plane sections instead of 520, as used in models 1, 2, and 3.

	Model 1	Model 2	Model 3
	Model 7	Model 8	Model 9

0.00 – 0.30	Unsatisfactory intelligibility
0.30 – 0.45	Poor intelligibility
0.45 – 0.60	Good intelligibility
0.60 – 0.75	Very good intelligibility
0.75 – 1.00	Excellent intelligibility

	Model 1	Model 2	Model 3
	Model 4	Model 5	Model 6

$C_{50} \geq 0dB$, good speech clarity
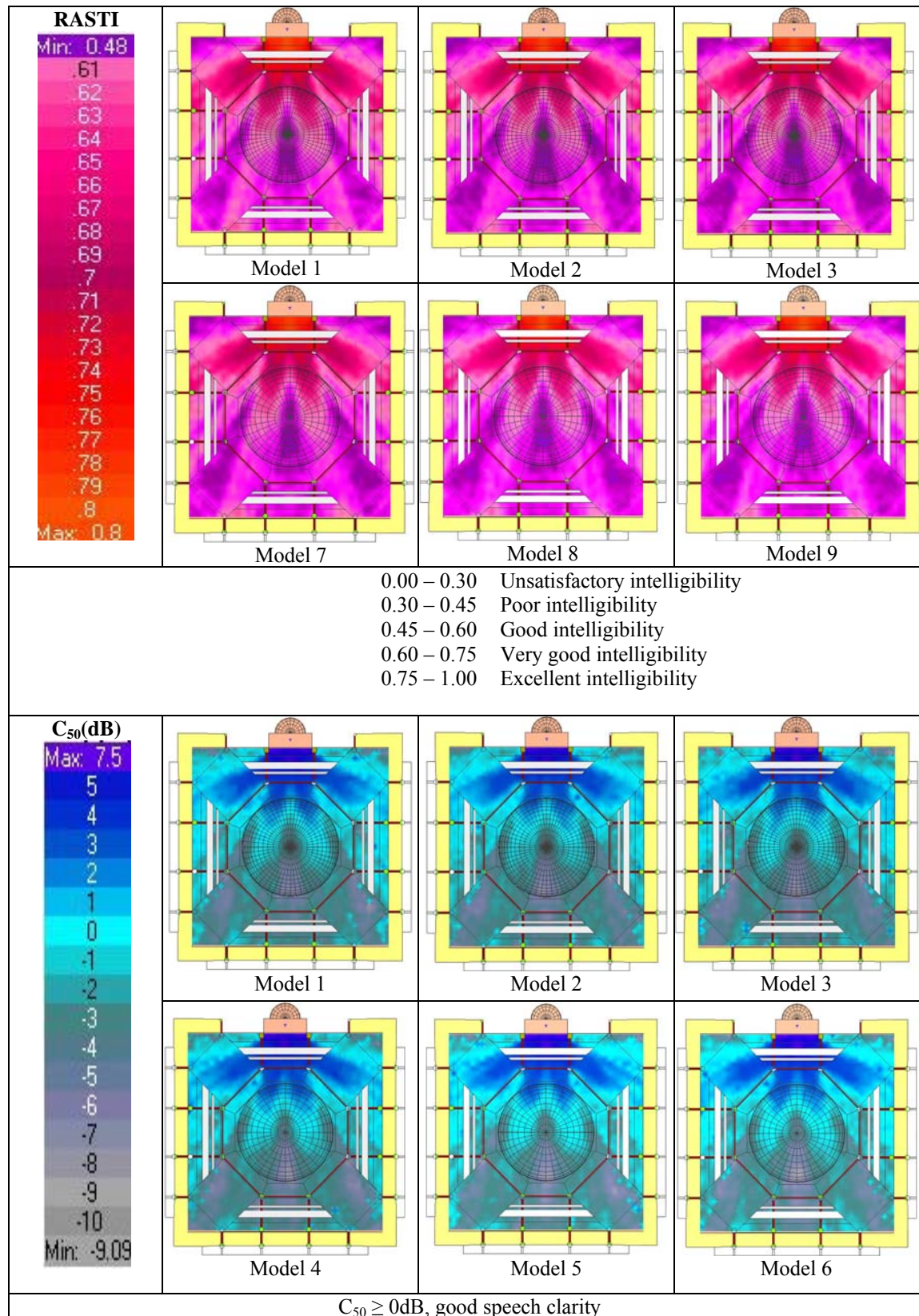
Figure 4.31. RASTI and C_{50} mappings of models 1, 2, 3, 7, 8 and 9 for comparison on number of dome sections.
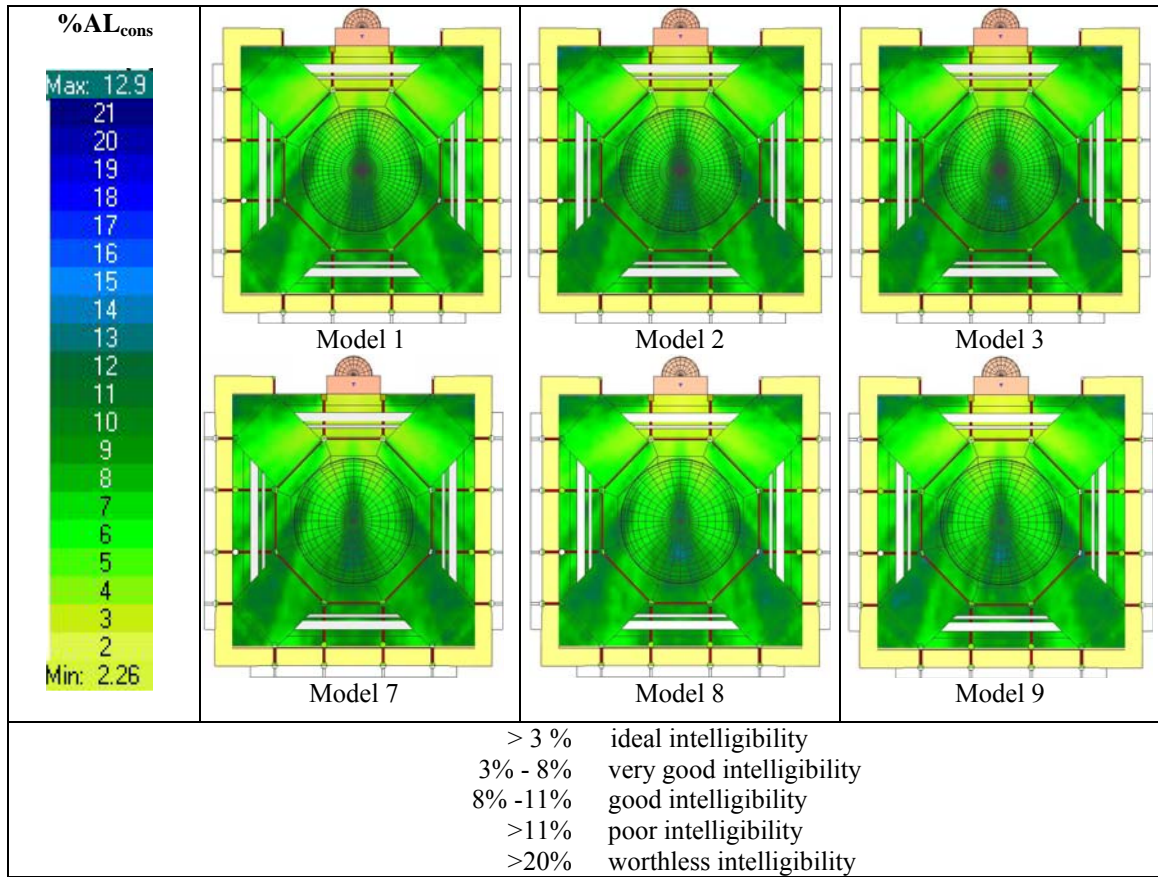
Figure 4.32. %AL$_{cons}$ mapping of models 1, 2, 3, 7, 8 and 9 for comparison on number of dome sections.

Comparative mappings are given in Figs. 4.31 and 4.32. Visually, the overall mappings for the three parameters show no differences between related pairs of models, i.e., model 1 vs. 7, model 2 vs. 8 and model 3 vs. 9. Furthermore, all six models appear to be consistently uniform in their predictions.

It is a straightforward matter to conclude from the *F-statistic* in Table 4.16 that there is no evidence that there are differences in the models.

Table 4.16 ANOVA test of models 1, 2, 3, 7, 8 and 9

ANOVA Test	*F-statistic*	*p*-observed	*F*-critical	Conclusion
RASTI (1,2,3,7,8,9)	0.263711	0.932465	2.257067	Does not reject H$_0$
C$_{50}$ (1,2,3,7,8,9)	0.028498	0.999606	$\alpha = 0.05$ $df_1 = 5$	Does not reject H$_0$
%AL$_{cons}$ (1,2,3,7,8,9)	0.293625	0.916115	$df_2 = 210$	Does not reject H$_0$

Three of the paired *t*-tests (Table 4.17) showed that there is evidence to reject the null hypothesis for differences between each model pair, although this did not hold for the C_{50} parameters.

<p style="text-align:center">Table 4.17. Paired *t*-test of models 1, 2, 3, 7, 8 and 9.</p>

Paired *t*-test	*t-statistic*	*p*-observed	*t*-critical	Conclusion
RASTI model 1 and 7	8.159	0.0000	2.028	Reject H_o
RASTI model 2 and 8	2.235	0.0319	$\alpha = 0.05$	Reject H_o
RASTI model 3 and 9	-0.26	0.7961	$df = 35$	Does not reject H_o
C_{50} model 1 and 7	-1.001	0.3235		Does not reject H_o
C_{50} model 2 and 8	-1.474	0.1493		Does not reject H_o
C_{50} model 3 and 9	-0.438	0.6641		Does not reject H_o
%AL_{cons} model 1 and 7	-6.785	0.0000		Reject H_o
%AL_{cons} model 2 and 8	-1.382	0.1756		Does not reject H_o
%AL_{cons} model 3 and 9	-0.123	0.9025		Does not reject H_o

Figures 4.33 through 4.35 are the speech parameters of seats in model comparisons, which provided evidence of differences, by rejecting the null hypothesis of the paired *t*-test in table 4.17. In the subjective RASTI range, there are no differences in the comparison.
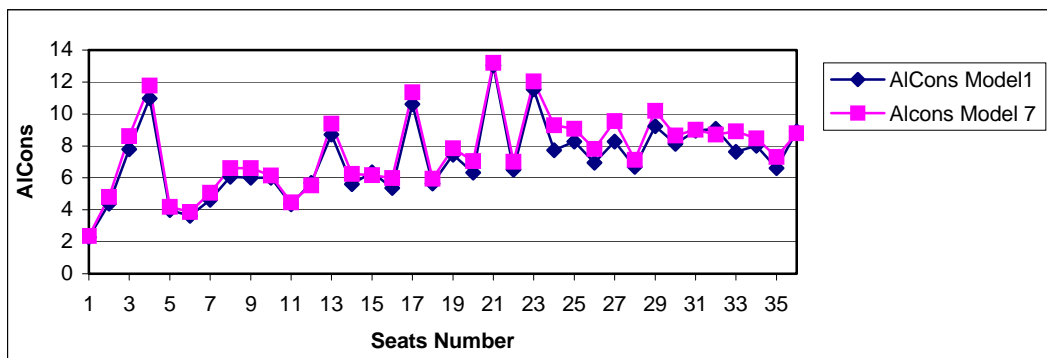
<p style="text-align:center">Figure 4.33 %AL_{cons} of model 1 and model 7 at 36 seats observed.</p>
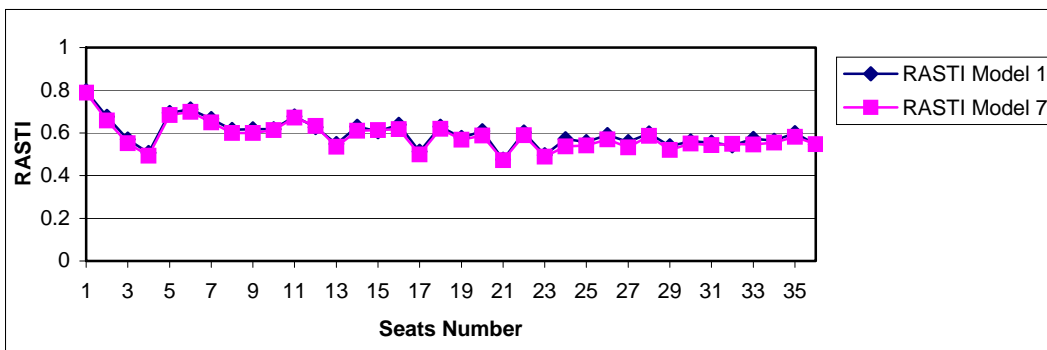
<p style="text-align:center">Figure 4.34. RASTI of model 1 and model 7 at 36 seats observed.</p>

Seat 24 and 27 in model 1 have very good intelligibility, slightly better than model 7, which is good intelligibility.
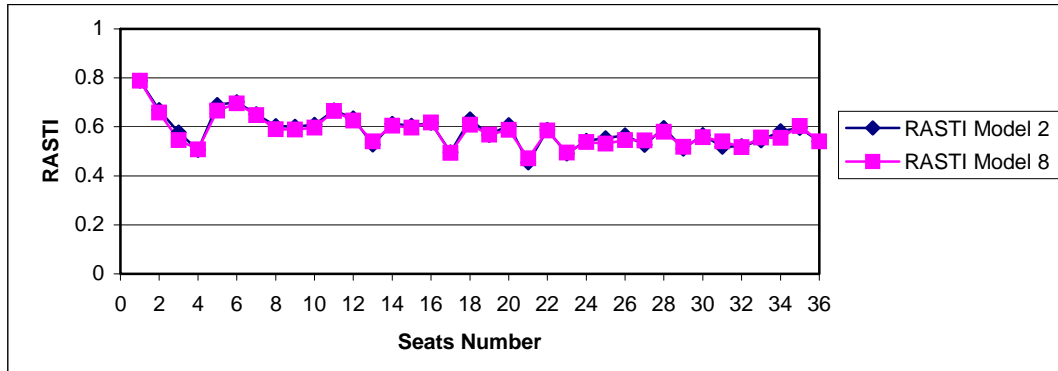
Figure 4.35. RASTI of model 2 and model 8 at 36 seats observed.
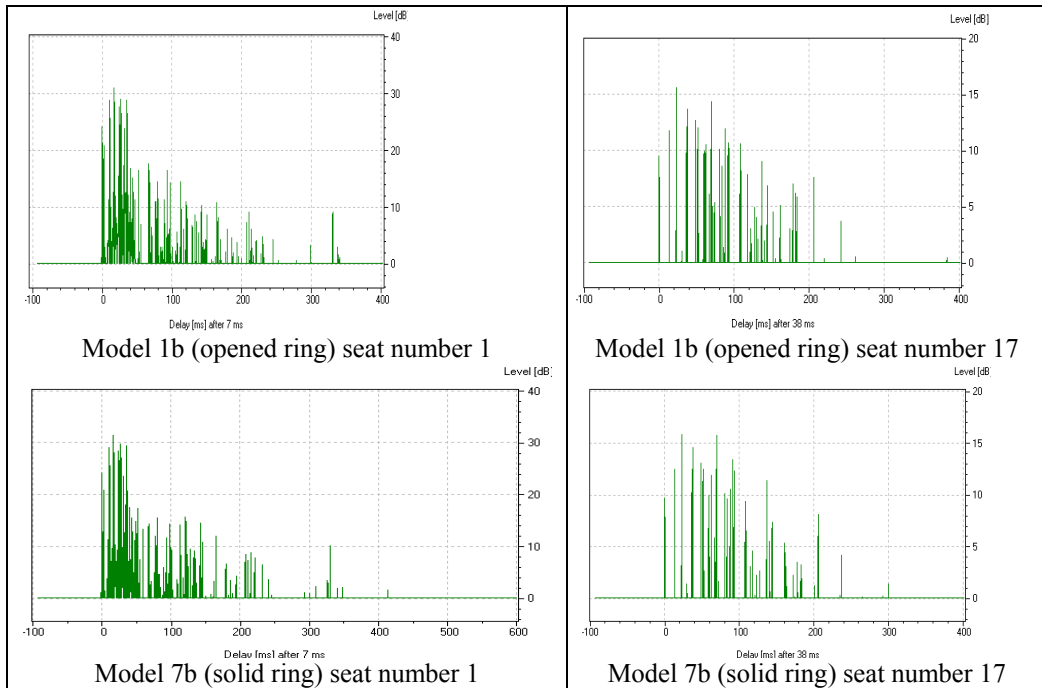
Figure 4.36. Comparison of model 1b to model 7b using energy time curves.

Figure 4.36 shows that significant differences in impulse responses do not occur in the comparison of model 1b and 7b, which are the models with the same dome ceiling configurations but with different number of planes. This comparison verified the conclusion addressed by the statistical analysis and the visualization of the speech parameters.

CHAPTER 5
ACOUSTICAL SCALE MODELING

The most significant portion of the work for this thesis involved the development of a 1:12 acoustical scale model of the mosque. An acoustical scale model is a physical model used principally for four purposes:

- To study the sound-reflection processes due to structural boundaries.

- To include diffraction, scattering, and other wave-related properties.

- To test room shapes and their geometrical acoustic properties.

- To measure room impulse responses and corresponding subjective parameters.

The following sections address the effects of this research to utilize the acoustical scale modeling methods. They first discuss the principles of acoustical scale modeling, and constructions of the model. They then discuss the source development process and measurement techniques. They finally present results and discuss their significance.

5.1 Applications of Principles in Acoustical Scale Modeling

Acoustical scale model measurements rely on the law of acoustical similarity[56] by carrying the scale factor throughout the acoustical characteristics of the model. This law should be applied in the use of the model for all four purposes mentioned above. Relationships that can be derived from the law of acoustical similarity between a full-sized room and a model include

$$\frac{\lambda_m}{\lambda_r} = \frac{l_m}{l_r} = S \,,$$

(5.1)

where in this research $S = 1:12$, and

$$\frac{c_m}{c_r} = K , \qquad (5.2)$$

$$\frac{f_m}{f_r} = \frac{K}{S} , \qquad (5.3)$$

$$\frac{t_r}{t_m} = \frac{S}{K} , \qquad (5.4)$$

and where, λ_m = wavelength in scale model λ_r = wavelength in actual room
l_m = length in scale model l_r = length in actual room
c_m = speed of sound in scale model c_r = speed of sound in actual room
f_m = frequency in scale model f_r = frequency in actual room
c_m = speed of sound in scale model c_r = speed of sound in actual room
t_m = time in scale model t_r = time in actual room

Scale factors ranging between 1:5 and 1:40 are often found in practice. A scale factor of 1:12 was chosen in this research, based on technical and practical considerations:

- A suitable size of the model for the laboratory and wood shop where the model was assembled, and a suitable size for the anechoic chamber where the acoustical measurements were taken.

- An adequate frequency range of operation related to apparatuses available in the BYU Acoustics Research Group.

The frequency range used for acoustical measurements in actual rooms is typically the 125 Hz octave band for the lower band limit and 4 kHz or 8 kHz octave band for the upper band limit. For the 1:12 scale model, the desired frequency range was then 1,2 kHz to 72 kHz or up to 120 kHz. As indicated earlier, the main focus of this research is speech intelligibility in the mosque. In general, the majority of speech energy is contained in the frequency range of approximately 250 to 4000 Hz. In the telephone industry, 300 to 3000 Hz would be the common frequency range used.[57] The strongest frequency range is

between 1800 to 2500 Hz for consonants of speech.[58] Following these trends, the scaled frequency range used in this research was then 3 to 48 kHz.

There were several important factors that needed to be considered when designing and building the experimental apparatus and doing the acoustical analysis. Many were related to the relationships in equations (5.1) through (5.4). They included

- Materials used in the scale model.

- Construction of the scale model.

- Sources and receivers.

- Measurement techniques.

- Sound field medium.

5.2   Materials Used in the Scale Model

In a 1:12 scale model, the linear dimensions of the model are reduced to one-twelfth their original size. The materials chosen to construct the model must have absorption coefficients similar to those in the full size room, but at frequencies twelve times higher. They should also have mass densities that are similar to those in the full size room, which means that the mass densities are not scaled.

Beyond geometrical considerations, choosing the absorption coefficients of materials is the most important task for evaluating the time sequence of early reflections from the room boundary surfaces at specified frequencies. It is sufficient to use backing materials in the model that are capable of minimizing the sound absorption. The boundary conditions must be scaled to match the acoustic impedances of the walls and medium where the sound propagates. This relates to the fact that absorption coefficients

may be defined in terms of specific acoustic impedances in room acoustics. The absorption coefficient is typically represented as

$$\alpha = 1 - |R|^2,\qquad(5.3)$$

where R is the pressure-amplitude reflection coefficient. If Z_s is the normal specific acoustic impedance of the boundary, the reflection coefficient for a given angle of incidence θ_i is

$$R(\theta_i) = \frac{Z_s \cos\theta_i - \rho_0 c}{Z_s \cos\theta_i + \rho_0 c},\qquad(5.4)$$

where $\rho_0 c$ is the characteristic specific acoustic impedance of the adjusted medium (in the scale model).

For high frequencies, the porosity and structural factor of a boundary material have the tendency to influence the absorption coefficient. The porosity factor σ represents the porosity of a material as the ratio of the volumes of the interior pores of a sample to the total volume.[55] Porosity factors are conditions that we can actually measure and control. Sound waves in air that enter pores will be efficiently absorbed only if the holes within the material are interconnected. If the pores are closed, as in aerated concrete, the waves cannot penetrate the material.

In some materials, the particle velocity of the air inside the material is increased by the influence of the internal structure of the material defined by a structural factor χ. The porosity factor alone is not sufficient to determine the velocity. The sound absorption for an infinitely thick boundary material composed of a rigid skeleton structure is given by the following equation for a normal–incidence wave:

$$\alpha_{(0)} = \cfrac{1}{\cfrac{1}{2} + \cfrac{1}{4} + \left(\cfrac{\sigma}{\sqrt{\chi}} + \cfrac{\sqrt{\chi}}{\sigma} \right)} \ . \qquad (5.5)$$

For studies that are most concerned with sound reflection paths inside rooms, the materials can be chosen to have small porosity factors and high densities. Such materials tend to have large reflection coefficients.

The appropriate acoustical conditions in the twelfth-scale prototype mosque were achieved by scaling the absorption characteristics of the various surfaces so that the correct reverberation time was obtained. Ideally, this would have taken into account the variation of absorption with angle of incidence and actual impedances of the surfaces. However, this degree of matching would be extremely time consuming to realize and it has been shown elsewhere that it is satisfactory to model only the absorption coefficient at random incidence.[59]

Most of the building materials used in the actual mosque were bricks and concrete. It has been reported[55] that with a structural factor $\chi = 4$, the porosity factor for bricks are values between 0.25 and 0.30, which is relatively small value in the range of 0 to 1. This means that these materials have narrow pores. Cremer stated that reflecting materials could be achieved by increasing the resistance differences of the surface by narrowing the cross-sections of the pores inside the materials. Therefore, in the study to analyze the reflections of sound in the mosque in an unoccupied condition, it may be sufficient to use materials with narrow pores. Other considerations were mostly based on practical needs in the construction process.

Medium density fiberboard (MDF),[60] a type of hardboard made from wood fibers glued under heat and pressure, was used for the main structure. Characteristics of MDF

that satisfied the scale model requirements were its density, flatness, and stiffness. Because it was made up of fine particles, it had no knots. It was easily machined without damaging the surface and could be painted to produce a smooth-quality surface with a minimal absorption coefficient for modeling plastered and painted concrete, brick and tiles. High reflective marble tiles on pillars in the actual mosque were modeled using MDF with layers of glossy varnish. Velvet was used to model the carpet surface of the prayer hall since it proved to give significant absorption inside the mosque as shown in Fig. 4.6.

5.3   Construction of the Model

Ideally, the model should be as similar as possible to the actual room, although simplifications are commonly used in scale modeling for practical reasons. This simplification is acceptable as long as the model still represents the important acoustical properties of the room. It must be carried out with an understanding of the actual building structure and acoustical analogies of the architectural concepts (functional and spatial).

Figure 5.1. The scale model in the BYU anechoic chamber.

Figure 5.1 shows the scale model, a simplification of the second floor of Darussholah mosque.

A construction guide is needed in the design simplification process. Additional details on the construction process are provided in Ref. 61. Figures 5.2 and 5.3 show the elements of the mosque, including the mihrab, that were considered most important.

Annotations:

1   Dome Structure
2   Ring Structure (Type N)
3   Elevated Ceiling/
    Octagonal structure
4   Side Roofs
5   Flat Roof 1
6   Windows
7   Flat Roof 2
8   Column 1
9   Column 2
10 Overhanging Side Wall
11 Column 3
12 Corner Walls
13 Thin velvet as carpet
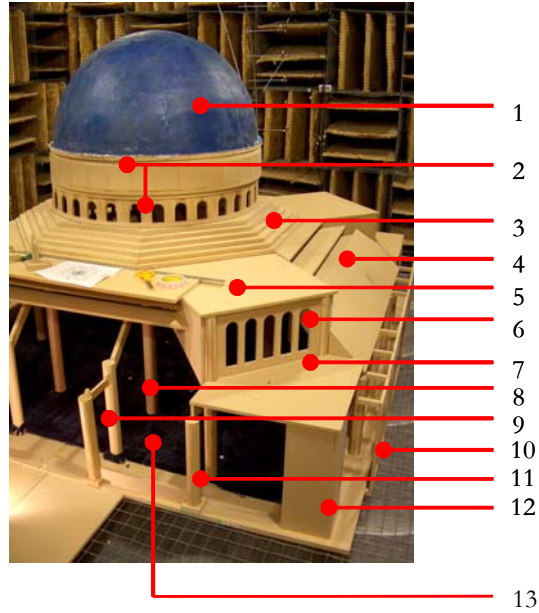
Figure 5.2. The main parts of the model.
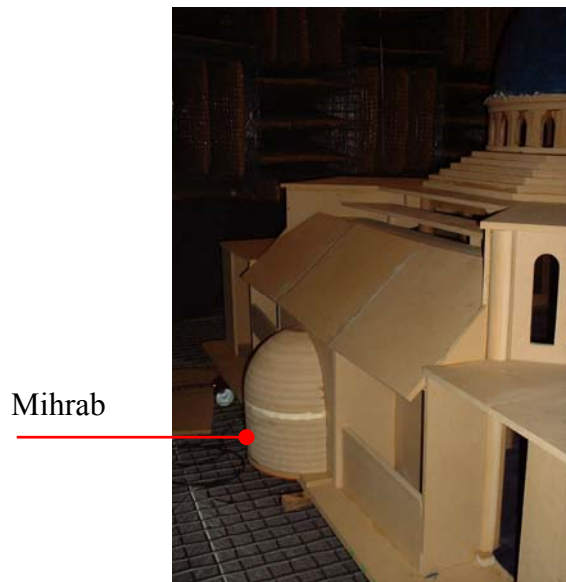
Mihrab

Figure 5.3. Mihrab from the exterior view.

The first item to be constructed were columns and beams, followed by the roof structure and the central ceiling structure (ring and dome structures). The step-by-step process of building the dome structure is shown in Fig. 5.4.
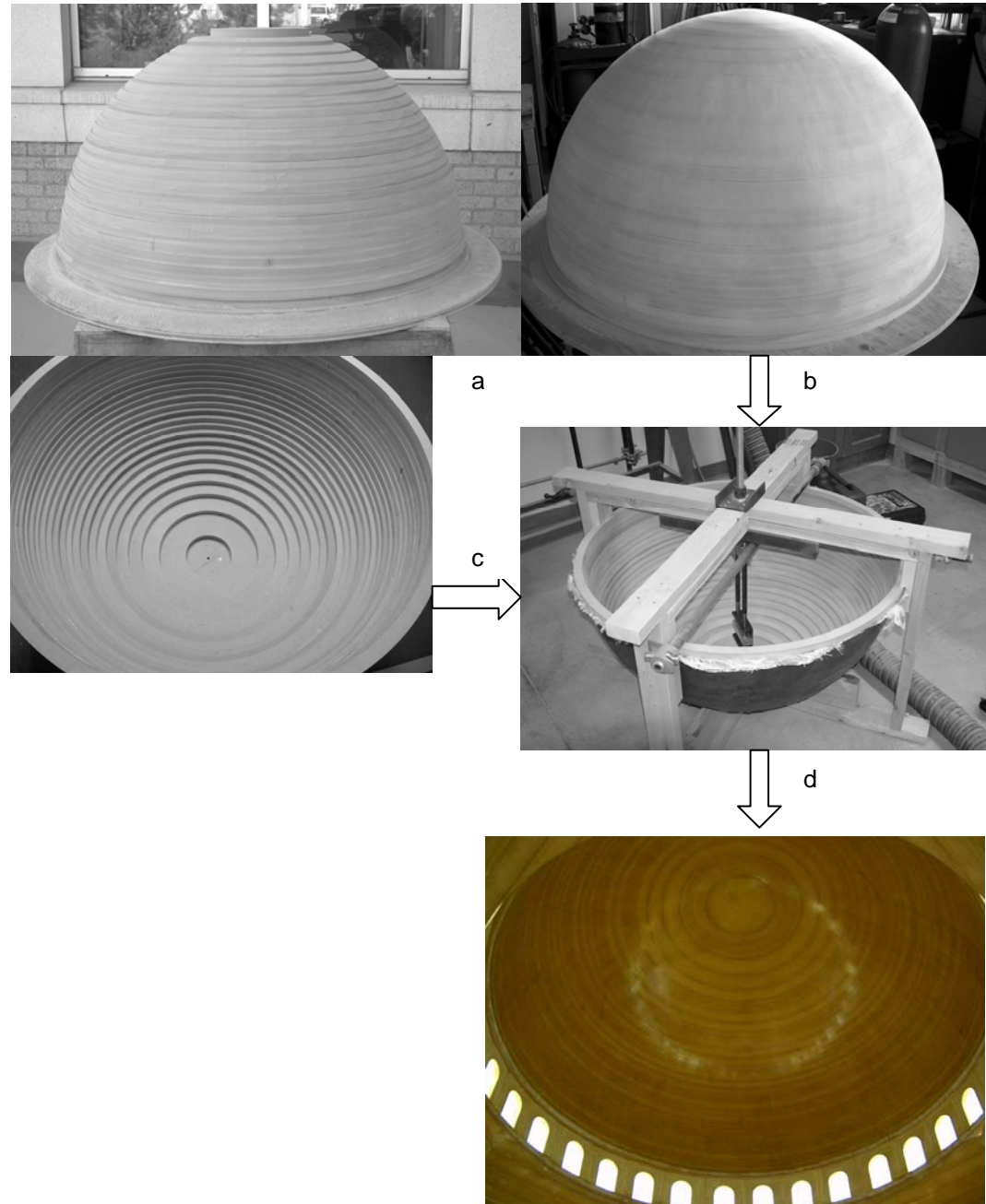
Figure 5.4. Spherical dome construction processed. (a) Rings of 1.9 cm thick MDF were glued and stacked. (b) The outer portion was sanded then covered with a layer of fiberglass for additional strength. (c) A pneumatic grinder on a jig was used to sand the inside, to create uniform-radius dome (d) The inner surface was sealed and coated with a glossy finish.

The dome was then placed on different ring structures to provide variations in the ceiling configurations (see Fig. 4.2 and Fig. 5.13). The rings were set on an octagonal base as a support structure.

Columns of three different heights were constructed of MDF as described in Ref. 75. Each of them was placed as a removable element in bases that were glued to the floor board. The process of building the mihrab (see Fig. 5.5) was essentially the same as that of the dome. Each partition and element had a certain detail size, assembling, and place that needed to be indicated. No matter how accurate the wood working was, all of these elements were still machined and fitted by hand.

After all the boundaries were set up, additional boards were placed on the floor to achieve the height level of the prayer hall and distinguish it from the circulation area (see Fig. 5.6). Finally, a thin layer velvet (less than 1 mm thick) was glued to the floor to represent carpeting that would be approximately 1.2 cm thick in the actual mosque.

Figure 5.5. Mihrab already sealed but not yet coated.

Figure 5.6. The Prayer hall and the circulation area.

5.4   Source and Receiver

An appropriate source and receiver were needed to carry out measurements in the scale model and obtain impulse responses. Sound sources are generally categorized in two types:

- Impulsive sources (e.g., a spark discharge).
- Continuous excitation sources.

This research focuses on speech intelligibility assessment for a male speaker. To carry out the assessments in the model, the scaled source must have three fundamental attributes at its upward-scaled frequencies: (1) sufficient linear acoustic output to provide good signal-to-noise ratio, (2) an adequate frequency range, and (3) the same directivity as that of a male speaker.

An omnidirectional microphone was needed to pick up the direct acoustic signal produced by the source and the reflected signals from the scale model boundaries. Small dimensions were required because of the small wavelengths associated with the scaled excitation frequencies.

5.4.1 Past Work on Speech Sources

Dunn and Farnsworth[62] conducted what was perhaps the first major study exploring the pressure field around the human head during speech. It demonstrated that the speech sound pressure has both spatial and frequency dependence. In 1977, Moreno and Pfretzschner[63] provided a new approach for studying directional properties of human speech radiation. Their research concluded that in the frequency interval studied (100-5000 kHz), variations in head shape, head dimensions, clothing, and lip movements are not major factors in controlling the directional properties of human speech radiation. Several speakers were shown to produce only slightly different radiation patterns.

Flanagan first developed a full-sized speech source by installing a transducer in the head of a full-sized mannequin.[64] Its aperture was similar to the human mouth size. Measurements of the sound field in vertical and horizontal planes around the head produced results that agreed fairly well with the pressure distributions for speech reported by Dunn and Farnsworth. Chu & Warnock reported a detailed measurement of the sound fields around human talkers in an anechoic environment.[65] The measurements also agree with other measurements made previously and provide detailed results for the same speech levels measured 1 m in front of the mouth in the 'straight head' position.

Orlowski developed an eighth-scale speech source for acoustic models using the same principles as Flanagan, but in this case the aperture was much smaller than the driving assembly.[59] A long tapered tube was mounted over the diaphragm of a selected high-frequency loudspeaker in order to avoid interference with the mouth radiation. Different shapes and sizes of tubes were investigated to provide an arrangement that suitably simulated the directional and frequency response characteristics of human speech

at the scaled frequencies. He demonstrated that it was possible to construct a model speech source by acoustically loading a suitable high frequency loudspeaker (at scaled frequencies) with an inverted conical horn. This source had directional characteristics similar to those of a human speaker and was capable of reproducing speech of a good quality.

5.4.2   Source Development Process

The limitation of finding a commercially available speaker that could operate in the test frequency range was the main concern while building the source. A KEF Hypertweeter loudspeaker was found to produce the needed acoustic output. The loudspeaker unit has a reasonably flat frequency response up to about 70 kHz so that speech frequencies from 250 Hz to 4 kHz in actual scale can be reproduced at the scaled frequencies for the 1:12 scale model.

A 1/8 inch Brüel & Kjaer precision microphone was mounted on a stand and pointed toward the speaker in the same horizontal plane. Measurements were performed in the Eyring Science Center anechoic chamber, at BYU. Details on the equipment used, the apparatus settings, the technical steps to run the measurements, and the subsequent calculations are provided in Ref 61.

Initial measurements were made on the KEF Hypertweeter (tweeter) alone in order to determine its capability. As each part of the source arrangement was added, the three fundamental attributes that a speech source must have (see page 75) were tested to produce the best design. An integrated signal source (periodic chirp) was fed into the source. The coherence was measure to assess how well the source would function in providing frequency response functioins and impulse response functions. Besides

checking the desired frequency range that it could cover, the frequency response was used to evaluate if resonances occurred in the emitted sound. To obtained an adequate signal-to-noise ratio and and flat frequency response, the source output level, microphone gain and distance between the source and receiver were carefully adjusted. Since the test signals were in the high frequency range, i.e., with very short wavelengths, scattering from electrical wiring and some surfaces inside the anechoic chamber would have produeced problematic results. In order to prevent these anomalies, SONEX [TM] foam rubber was placed around the source and the receiver for these measurements. The directivity measurements could be conducted after the coherence and frequency response measurements were determined to be adequate.

The scaled frequency-dependent directivities of the tweeter alone at the observed frequencies do not compare well to those of human speech, as given by Chu & Warnock. Results from Orlowski were adapted to this study by using an inverted conical horn made from copper sheet. The small mouth aperture of the horn had a 4-5 mm diameter to approach as close as possible the size of a human mouth in the 1:12 scale, while still producing sufficient output for suitable coherence and frequency response. Two different lengths of horns were tested: which are 10 cm and 30 cm (see Fig. 5.7).

(a)   (b)
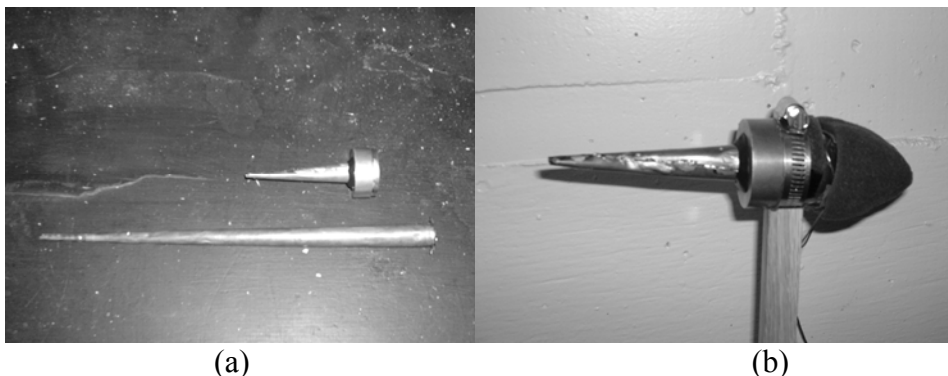
Figure 5.7. (a) Short horn and long horn, (b) The design proceeded with the short horn.

The final design used the short horn, since after testing it was shown that the long horn did not have sufficient output and did not produced sufficient coherence (see Fig. 5.8).
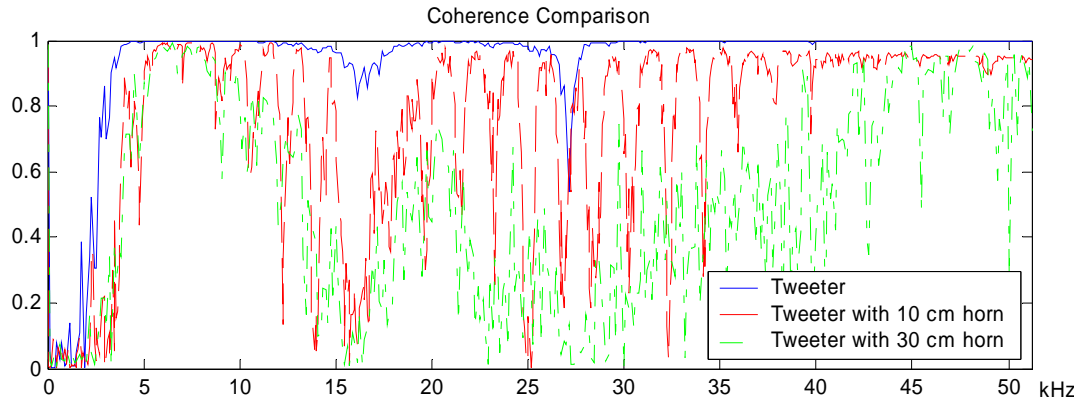
Figure 5.8. On-axis comparison of coherence from tweeter, tweeter with 10 cm horn, and tweeter with 30 cm horn.
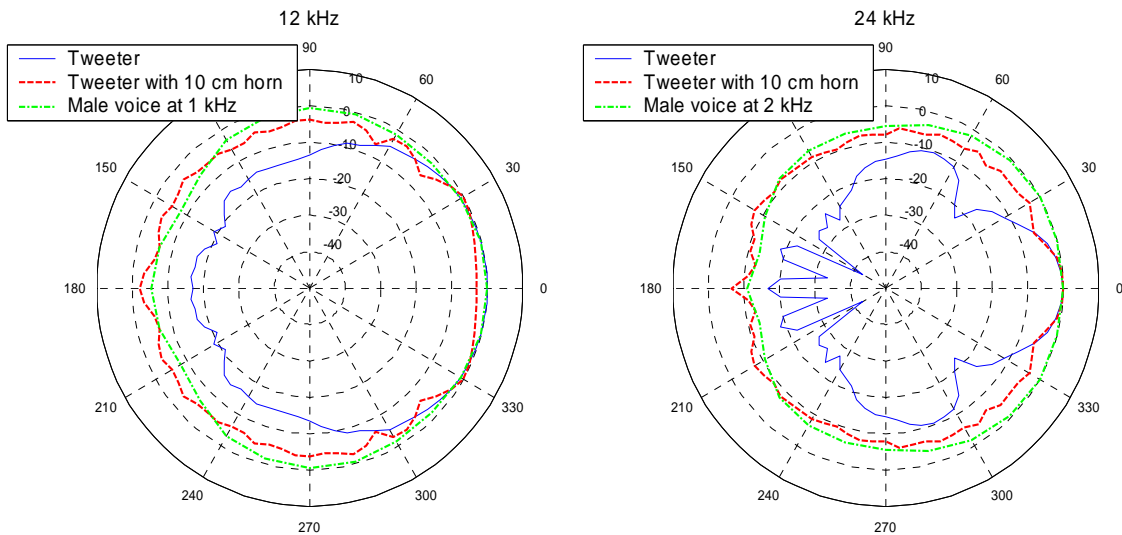
Figure 5.9. Comparison of the directivity of tweeter itself and tweeter with 10 cm horn against Chu & Warnock male speaker at 12 kHz and 24 kHz.

The short horn frequency response was shown to have resonances as evidenced by Fig. 5.8. However, as shown in Fig 5.9, the directivity is better than the tweeter alone and is similar to the directivity of a male voice. The resonances then reduced by inserting a segment of open-cell foam into the end of the horn nearest the tweeter. This needed to be a certain length (approximately 1 cm) in order to maintain sufficient output level. The

directivity of the short horn mounted on the tweeter with and without the foam was compared to check the consistency in directivity (see Fig. 5.10).
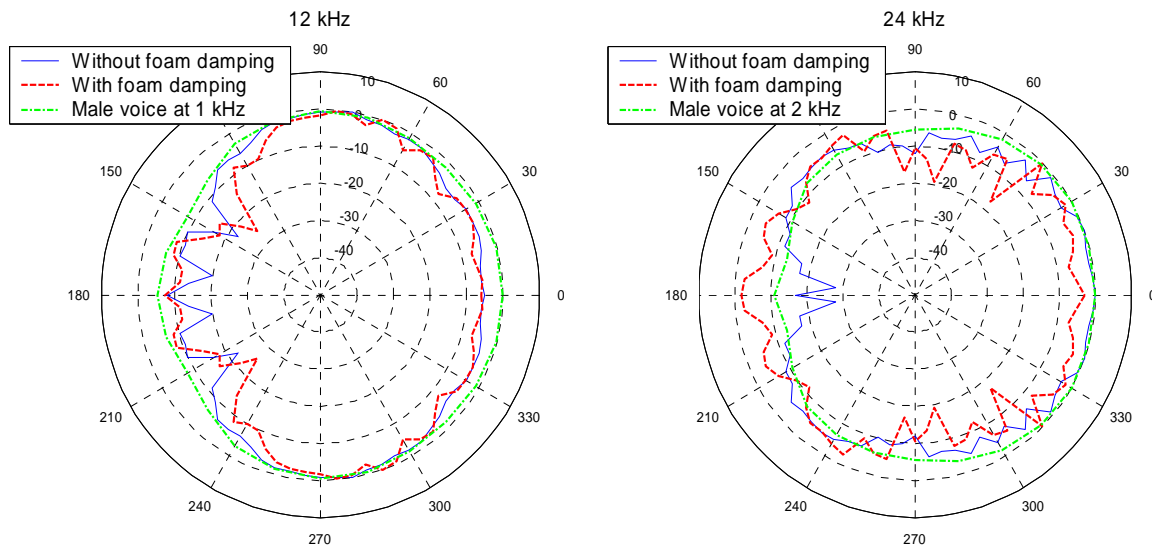
Figure 5.10. Comparison of the directivity of the tweeter with and without inserted foam damping inside the 10 cm horn at 12 kHz and 24 kHz.

An ideal speech source would actually come out from a human mouth. In order to fit that idealized condition, a 1:12 scale mannequin with an open mouth was mounted at end of the horn with the small aperture. The mannequin was modeled from a real human head with an upper part of a human torso (Fig. 5.11), adapted from other research.
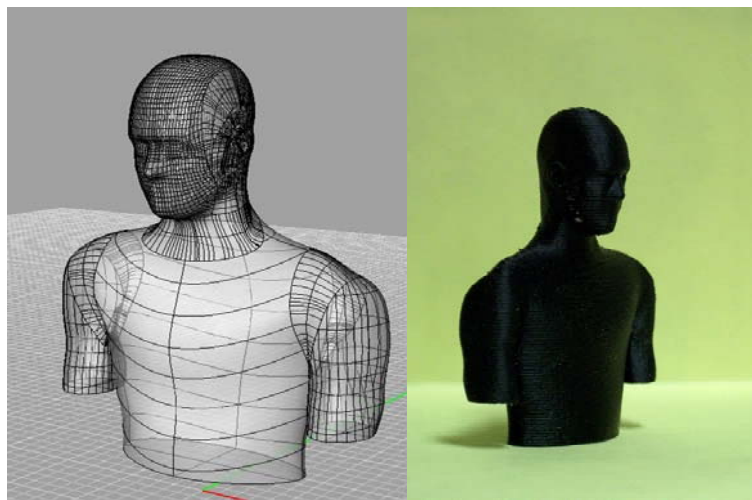
Figure 5.11. Scale model mannequin made with Fused Deposition Modeling (FDM), process of depositing polymer in layers.

It was also used to model a gathering of worshipper in one of the scale model settings. Finally, the directivity of this last configuration was checked (Fig. 5.12) and it was used as the final design.
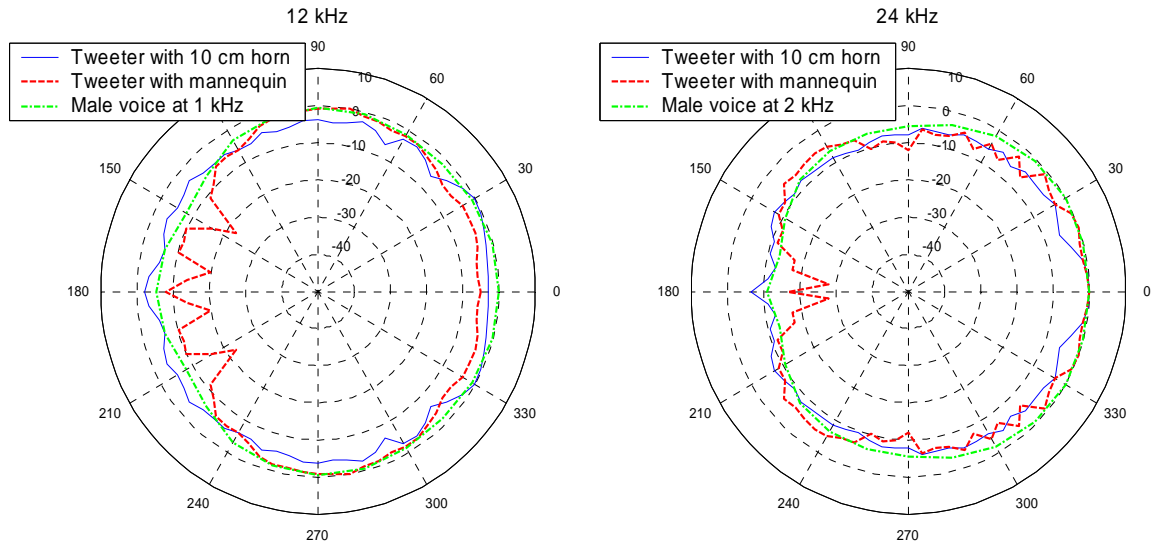
Figure 5.12. Directivity of the short horn with mannequin.

5.4.3 Analysis and Discussion of the Source Development

Generalized from the tweeter coherence plot (see Fig. 5.8), measurements in the 1:12 scale model were limited in frequency from 2.1 kHz to 76.8 kHz, which approximately fulfil an adequate frequency range for actual scale (250 to 4000 Hz). However, it is also shown that at frequencies around 3 to 3.5 kHz the coherence was poor due to uncorrelated noise in the measurement or possibly due to non-linearity in the transducer. Adjusting the signal output level through amplifying and adjusting the distance between source and receiver did improve the coherence and directivity consistency.

This thesis only provided directivity plots for measurements at 12 and 24 kHz, corresponding to 1000 and 2000 Hz in the full size room under the assumption that these

would be the main frequencies of interest in the observation because the intelligibility of male speech at a raised level would be controlled to a large extent by these octave bands. Directivity in the 12 kHz range fit best with the directivity in the Chu and Warnock report, especially the general pattern from -90° to 90°, passing through 0°. For a measurement at 24 kHz, details on the side angles seemed to be better having the source without the mannequin, although from -30° to 30° passing through 0° the directivity was closer. This effect would be more important since in the scale model measurement sound emitted from the front part of the source would be the priority.

5.5   Measurement Techniques

Measurement in the scale model in order to get the acoustical parameters is principally the same as measurement in an actual room. The difference is in the apparatuses and settings due to the scale factor.

5.5.1   Detail of Elements of Measurement Configurations

The scale model configurations were based on model 1, 2 and 3 of the computer modeling (Table 4.1). Using these models, the observation was classified further into sets of measurement due also to variations in the receiver's position horizontally (seat number) and vertically (standing or seating position) and also the source orientation [preaching or praying (Table 5.1)]. The receiver positions are the same with the positions in the computer models (see Fig. 4.4) but with a total of 20 positions instead of 36 in the same numbering sequence. See Figs 5.13 and 5.14 for details on the set up configurations.

Table 5.1. Details of measurement settings.

Setting	Receiver's position	Model	Source Orientation	Number of Seats
1c	Standing	3	Preaching	20 positions
1d	Seating			(1-4, 9-12,17-20, 25-28, 33-36)
2c	Standing	3	Praying	20 positions
2d	Seating	3		(1-4, 9-12,17-20, 25-28, 33-36)
3c	Hanging down from the ceiling, standing height	3	Praying	6 positions (1, 4, 17, 20, 33, 36)
4c	Hanging down from the ceiling, standing height	3	Preaching	6 positions (1, 4, 17, 20, 33, 36)
5d	Seating with scaled people	3	Preaching	6 positions (9, 11, 17, 19, 25, 27)
6c	Standing	1	Praying	20 positions
6d	Seating	1	Praying	(1-4, 9-12,17-20, 25-28, 33-36)
7c	Standing	2	Praying	20 positions
7d	Seating			(1-4, 9-12,17-20, 25-28, 33-36)
8c	Standing	2	Preaching	6 positions
8d	Seating	no carpet		(1, 4, 17, 20, 33, 36)
9c	Standing	2	Praying	6 positions
9d	Seating	no carpet	Praying	(1, 4, 17, 20, 33, 36)

Model 3 (Used for setting 1 through 5)

Model 1 (Used for setting 6)
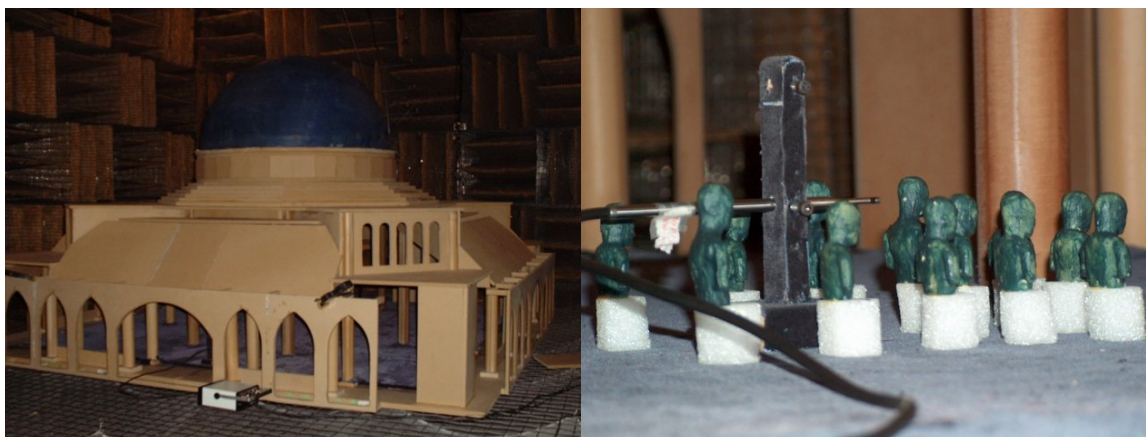
Model 2 (Used for setting 7 through 9)

Miniature people seating surrounding the microphone, used for setting 5

Figure 5.13. Settings and measurements configurations.
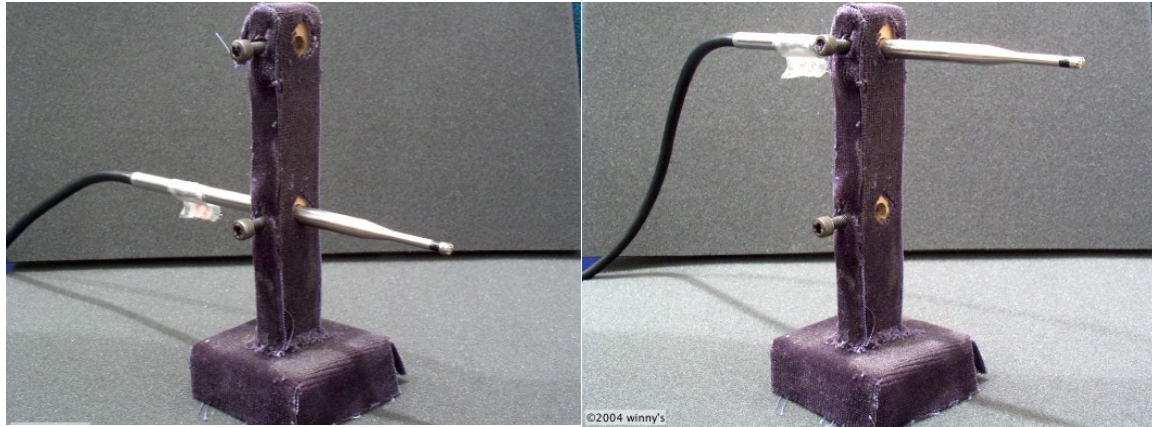
Receiver in a seatng position height (Used for setting 1, 2, and 5 through 9)

Receiver in a standing position height (Used for setting 1, 2, 6 through 9)
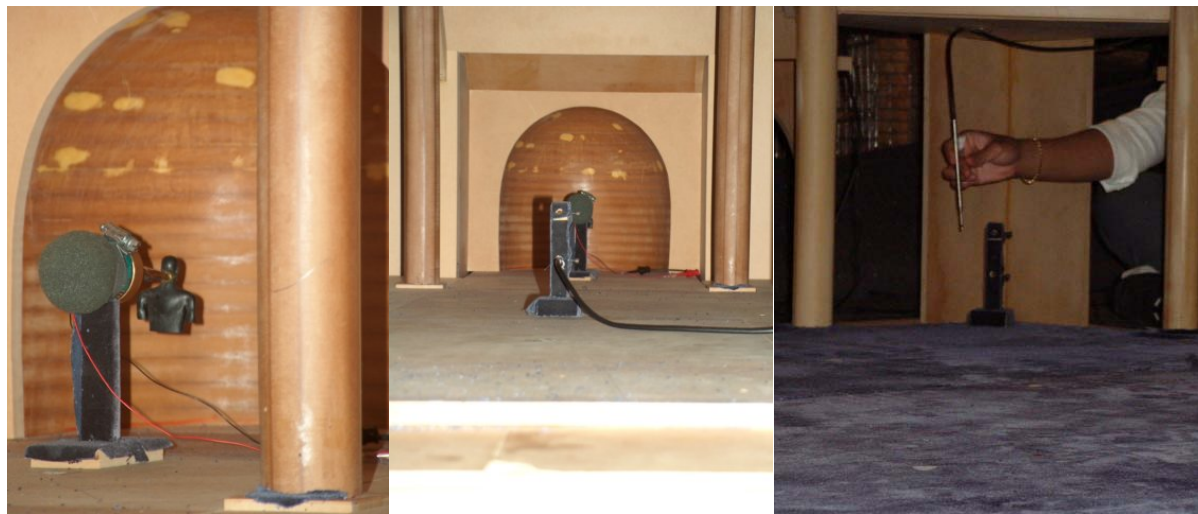
Praying, source facing mihrab. For preaching the source facing receiver, turned about 180°

Receiver hanged (Used for setting 3 and 4)

Figure 5.14. Settings and measurements configurations of the source and receiver.

5.5.2 Generalizing the Impulse Response

There are several techniques used to derive the speech intelligibility parameters from the scale model measurements. Impulse responses as the preliminary output of a system are used widely in most architectural acoustics studies. The response to the source at the various receiver measurement points is captured by a 1/8" microphone (B&K 4138) with a corresponding preamplifier (Larson Davis 910B) and connected through a microphone power supply (Larson Davis 2200C). These devices are in turn connected to

a DATA Physics DP620 Analyzer. Since it was measured in a 1:12 scale model, the impulse response needed to be scaled to the actual frequency range before further calculation could be done. The scaling was done in the time domain. From the comparison on the time length it is shown that the impulse response in the actual size (Fig. 5.16) is twelve times longer (1.2 seconds) than the impulse response from the measurement (0.1 seconds), both with the same magnitude.
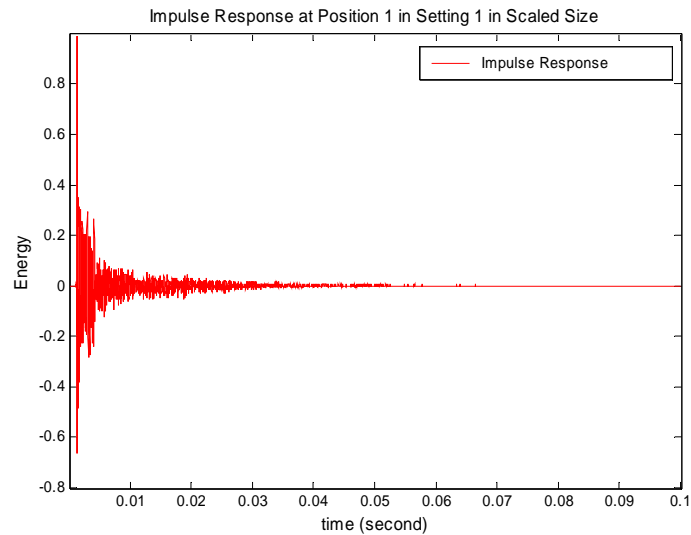
Figure 5.15. Impulse responses of position 1 from the measurements (h(t)).
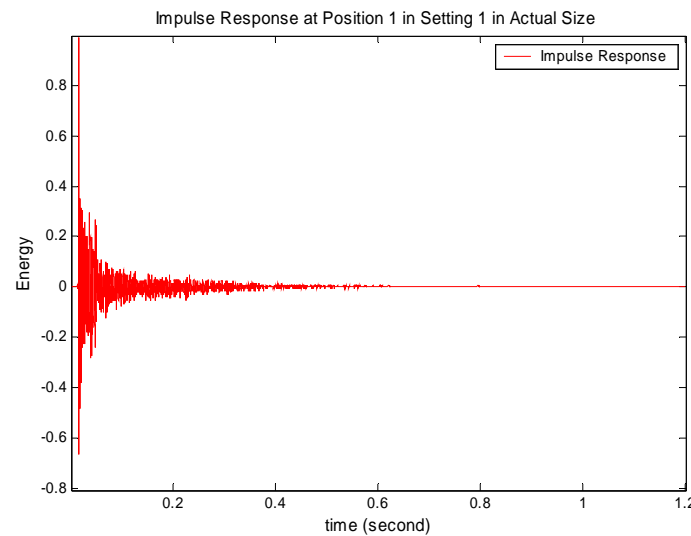
Figure 5.16. Impulse responses of position 1 in the actual size (h_1(t))

Acoustical parameters are determined in octave bands. Octave band filtering of $h_1(t)$ was therefore the next digital process. Based on the main frequency bands of interest for speech intelligibility evaluation in the model and limitations on the source frequency range output, the speech parameter calculations were done for the octave bands in Table 5.2 below.

Table 5.2. Octave bands measured and used in the filtered impulse responses.

Centre frequency of octave bands in scaled model (Hz)	Centre frequency of corresponding octave bands in the actual room (Hz)
3000	250
6000	500
12000	1000
24000	2000
48000	4000

Correcting the impulse response due to the freqeuncy-dependant air absorption effects was the last correction before the acoustical parameters were generated. This will be discussed further in the following subsection.

5.5.3   Air Absorption in the Scale Model

Absorption of sound in air is related to the properties of the medium of the sound field. As the frequencies increase, the air in the scale room becomes more absorbent than the corresponding air in the full size room, due to two-mechanisms of sound absorption. This include classical absorption and molecular absorption. Classical absorption is a mechanism of sound energy dissipation in air by viscous losses due to friction between air molecules, which results in heat generation. The classical absorption coefficient is therefore the sum of the shear viscosity and thermal conductivity absorption coefficient and depends upon the frequency of sound propagating in the air:

$$\alpha_C = \frac{\omega^2}{2\rho_o c^3}\left[\frac{4}{3}\eta + \eta_B + \frac{(\gamma-1)k}{C_p}\right] \sim f^2 \quad , \qquad (5.5)$$

where,

α_c = classical absorption coefficient
η = the shear viscosity coefficient
η_B = the bulk shear viscosity coefficient
γ = adiabatic constant
k = the thermal conductivity
C_p = coefficient for the specific heat capacity at constant pressure

The classical absorption coefficient for air is given in tables as α_c= 1.61 x $10^{-10} f^2$ dB/m.

Molecular absorption deals with molecular thermal relaxation in gases composed of polyatomic molecules. For sound propagation, the most important polyatomic gas is air. It consists of oxygen and nitrogen, with traces of other gases, including water vapor and carbon dioxide. The process involves a relaxation process where the sound is absorbed in the air molecules and causes the molecules to vibrate and rotate, then reradiate the sound at a later instant. This conversion of vibrational energy in the oxygen molecule into translation energy is catalysed by the presence of water vapour molecules.

For molecular absorption, the actual relationship between molecular absorption (m_m) and frequency is given by[66]

$$m_m = \frac{1.25\times10^{-5}\times f_{max}}{1+\left[\dfrac{f_{max}}{f}\right]^2}, \qquad (5.6)$$

where f_{max} is the "Napier" frequency, the frequency of maximum absorption per wavelength which the existing humidity produces. The Napier frequency in oxygen and in air is shifted to higher values by water vapor. Several researchers have proposed the relation between the Napier frequency and humidity (h).

Monk[67]
$$: f_{max} = 175\,h + 6140\,h\left[\frac{1.12 + h}{10.4 + h}\right] \qquad (5.7)$$

Other researchers [68]

Knudsen & Obert $: f_{max} = 4.96 \times 10^2 h + 6.05 \times 10^3 h^2 \qquad (5.8)$

Clark & Henderson $: f_{max} = 40 + 1.95 \times 10^3 h + 1.32 \times 10^4 h^2 \qquad (5.9)$

Harlow & Kitching $: f_{max} = 3 + 1.66 \times 10^3 h + 1.45 \times 10^4 h^2 \qquad (5.10)$

As sound travels through the air, the intensity is attenuated exponentially at a rate determined by $m = 2\alpha$ in the equation

$$I = I_o e^{-mx} \qquad (5.11)$$

This variable m is different than m_m in Eq (5.6) in that it includes both molecular and classical absorptions. Sabine's reverberation time introduced the air absorption variable m (see section 4.4). However, it is only acceptable for the frequency range up to 10 kHz. From the discussion above, it is obvious that air absorption is sensitive to temperature, air composition, particularly water vapour concentration, and frequency. The correction factor of an appropriate air attenuation applied in the model follow the relationship

$$\frac{I = I_o e^{-mx}}{I_c = I_o e^{-m_c x}} = \frac{I}{I_c} = \frac{e^{-mx}}{e^{-m_c x}} = e^{(m_c - m)x} \Rightarrow I_c = \frac{I}{e^{(m_c - m)x}} \Rightarrow \ln\left(\frac{I}{I_c}\right) = (m_c - m)x, \quad (5.12)$$

Where I = Intensity in the scale model measurement
I_c = Intensity corrected
$m = 2\alpha$ = air attenuation in the scale model measurement
$m_c = 2\alpha_{corrected}$ = air attenuation corrected
x = distance of source to receiver

Equation 5.12 would be acceptable if the air absorption in the actual size room is known and both source intensities are defined. Boone & Eggen[69] proposed a method to deal with the correction for the difference between air absorption in the scale model and air

absorption in the full-sized room. A reference condition on temperature, air pressure, and relative humidity needs to be assumed to define the air absorption coefficient ($a = 8.69 \times \alpha$) of reference called $a_{ref}(f)$. It is the frequency-dependent air absorption in dB/m under the reference conditions defined. Based on the law of similarity in scale models, the reference absorption in the model ideally should be:

$$a_{ref,mod}(12f) = 12\, a_{ref}(f),\qquad (5.13)$$

In reality another condition, $a_{meas,mod}(12f)$, would be found. Therefore

$$b_n = a_{meas,mod}(12f_n)\cdot c_{meas} - 12\, a_{ref}(f_n)\cdot c_{ref}, \qquad (5.14)$$

and

$$m_n(t) = 10^{b_n t/20}, \qquad (5.15)$$

where $m_n(t)$ is the time-dependent amplification factor to correct the impulse response for the absorption discrepancy. The variable t is defined by the distance between source and receiver divided by the speed of sound under reference conditions, since the speed of sound, c_{ref} (m/s) is a variable built into b_n. The air absorption has been empirically quantified and codified for calculation in the international standard ISO 9613-1:1996 and ANSI Standard S1-26:199. The calculation given here was based on the ISO standard: [70]

$$a = 8.686 \times f^2 \left[\begin{array}{l} 18.4 \times 10^{-12} \left(\dfrac{p_s}{p_{s,r}} \right)^{-1} \left(\dfrac{T}{T_{20}} \right)^{-\frac{1}{2}} \\[2em] + \left(\dfrac{T}{T_{20}} \right)^{-\frac{5}{2}} \left(0.1068 \dfrac{e^{(-3352/T)}}{\left(f_{rN} + f^2 \right)/ f_{rN}} + 0.01275 \dfrac{e^{(-2239.1/T)}}{\left(f_{rO} + f^2 \right)/ f_{rO}} \right) \end{array} \right] \qquad (5.16)$$

Where f = center-frequency of the octave band of interest
f_{rN} = relaxation frequency of Nitrogen
f_{rO} = relaxation frequency of Oxygen
p_s = static pressure
$p_{s,r}$ =101325 Pa, the reference static pressure
$T = T_0 + t$, the thermodynamic temperature in K
T_0 = 273.15 K (0 ^{o}C)
T_{20} = 293.15 K (20 ^{o}C)

The air absorption defined in Eq. (5.16) consists of the classical absorption and the molecular absorption. The first term inside the bracket is the classical absorption. The remainder of the terms quantify the molecular absorption. The relaxation frequency for nitrogen and oxygen is given by these following equations:

$$f_{rN} = \frac{p_s}{p_{s,r}}\left(\frac{T}{T_{20}}\right)^{-\frac{1}{2}}\left[9 + 28\times 10^3\, h\exp\left(-4.170\left(\left(\frac{T}{T_{20}}\right)^{-\frac{1}{3}} - 1\right)\right)\right],$$ (5.17)

and

$$f_{rO} = \frac{p_s}{p_{s,r}}\left[24 + 4.04\times 10^6\, h\left(\frac{0.2 + 10^3 h}{3.91 + 10^3 h}\right)\right]$$ (5.18)

The mole fraction of water vapour in air h is defined by the relative humidity H (%) as follows:

$$h = \frac{H}{100}\frac{p_{sv}(t)}{p_s},$$ (5.19)

$$p_{sv}(t) = p_{s,r}10^C,$$ (5.20)

and

$$C = 4.6151 - 6.8346\left(\frac{T_0 + 0.01}{T}\right)^{1.261},$$ (5.21)

where $p_{sv}(t)$ is the saturation water vapour pressure in Pa.

Air absorption compensation on the measured data was done in MATLAB® [Appendix A]. For the auralization used, the octave band impulse responses were then added together to get the whole compensated impulse response.

5.6   Observation of Different Ceiling Structures (Dome and Ring Structures)

Speech parameters were calculated with MATLAB® code from the impulse responses at certain positions and with different measurement settings (see Table 5.1). Visual inspection of the parameter mappings and statistical analysis using data from

certain positions were used in order to accommodate further discussion of the effects of variations in the settings. The parameter mappings themselves were created using AutoDesk Land Desktop software, from 20 measurement positions.

Results from setting numbers 2, 6 and 7 were used to evaluate models 1, 2, and 3 that have variations in the ceiling structure. All three settings were measured with the source orientated toward the mihrab, which represented the praying mode.
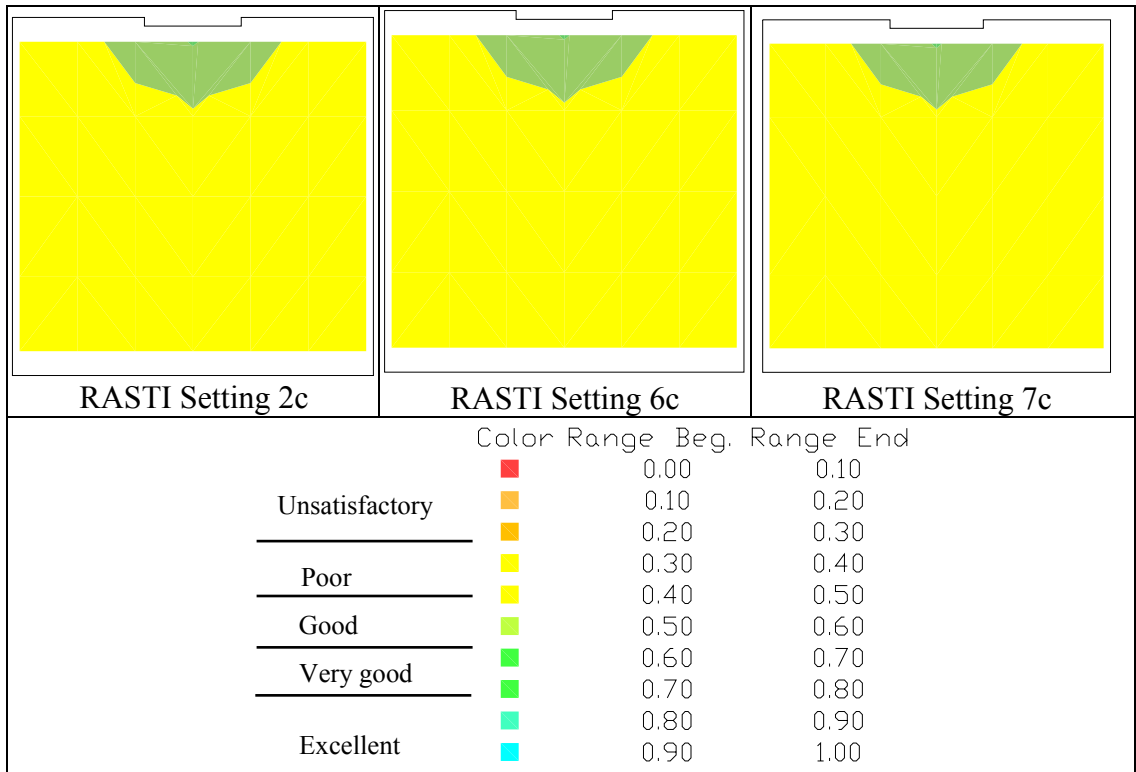
Figure 5.17. RASTI mapping of settings 2c, 6c, and 7c.

RASTI mappings (see Fig. 5.17) show that there are no significant differences in the distribution of values, where all receiver positions fall in the subjective range of good speech intelligibility, except seat number 1, which has very good intelligibility. Good intelligibility is sometimes defined as $C_{50} \geq 0dB$, which includes all area shaded green and blue (see Fig. 5.18).

| | C$_{50}$ Setting 2c | C$_{50}$ Setting 6c | C$_{50}$ Setting 7c |

Good intelligibility of speech
C$_{50}$ ≥ 0 dB

Color Range	Beg.	Range End
	−6.00	−5.00
	−5.00	−4.00
	−4.00	−3.00
	−3.00	−2.00
	−2.00	−1.00
	−1.00	0.00
	0.00	1.00
	1.00	2.00
	2.00	3.00
	3.00	4.00
	4.00	5.00
	5.00	6.00

%AL$_{cons}$ Setting 2c   %AL$_{cons}$ Setting 6c   %AL$_{cons}$ Setting 7c

%AL$_{cons}$ ≤ 3%   ideal intelligibility

%AL$_{cons}$ = 3%-8%   very good intelligibility

%AL$_{cons}$ = 8%-11%   good intelligibility

%AL$_{cons}$ >11%   poor intelligibility

%AL$_{cons}$ >20%   Worthless intelligibility

Color Range	Beg.	Range End
	0.00	2.00
	2.00	5.00
	5.00	8.00
	8.00	10.00
	10.00	13.00
	13.00	16.00
	16.00	18.00
	18.00	21.00
	21.00	24.00
	24.00	26.00
	26.00	29.00
	29.00	32.00

Figure 5.18. C$_{50}$ and % AL$_{cons}$ mappings of settings 2c, 6c and 7c.

Setting 6c and 7c have similar C_{50} distributions that differ from setting 2c. They also have a wider area of poor intelligibility toward the back of the prayer hall. Among the three settings, setting 2c is shown to have the widest area for very good and good intelligibility.

In the statistical analysis with the ANOVA test (Table 5.3), all parameters failed to reject the null hypothesis. There were accordingly no statistically significant differences in the models.

Table 5.3. ANOVA test on RASTI, C_{50}, %AL$_{cons}$ for setting 2c (Model 3), setting 6c (Model 1) and setting 7c (Model 2).

Test	*F*-statistic	*p*-observed	*F*-critical	Conclusion
ANOVA RASTI	1.7845	0.1771	3.1588	Does not rejectH_o
ANOVA C_{50}	0.2293	0.7959	$\alpha = 0.05$	Does not rejectH_o
ANOVA %AL$_{cons}$	0.176	0.839	$df_1 = 2$, $df_2 = 57$	Does not rejectH_o

Table 5.4. Result of the listening test from 12 listeners comparing settings 2c, 6c and 7c.

Comparison	Receiver position	Differences (%)	Preferred Condition (%)	
Setting 2c,6c &7c	1	100	6c ~50 %	7c ~ 50 %
Setting 2c,6c &7c	17	83	6c ~ 50 %	7c ~ 40%

Differences in the dome structure did not create different results in the RASTI distribution. RASTI values were based on reverberation times in the 500Hz and 2000Hz octave bands. The reverberation times at the receiver positions for the three different dome structures must therefore have been similar. Although they were calculated using reverse Schroeder integration, the reverberation time inside an enclosure is determined by the absorption from boundaries and the samples being compared were measured in the same rectangular room but with different dome ceilings. Therefore, it can be further assumed that the dome ceiling absorption was not significant to the total absorption in the mosque, due to its size and proportion relative to the much larger rectangular room.

All listeners in an auralization listening test judged that the male voice received at receiver position 1 and 17 sounded different in those three different dome structure

settings, but most of them could not tell the difference between settings 6c and 7c. Based on this result, dome models 1 and 2 used in settings 6 and 7 did not yield significant perceptual differences in the speech parameters. These dome structures basically had the same height, but one had a massive ring structure and the other had windows, meaning different ring structures did not appreciably influence the speech parameters.

The echograms of these settings shown in Fig. 5.19 may be compared to verify these results.
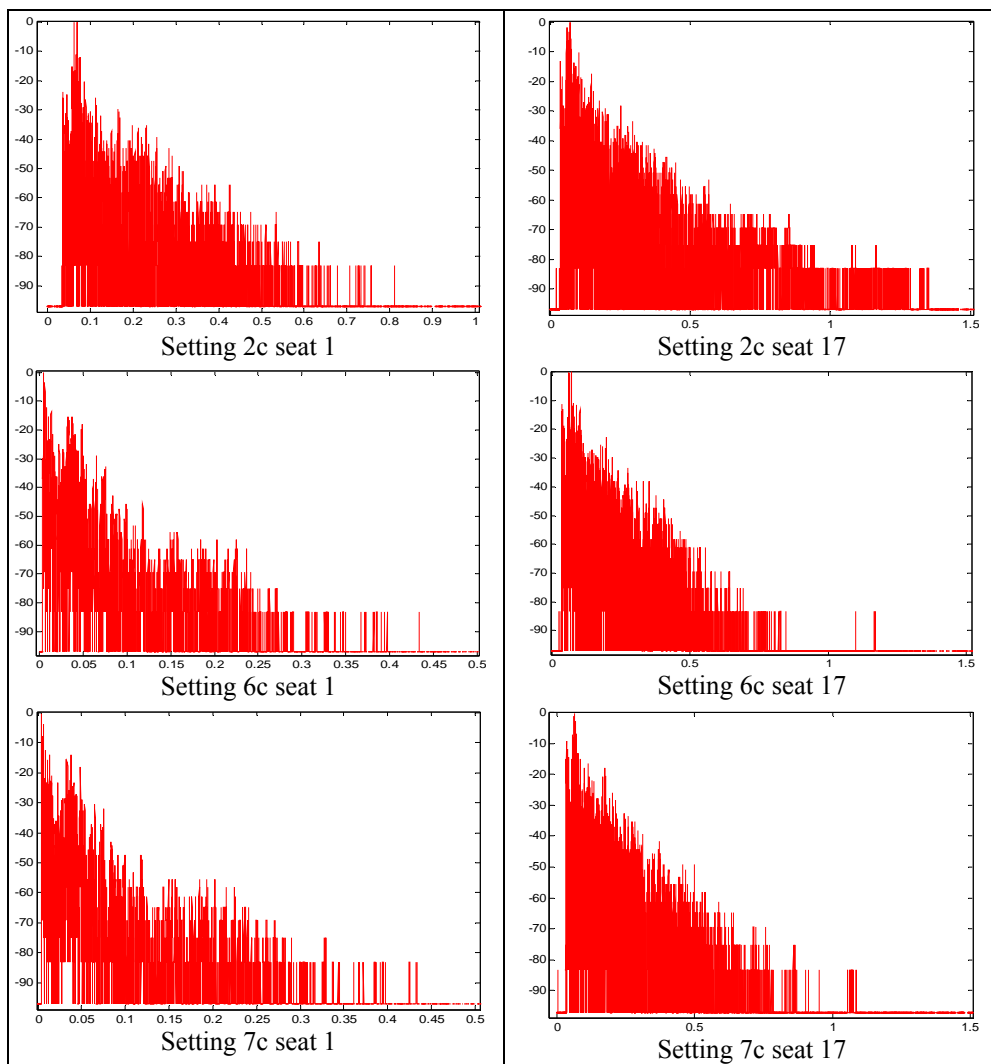
Figure 5.19. The energy time curves comparison of settings 2c, 6c, and 7c of positions 1 and 17.

www.manaraa.com

Setting 2c is shown to have the longest decay time, both in the echograms at positions 1 and 17. It also has the most significant differences in early arrivals of sound energy, particularly at seat 1. These conditions are related with the reflection done by the ring configuration since now the sounds have a longer propagation time before they reached the receiver. In general, there are significant differences in the echograms but these differences are not always shown in the speech parameters values.

5.7   Observation of Different Source Orientations

The source orientations represent the praying and preaching modes as they did in the computer models. Settings 1c and 2c have the same detail configurations. Settings 8c and 9c have the same detail configurations as setting 7c, but these settings are without carpeting. Only the C_{50} in the comparison of setting 1c to setting 2c provided evidence of statistical differences (Table 5.5). In the comparison of setting 8c to setting 9c, there are strong evidences that the source orientation created different results in the speech parameters.

Table 5.5. Paired *t*-test for settings 1c to 2c and settings 8c to 9c.

Parameter	*t*-statistic	*p*-observed	*t*-critical	Conclusion
Settings 1c-2c				
RASTI	0.605	0.5524	2.086	Does not reject H_0
C_{50}	4.876	0.0001	$df = 19$	Reject H_0
%AL_{cons}	-1.286	0.2140	$\alpha = 0.05$	Does not reject H_0
Settings 8c-9c				
RASTI	2.95	0.0319	2.447	Reject H_0
C_{50}	3.498	0.0024	$df = 5$	Reject H_0
%AL_{cons}	-3.670	0.0016	$\alpha = 0.05$	Reject H_0

There are no differences in the RASTI mappings (Fig 5.20). Some similarities are apparent for the %AL_{cons} mappings. Setting 1c appears to have a better clarity throughout the prayer hall, particularly for the area underneath the domed ceiling. This setting is for the preaching mode, that is, with the source facing the prayer hall.

| RASTI Setting 1c | C₅₀ Setting 1c | %AL_cons Setting 1c |
| RASTI Setting 2c | C₅₀ Setting 2c | %AL_cons Setting 2c |

| | 6.00 | 7.00 |
| | 7.00 | 8.00 |
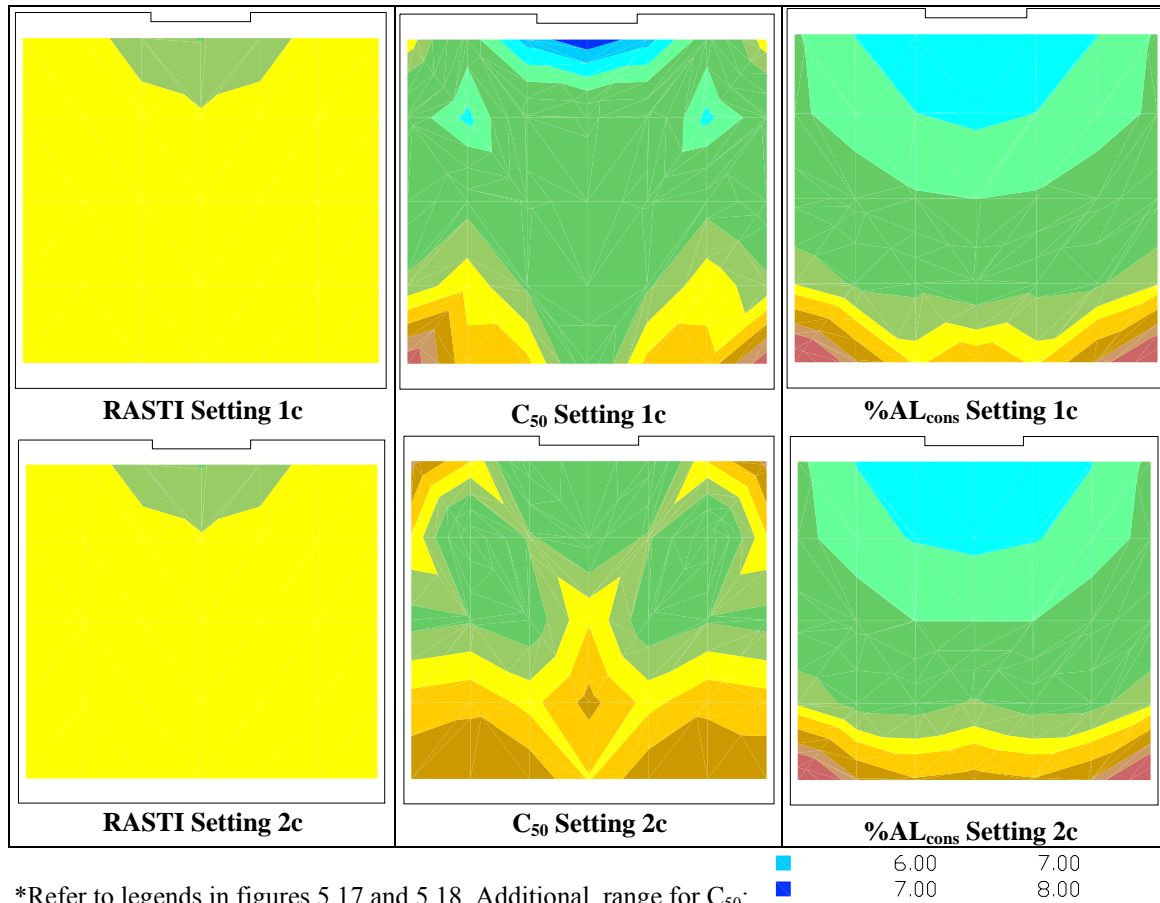
*Refer to legends in figures 5.17 and 5.18. Additional range for C_{50}:

Figure 5.20. Mapping of parameters of settings 1c and 2c.

The mapping of C_{50} shows significantly different patterns and these differences were verified by the *t*-test. A C_{50} parameter for good intelligibility would have values $\geq$ 0dB, which means the early energy, has to be larger than the late energy. Clearly, having the source facing the audience will then yield a higher C_{50} value, since the early energy consists of stronger direct energy. The listener test results using 12 listeners verified this assumption, given by the data that 100% of the listeners assumed setting number 1 is better for receiver position 1 (Table 5.6).

Table 5.6 Result on the listening test from 12 listeners comparing setting 1c and 2c

Comparison	Receiver position	Differences (%)	Preferred Condition (%)	
Setting 1c-2c	1	100	1c ~100 %	2c ~ 0 %
Setting 1c-2c	17	100	1c~ 50 %	2c ~ 50%

For receiver position number 17, underneath the dome, both settings were judged equally good since here the echo created by the dome ceiling was recognized and some people tended to like more reverberant rooms. On the other hand, some people prefer more dead rooms for better speech intelligibility.

With regard to the comparison between setting 8 and setting 9, all *t-statistic* and *p-*observed values reject the null hypothesis, which means in the measurements without carpeting, the source orientation did create different results. However, this assumption could only be implemented on 6 receiver positions observed.
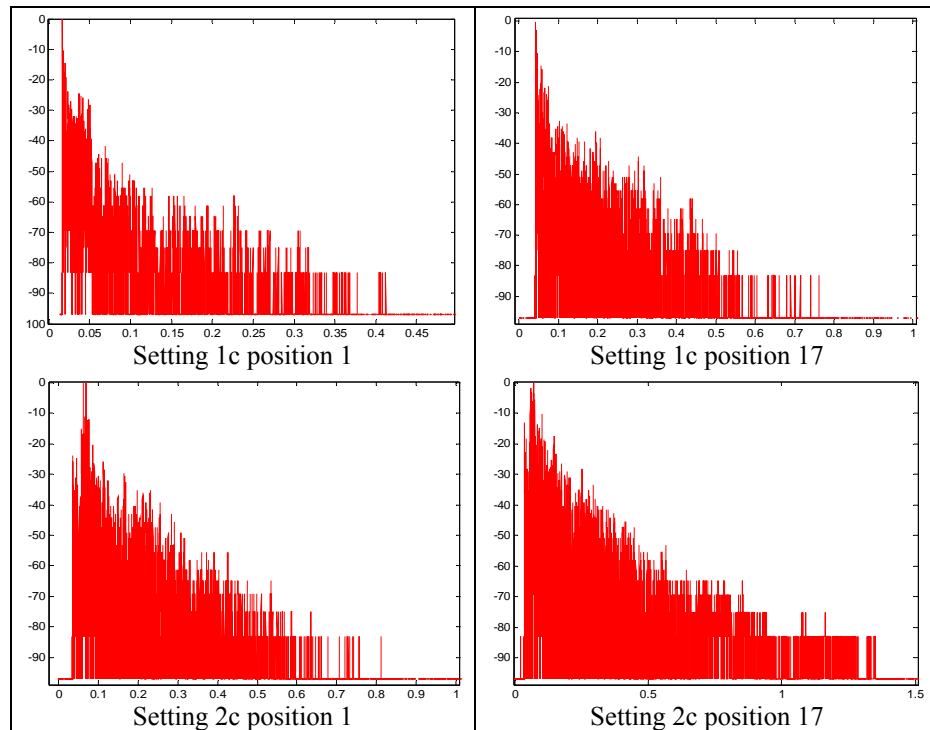
Figure 5. 21. The energy time curves comparison of settings 1c to 2c at positions 1 and 17.

In the echograms for settings 1c and 2c at seats 1 and 17 (Fig 5.21), it may be seen that the direct sound is stronger for setting 1c. This was expected since in the praying mode where the source is facing the mihrab, direct sound is coming from the rear of the source. The strong reflections arriving immediately after the weaker direct sound in

setting 2c are sound reflections from the mihrab. Therefore, it is shown here that the mihrab has an important role in the acoustics of the room.

5.8   Observations for Different Receiver Positions

Preaching and praying modes are the two main activities inside the mosque, as mentioned in Chapter 1. In these activities, worshippers will perform several different body movements and in general these can be classified by having two different heights of ear level, that is, i.e., standing (setting 1c) and sitting (setting 1d) height. In the computer model, the seats and audience area represented these heights. Another consideration in scale model measurements is the position where the microphone is placed inside the model.

5.8.1   Results for Standing and Seating Positions

In the scale model measurements, the settings are classified with two different heights for the microphones. Table 5.7 provides the results of the paired *t*-test for settings 1, 2, 6, and 7.

Table 5.7. Paired *t*-test for all parameters comparing result from receiver in standing and seating positions.

Parameter	*t*-statistic	*p*-observed	*t*-critical	Conclusion
RASTI			2.086	
Setting 1c-1d	1.438	0.1666	$df = 19$	Does not rejectH_0
Setting 2c-2d	-0.634	0.5336	$\alpha = 0.05$	Does not rejectH_0
Setting 6c-6d	-0.608	0.5503		Does not rejectH_0
Setting 7c-7d	-0.962	0.3479		Does not rejectH_0
C_{50}				
Setting 1c-1d	-1.194	0.2473		Does not rejectH_0
Setting 2c-2d	0.954	0.3522		Does not rejectH_0
Setting 6c-6d	-0.432	0.6709		Does not rejectH_0
Setting 7c-7d	-0.892	0.3836		Does not rejectH_0
$\%AL_{cons}$				
Setting 1c-1d	1.196	0.2466		Does not rejectH_0
Setting 2c-2d	-1.686	0.1016		Does not rejectH_0
Setting 6c-6d	0.502	0.6214		Does not rejectH_0
Setting 7c-7d	0.506	0.6186		Does not rejectH_0

It showed that doing the measurements with two different heights did not affect the speech parameters at 20 receiver positions.

This result agreed with the parameter mapping of Setting 1 except for C_{50} (see Fig. 5.22). Clarity is better for the standing position toward the front of the prayer hall. Toward the back, clarity seems to be better for the sitting position. It is possible that the measurements for the standing position were affected more by the dome ceiling because the elevation was higher.

| RASTI Set 1c | C_{50} Set 1c | %AL$_{cons}$ Set 1c |
| RASTI Set 1d | C_{50} Set 1d | %AL$_{cons}$ Set 1d |
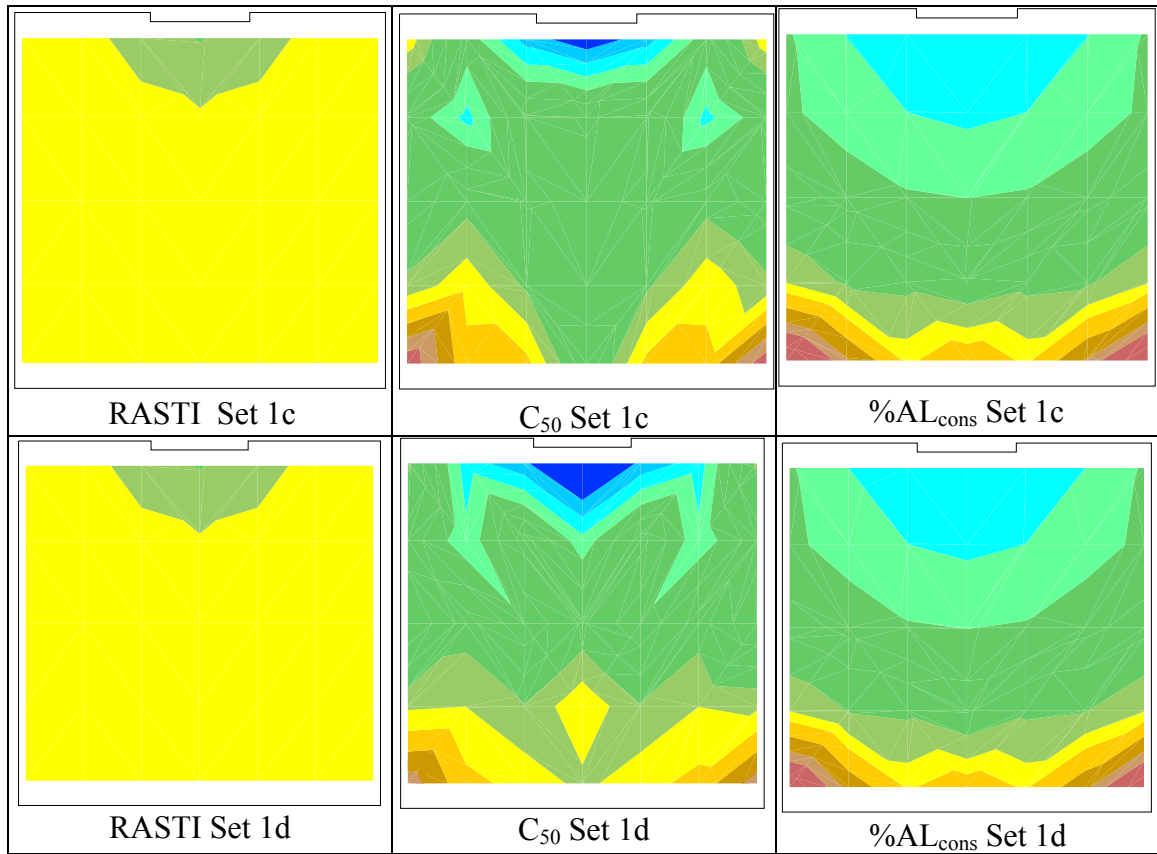
*Refer to legends in figure 5.17. Additional range for C_{50}:

| | 6.00 | 7.00 |
| | 7.00 | 8.00 |

Figure 5.22. Mapping on all parameters for settings 1c and 1d.

From listening test using three settings, setting 2 was the only setting where all listeners were able to distinguish the difference between the speech at positions 1 and 17 (see Table 5.8). For setting 6, receiver position 1 had 50% of the listener samples that

could tell the difference between standing and sitting position, while the other comparisons had 83-100% agreement for differences. In all comparisons, the majority of the listeners agreed that the speech was better in a seated position, which verified the statement regarding the mapping analysis of setting 1 above.

Table 5.8. Result on the listening test from 12 listeners.

Comparison	Receiver position	Differences (%)	Preferred Condition (%)	
Setting 2c-2d	1	100	2c ~ 17 %	2d ~ 83%
Setting 2c-2d	17	100	2c ~ 25 %	2d ~ 75%
Setting 6c-6d	1	50	6c ~ 33.33 %	6d ~ 66.67%
Setting 6c-6d	17	100	6c ~ 17 %	6d ~ 83%
Setting 7c-7d	17	83	6c~ 60%	6d ~ 40%

The echograms in Fig. 5.23 suggest that there are only minor differences due to different receiver heights.
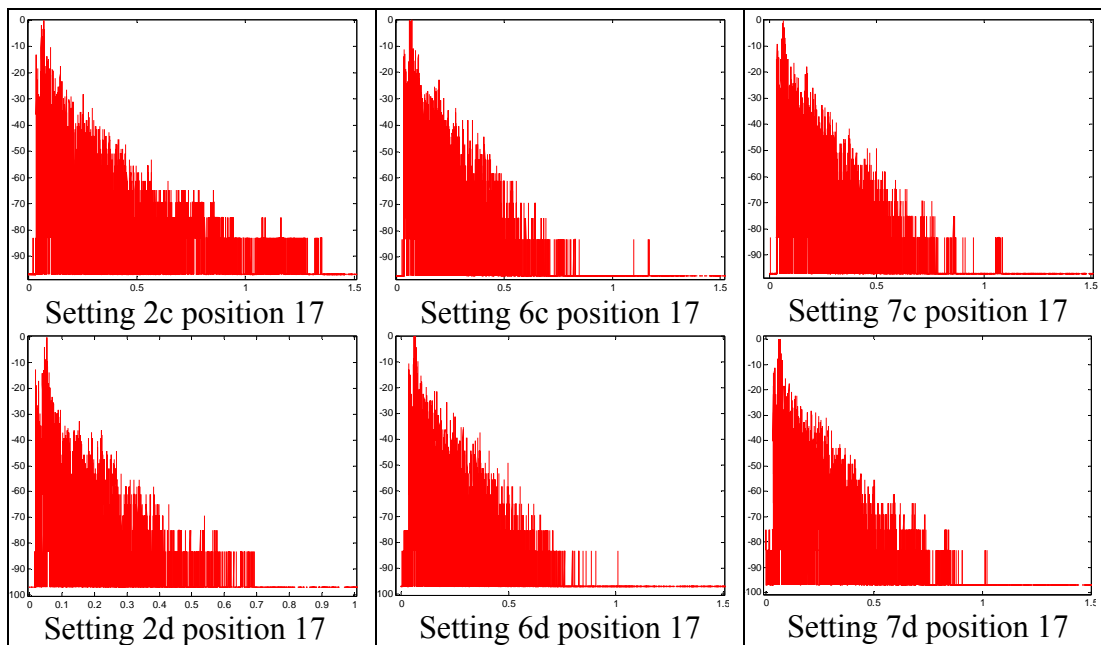
Figure 5.23. The echograms comparison of different receiver heights at position 17.

5.8.2   Results for the Receiver Hung and Placed on a Supported Stand

In this observation, setting 1c and 2c (microphone placed on a stand) were compared with setting 3 and 4 (microphone hung from the ceiling) at six different seats.

Table 5.9. Paired *t*-test for all parameters comparing results from the receiver hung and placed on a stand.

Parameter	*t*-statistic	*p*-observed	*t*-critical	Conclusion
Settings 1c-4 (preaching, source facing audience)				
RASTI	2.697	0.0429	2.447	Reject H_0
C_{50}	2.556	0.0431	$df = 5$	Reject H_0
%AL$_{cons}$	-2.124	0.0470	$\alpha = 0.05$	Reject H_0
Settings 2c-3 (praying, source facing *mihrab*)				
RASTI	1.032	0.3498	2.447	Does not rejectH_0
C_{50}	6.542	0.0017	$df = 5$	Reject H_0
%AL$_{cons}$	-5.408	0.0000	$\alpha = 0.05$	Reject H_0

Results from the statistical analysis (Table 5.9) showed that hanging the receiver from the ceiling and placing it on a stand gave significantly different speech parameters. This could be concluded only for the 6 seats observed. For subjective ranges of RASTI, all receiver positions in both settings were in the same range: good to very good intelligibility. They therefore had the similar results. An assumption can be made that the 1/8" microphone was not omni-directional over the entire frequency range measured. As a consequence, changing the microphone's direction did change the results of the measurements.

Listeners in the listening test (see Table 5.10) felt that hanging the microphone on the ceiling created a better speech quality inside the model.

Table 5.10. Results of the listening test from 12 listeners comparing setting 2c and 3.

Comparison	Receiver position	Differences (%)	Preferred Condition (%)	
Setting 2c – 3	1	100	2c ~ 0 %	3 ~ 100 %
Setting 2c – 3	17	83	2c ~ 40 %	3 ~ 60 %

Interestingly, Figs 5.24 and 5.25 contradict this result by showing that the measured %Al$_{cons}$ and the C_{50} values are better in setting 2c, which is the model with the microphone placed on a stand. It should be noticed that the surfaces of the stand were large enough for the high-frequencies sound waves to see them as reflecting surfaces.
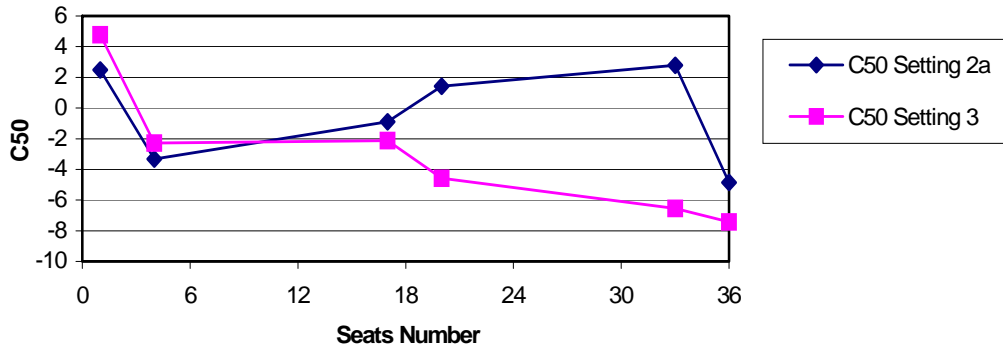
Figure 5.24. Comparison of C_{50} in setting 2c to setting 3 for 6 receiver positions.
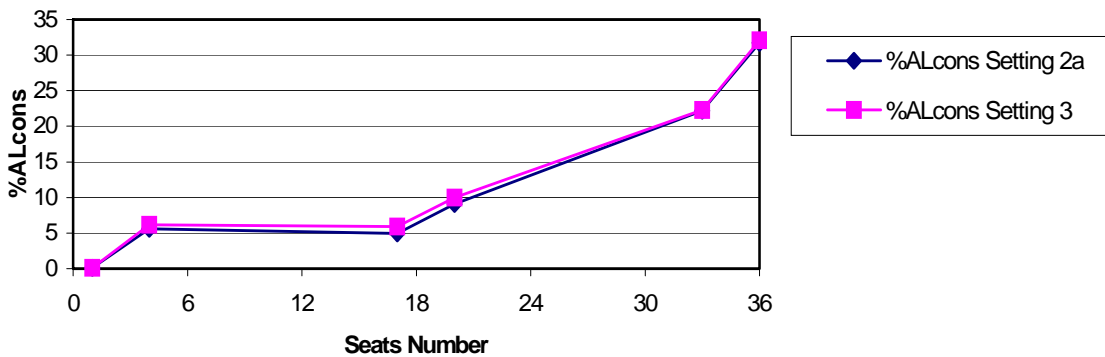
Figure 5.25. Comparison of %AL_{cons} in setting 2c to setting 3 for 6 receiver positions.

Eventually, the stand was wrapped with velvet lining, which absorbed some of the sound energy that hit the surfaces. However, residual scattering created non-uniform sound reflection that was picked by the microphone.

The echograms in Fig. 5.26 show some of the differences produced by the different microphone orientations.
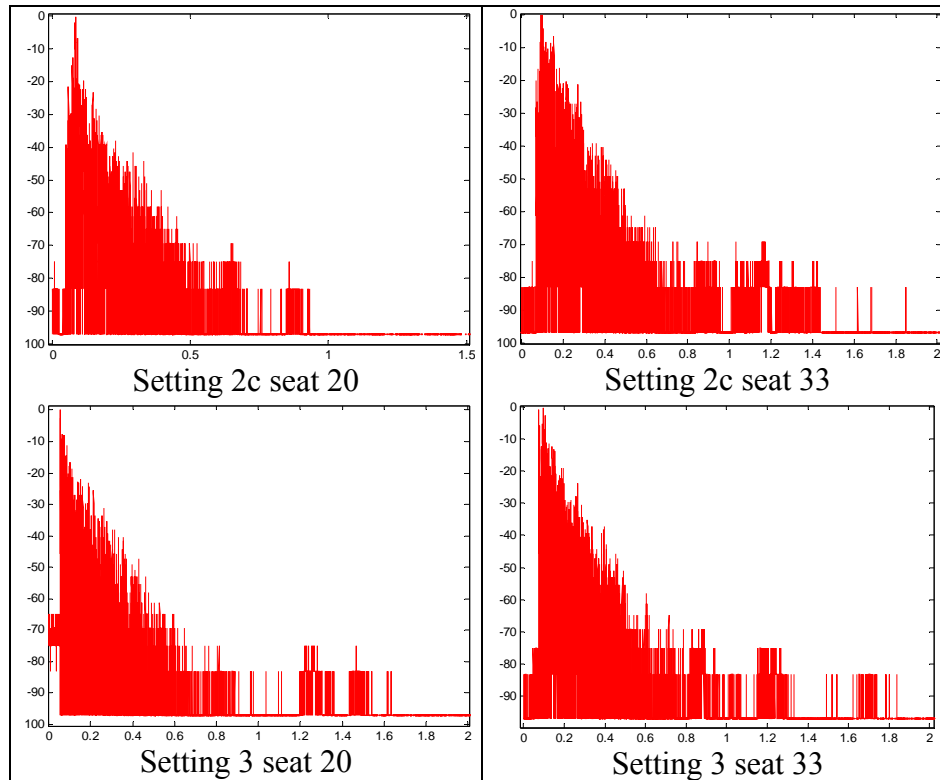
Figure 5.26. The echograms comparison of setting 2c to setting 3 for receiver positions 20 and 33.

5.9 Observation of Differences Due to Miniature Mannequins Surrounding the Receiver

Setting 5 is model 3 with miniature mannequins surrounding the receiver in a sitting position. This configuration represented the condition of worshipper inside mosques during preaching. Setting 5 was compared to setting 1d on 6 seats (9, 11, 17, 19, 25 and 27). These seats are underneath the domed ceiling. The paired t-test in Table 5.11 show that there are no strong evidences that there are differences from measurement with and without placing mannequins around the microphone.

Table 5.11. Paired *t*-test for all parameter comparing result from setting 1d with setting 5.

Parameter	t-statistic	p-observed	t-critical	Conclusion
RASTI	1.790	0.1335	2.447	Does not rejectH_0
C_{50}	0.499	0.6388	$df = 5$	Does not rejectH_0
%AL_{cons}	-2.720	0.0418	$\alpha = 0.05$	Reject H_0

Using the echograms comparison (Fig. 5.27), it is shown that there are differences in the energy received by the receiver due to presence of the mannequins.
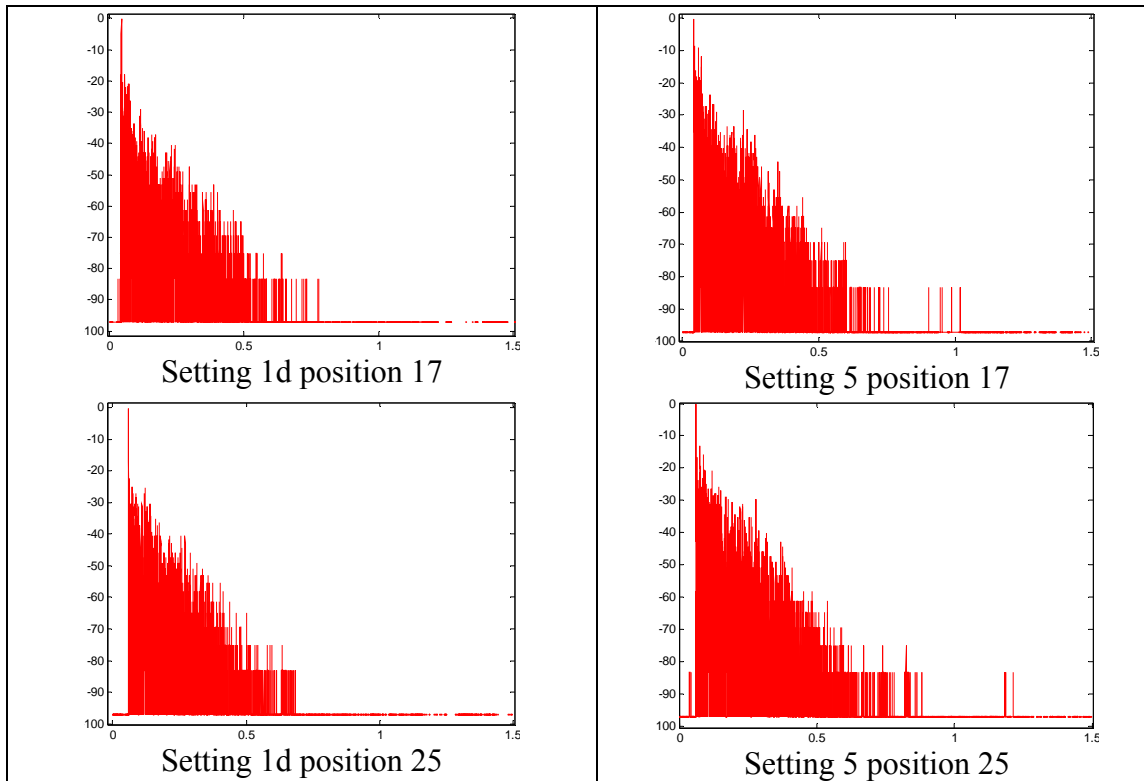
Figure 5.27. The echograms comparison of setting 1d to setting 5 for receiver positions 17 and 25.

5.10 Observation of Differences Due to Floor Material

A final observation (setting 9) was used and compared with setting 7 to assess the impact of floor material. In the real world, carpet has a significant role in the room absorption and is commonly used to control room reverberation. Measurements were done only at 6 positions. Section 5.7 also provided evidence that without carpeting the parameters are significantly different for measurements with different source orientation.

Result from the statistical analysis (Table 5.12) and the listening test (Table 5.13) both show that measurements with and without carpet do create differences in the parameter values.

Parameter	t-statistic	p-observed	t-critical	Conclusion
RASTI	3.777	0.0129	2.447	Reject H_0
C_{50}	4.996	0.0001	$df = 5$	Reject H_0
%AL_{cons}	-5.231	0.0000	$\alpha = 0.05$	Reject H_0

Table 5.13. Result on the listening test from 12 listeners comparing settings 7c and 9c.

Comparison	Receiver position	Differences (%)	Preferred Condition (%)	
Setting 7c-9c	1	83	7c ~ 60 %	9c ~ 40 %
Setting 7c-9c	17	100	7c ~ 100 %	9c ~ 0 %

The echograms (Fig. 5.28) also show some differences resulting from the carpeting.

Setting 7c position 1

Setting 7c position 17

Setting 9c position

Setting 9c position 17
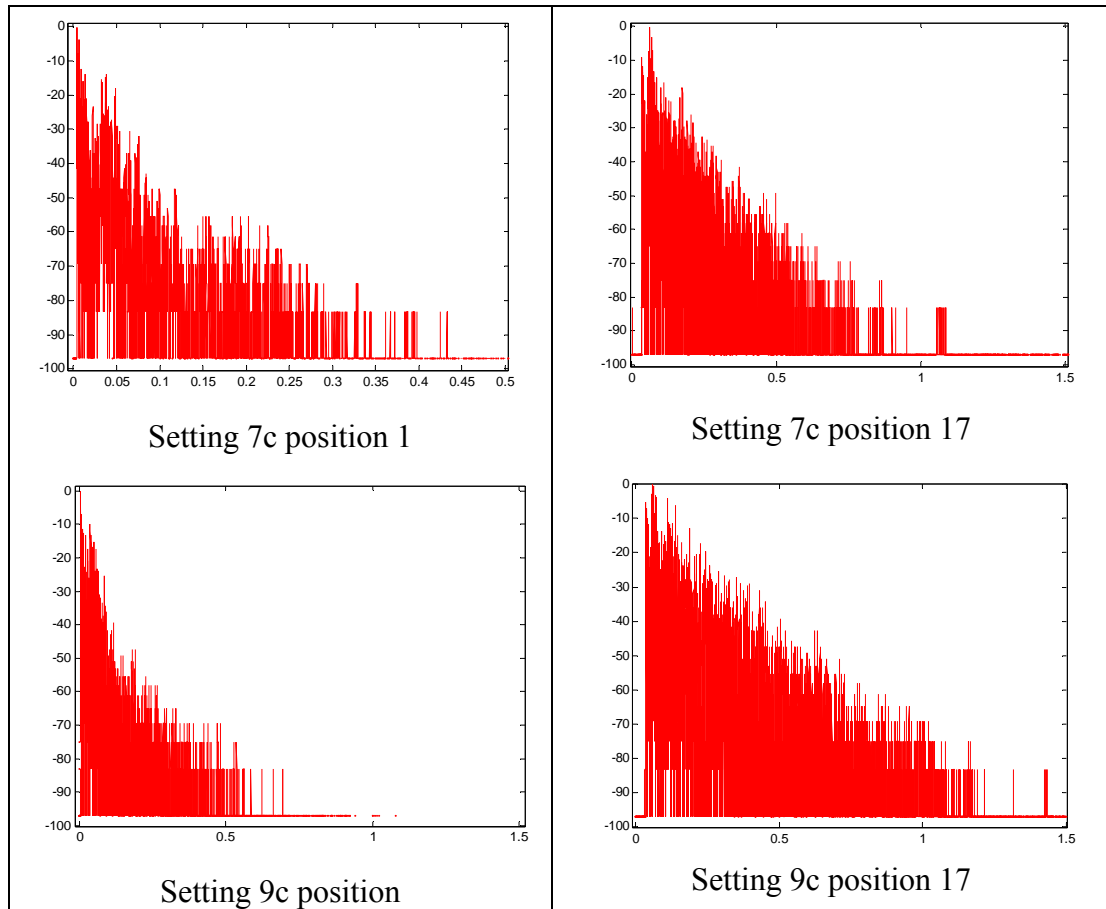
Figure 5.28. The echograms comparison of setting 7c to setting 9c for receiver positions 1 and 17.

The intelligibility scores at six seats observed in Setting 7c, which is with carpet lining, showed that the carpet produced better intelligibility (see Figs 5.29 through 5.31).
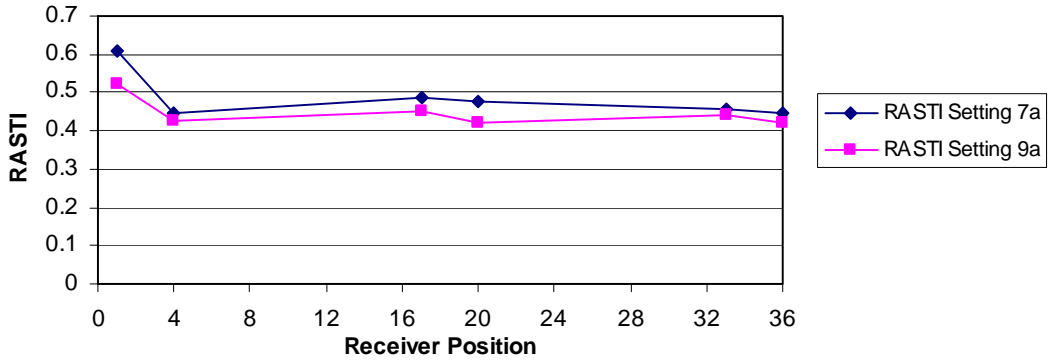
Figure 5.29. RASTI for setting 7c and setting 9c.
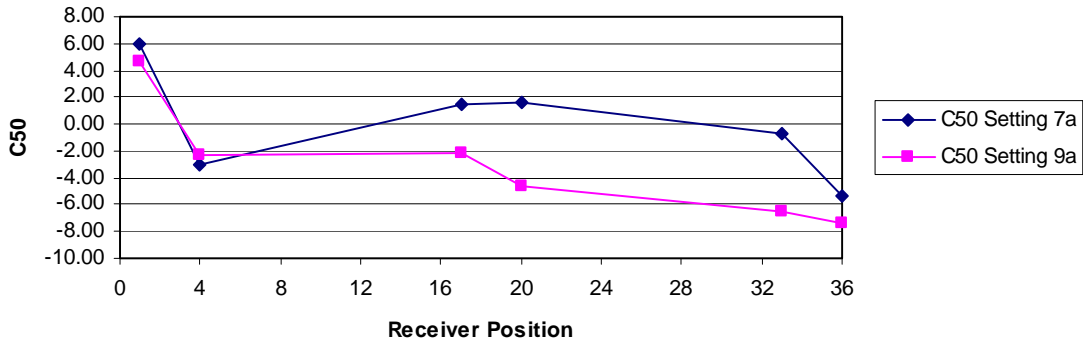
Figure 5.30. C_{50} for setting 7c and setting 9c.
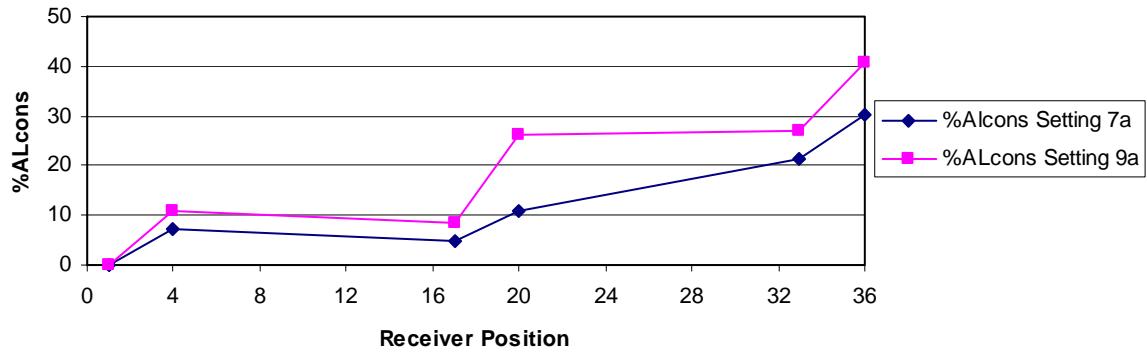
Figure 5.31. %AL$_{cons}$ for setting 7c and setting 9c.

CHAPTER 6
CONCLUSION

This research project involved the acoustical modeling and evaluation of a room with a domed ceiling structure, with special application to the Darussholah mosque in Jember (East Java), Indonesia. It was approached using analytical, numerical, and experimental (scale modelling) methods. Since each method had its own scope and set of limitations, some conclusions could not be derived simultaneously from all three methods. Comparisons using results from computer models and physical scale models were not complete; neither one alone could be used as an ideal approach to the problem. The conclusions presented here thus result from one or more of the methods and correspond to the chief points of emphasis in this research.

The central analyses corresponded to acoustical differences in the mosque due to variations in the ceiling structure. Observations of different shapes of domes were only made using computer modeling and an analytical approach. Different shapes of domes and ring structure configurations beneath the domes did not create significant differences in the speech quality inside the prayer hall of the mosque. This was likely due to the small geometrical proportion of the dome relative to the larger coupled rectangular room below it. Several physical conditions of a dome should be considered to determine whether it would produce significant effects in the coupled room.

In the case where the dome diameter is kept the same as the dome in the actual mosque (12.3 m), the chief geometrical variation is associated with the height of the dome. The higher the domed ceiling is from the prayer hall, the less the sound intensity

from reflections of the dome will cover the prayer hall. Some degree of reflected sound intensity might be needed to provide sufficient acoustical support in the hall.

Little in the way of focusing effects was observed in the modeled prayer hall, even underneath the dome. This was apparently because the base of the dome was high enough that the focusing actually occurred at points higher than the heights of the receivers (listener ears both in seated and standing positions). Accordingly, it did not affect speech quality appreciably. The research suggested that the greater the height of the receiver, the greater the effect the domed ceiling would produce. Prayer in mosques combines several movements and positions by participants. However, in this research, all positions were low enough in height that they were not strongly affected by the presence of the domed ceilings. In reality, worshipper activities are not only standing and sitting. However, it can still be concluded from the results of this work that speech clarity and intelligibility will generally be the same for all worshipper positions.

Source (Imam) orientation had significant impact on the results from the scale model. (Parameter mappings produced by the computer models did not show such significant differences.) It was apparent that for preaching, the speech quality was better because the source was facing the audience. Several conclusions can be reached, relative to this matter. First, while the mihrab did appear to play an important acoustical role in the mosque, there was a limitation of having reflected sounds coming toward the receiver when the source is facing the mihrab instead of the audience. In this case, the distance for the sound to travel is longer and the direct-to-reverberant sound ratio was smaller. The mihrab also created a nonuniformity of sound reflections in the hall.

Absorptive materials were found to be very important factors for producing good speech intelligibility inside the room. Applying BASWAphon^{TM} for the dome material in the computer models did affect the results significantly. Carpeting in the scale model also produced notable changes. In both cases, these absorptive materials produced better speech intelligibility. In a mosque, particularly with a domed ceiling, it is important to consider the dome material and other absorptive materials that might be inserted in the prayer hall.

A geometrical representation of a hemispherical dome was made by a series of flat plane surfaces in the computer models. The disadvantage of this approach was that the model might fail to produce accurate results from the simulations due to an insufficient number of planes. In this research it was shown that after a certain number, the larger the number of planes demanded longer computation time, but without producing a significant benefit. Meanwhile, in the scale modeling technique, the spherical dome had a smooth concave surface, which more closely represented the dome in the actual mosque. Measurement positions underneath the dome in the scale model may therefore have produced better results than in the computer model.

The results of the speech parameters and auralization listening test produced by both, the computer and scale modeling measurements provide a general prediction that the speech intelligibility and clarity inside the actual mosque would be good toward the front hall and beneath the dome. The presence of the dome does not significantly create speech intelligibility problems. Poor intelligibility would happen toward the back of the hall due to insufficient sound energy.

Additional points related to this research should be investigated in the future. The geometrical proportion of a domed ceiling relative to the room coupled to it should be a primary consideration in the room design process. For any room under consideration, this should be studied carefully in order to predict the impact of the dome on the acoustics of the room. The mihrab could be claimed to be a very important element inside the mosque, since in prayers it is the first boundary encountered by the strong direct sound and it becomes something of a sound projector. Therefore, further investigation and exploration of this element is needed, particularly a study of the materials used in its construction, its geometrical properties, and its acoustical relationship to the Qibla' wall. An approach that involves both computer modeling and scale modeling should be available in such a study. Algorithms designed to measure impulse responses and calculate acoustical parameters need to be compared and verified between numerical and experimental research methods. However, in order for this verification to take place, computer modeling packages need to become more transparent and detailed in their description of coded algorithms.

In order to specifically study the effects of different domed ceiling configurations on the acoustical performances in rooms, larger variations of models are needed. The domed ceiling configurations should involve significantly different shapes, heights, and diameters. In this research, these parameters were only explored to an extent. Different dome diameters were not addressed at all. Computer modeling techniques might be the most appropriate approach to conduct this kind of study.

Source positions in this research were based on practical mosque functions. As a result, a detailed study of focusing effects was not carried out. A detailed study of the

focusing effect created by the domed ceiling could be performed by placing the source underneath the dome during the measurements and changing the source and receiver elevations.

References

[1] S. Strom, A. Krokstad, S. Sorsdal, and S. Stensby, "Design of Room Acoustics and A MCR Reverberation System dor Bjergsted Concert Hall in Stavanger," Applied Acoustics **19**, 465–475 (1986).

[2] C. A. Weitze, C. L. Christensen, and J. H. Rindel, "Comparison between In-situ recordings and Auralizations for Mosques and Byzantine Churches," http://www.dat.dtu.dk/~odeon/pdf/NEM%202002%20paper.pdf (July, 2002).

[3] G. N. Papageorgiau, "Computer modeling of sound fields in bounded spatial systems; extension of the ray method to curve surfaces," Computational acoustics and its environmental applications II, International Conference on Computational Acoustics and Its Environmental (1997), pp. 99-109.

[4] R. Suarez, J.J. Sendra, J. Navarro, and A.L. Leon, "The acoustics of the cathedral-mosque of Cordoba, Proposal for architectural intervention," Acta Acustica **90**, 362–375 (2004).

[5] R. N. S. Hammad, "Rasti Measurements in Mosque in Amman Jordan," Applied Acoustics **30**, 335–345 (1990).

[6] H. A. Hamadah and H. M. Hamouda, "Assessment of Speech Intelligibility in Large Auditoria Case Study: Kuwait State Mosque," Applied Acoustics **54**, 273–289 (1998).

[7] A. A. Abdou, " Measurement of acoustical characteristics of mosques in Saudi Arabia," J. Acoust. Soc. Am. **113**, 1505–1517 (2003).

[8] I. Seralgeldin and J. Steele, *Architecture of the Contemporary Mosque* (Academy Group Ltd., London, 1996).

[9] D. L. Klepper, "The distribution column sound system at Holy Cross Cathedral, Boston, the reconciliation of speech and music," J. Acoust. Soc. Am. **99**, 417–425 (1996).

[10] E. A. Wetherill, "Translating acoustical requirements into architectural details," Journal of Sound and Vibration, July (1997).

[11] J. S. Bradley, "Predictors of speech intelligibility in rooms," J. Acoust. Soc. Am. **80**, 837–845 (1986).

[12] H. Kuttruff, *Room Acoustics* (Elsevier Science Publishing Ltd., 4th edition, 1991).

[13] J. H. Rindel, "The Use of Computer Modeling in Room Acoustics," Journal of Vibro-Engineering **3(4),** 219–224 (2000), Index 41-72 Paper of the International Conference BALTIC-ACOUSTIC (2000).

[14] A. Krokstad, S. Stroem, and S. Soersdal, "Calculating the Acoustical Room Response by the use of a Ray Tracing Technique," J. Sound Vibration **8**, 118–125 (1968).

[15] A. Kulowski, "Algorithmic Representation of the Ray Tracing Technique," Applied Acoustics **18**, 449–469 (1985).

[16] T. Lewers, "A Computer Beam Tracing and Radiant Exchange Computer Model of Room Acoustics," Applied Acoustics **38**, 161–178 (1993).

[17] J. H. Rindell, "Computer simulation techniques for the acoustical design of rooms-how to treat reflections in sound field simulation," Proceedings of the International Symposium ASVA 97, Tokyo, Japan, 1997, pp. 201–208.

[18] M. Vorländer, "International round robin on room acoustical computer simulations," Proceedings of the 15th Int. Cong. Acoust., Troundheim, Norway (1995), pp. 689–692.

[19] M. Vorländer, "Simulation of the Transient and Steady-State Sound Propagation in Rooms Using a New Combined Ray Tracing/Image-Source Algorithm," J.Acoust. Soc. Am. (1989).

[20] M. J. Howarth and Y. M. Lam, "An assessment of the accuracy of a hybrid room acoustic model with surface diffusion facility," Applied Acoustics **6**, 237–251 (2000).

[21] M. Lisa, J. H. Rindel, and C. L. Christensen, "Predicting the Acoustics of Ancient Open Air Theatres: The Importance of Calculation Methods and Geometrical Details," http://www.dat.dtu.dk/~odeon/pdf/BNAM_paper_04.pdf. (March, 2005).

[22] G. M. Naylor, "ODEON-Another Hybrid Room Acoustical Model," Applied Acoustics **38,** 131–143 (1993).

[23] M. R. Schroeder, "New Method of Measuring Reverberation time," J. Acoust. Soc. Am. **37**, 409–412 (1965).

[24] H. M. Smith, "Geometric Acoustic Modeling of the LDS Conference Center," Master thesis, Brigham Young University, Provo, Utah, USA (2004).

[25] J. H. Rindell, "Attenuation of Sound Reflections form Curved Surfaces," Proceedings of the 24th Conference on Acoustics, Strbské Pleso (1985), pp. 194–197.

[26]H. Kurtruff, "Some remarks on the simulation of sound reflection from curved walls," Acustica **77**, 176–182 (1992).

[27]A. Tisseyre, A. Moulinear, and Y. Rouard, "Intelligibility in various rooms: Comparing its assessment by (RA)STI Measurement with a direct measurement procedure," Applied Acoustics **53** (1-3), 179–191 (1998).

[28]L. Faiget and R. Ruiz, "Speech Intelligibility model including room and loudspeaker influences," J. Acoust. Soc. Am. **105**, 3345–3354 (1999).

[29]J. P. A. Lochner and J. F. Burger, "The influence of reflections on auditorium acoustics," J. Sound Vib. **1**, 426–454 (1964).

[30]H. J. M. Steeneken and T. Hougast, "RASTI: A Tool For Evaluation Auditoria," *B&K Technical Review* (1985).

[31]K. D. Kryter, "Validation of the Articulation Index," J. Acoust. Soc. Am. **34**, 1698–1702 (1962).

[32]Articulation Index Tutorial, http://www.audiologyinfo.com/ai/aitut.htm, (April, 2005).

[33] J. S. Bradley, R. D. Reich, and S. G. Norcross , "On the combined effects of the signal-to-noise ratio and room acoustics on speech intelligibility," *J. Acoust. Soc. Am.* 106 (4), Pt.1, October, 1820-1828 (1999).

[34]R. Thiele, "Richtungsverteilung und Zeitfolge der Schallruckwurfe in Raumen," Acustica 3, p 291-302, (1953)

[35]W. Ahnert and H. P. Tennhardt, "Acoustics for Auditorium and Concert Halls," Handbook for Sound Engineers, Ed. G. M. Ballou, Third Edition, Butterworth-Heinemann, USA (2002), pp. 118.

[36]J. S. Bradley, R. Reich, and S.G. Norcross, "A just noticeable difference in C_{50} for speech," Applied Acoustic **58**, 99–108 (1999).

[37]V. M. A. Peutz ,"Articulation loss of consonants as a criterion for speech transmission in room," J. Audio Eng. Soc. **19**, 915–919 (1971).

[38]K. D. Jacob, "Subjective and Predictive Measures of Speech Intelligibility-The Role of Loudspeaker Directivity," J. Audio Eng. Soc. **33**, No 12, 950–955 (1985).

[39]T. Houtgast and H. J. M. Steeneken, "The Modulation Transfer Function in Room Acoustics as a Predictor of Speech Intelligibility," Acustica **28**, 66–73 (1973).

[40]T. Houtgast and H. J. M. Steeneken, "The Modulation Transfer Function in Room Acoustics," *B&K Technical Review* (1985).

[41]M. R. Schroefer, "Modulation Transfer Functions: Definition and Measurement," Acustica **49**, 179–182 (1981).

[42]T. Houtgast and H. J. M. Steeneken, "A review of the MTF concept in room acoustics and its use for estimating speech intelligibility in auditoria," J. Acoust. Soc. Am. **77** 1069–1077 (1985).

[43]H. J. M. Steeneken and T. Houtgast, "A Physical Method for Measuring Speech-Transmission Quality," J. Acoust. Soc. Am. **67**, 318–326 (1980).

[44]H. J. M. Steeneken and T. Houtgast, "RASTI: A Tool for Evaluating Auditoria", *B & K Technical Review* (1985).

[45]Acoustic Design Ahnert, *EASE^{TM} 4.0 Tutorial* (Renkus-Heinz Inc., 2002).

[46]R. A. Johnson and G. K. Bhattacharyya, *Statistics Principles and Methods* (John Wiley & Sons, Inc., 4th Edition, New York, USA, 2001).

[47]D. S. Moore and G. P. McCabe, *Introduction to the practice of statistics* (W. H. Freman & Company, 4th edition, New York, USA, 2003).

[48]J. R. Swisher and S. H. Jacobson, "A survey of ranking, selection and Multiple Comparison Procedures for Discrete-Event Simulation," Proceedings of the 31st conference on Winter Simulation: Simulation--a bridge to the future – Volume 1, Arizona, USA (1991), pp. 492–501.

[49]F. L. Ramsey and D. W. Schafer, *The Statistical Sleuth: A course in methods of data analysis*, (Thomson Learning, 2nd edition, Duxbury, California, USA, 2002).

[50]BASWAphon, Diffuse Reflections **1** (2001), http://www.rpginc.com/cgi-bin/byteserver.pl/news/reflections/Drv7i1web.pdf (October, 2003)

[51] "The BASWA*phon* acoustic system", http://www.baswa.com/e/default.htm (October, 2003).

[52]V. O. Knudsen, *Architectural Acoustics* (John Wiley & Sons, Inc., New York, Third Edition, 1947).

[53] Kinsler and Frey, *Fundamentals of Acoustics* (John Wiley & Sons, Inc., Fourth Edition, New York, USA, 2000).

[54] W. Ahnert and H. P. Tennhardt, "Acoustics for Auditorium and Concert Halls," *Handbook for Sound Engineers* (Ed. G. M. Ballou, Third Edition, Butterworth-Heinemann, USA, 2002).

[55] L. Cremer and H. A. Muller, *Principles and Applications in Room Acoustics Vol. I.* (translated by T. J. Schultz, Applied Science, London, UK, 1982).

[56] J. D. Polack, A. H. Marshall, and G. Dodd, "Digital evaluation of the acoustics of small models: The MIDAS package," J. Acoust. Soc. Am. **85,** 185–193 (1989).

[57] J. Eargle and C. Foreman, "An examination of bandwidth, dynamic range and normal operating levels," http://www.livesoundint.com/archives/2003/jan/asa/asa.php, (February, 2004).

[58] Meyer Sound, "Factor that Affect Intelligibility in Sound Systems," http://www.meyersound.com/support/papers/speech/section2.htm, (March, 2005).

[59] R. J. Orlowski, "An Eighth-Scale Speech Source for Subjective Assessments in Acoustic Models," Journal of Sound and Vibration **77 (4)**, 551-559, 1981.

[60] "What is MDF?," Merbok, http://www.merbok.com/mdfoverview/whatis.htm (January 2004).

[61] R. T. Chester, "Construction and Evaluation of An Acoustical Scale Model of A Mosque and A Miniature Human Voice Source," Undergraduate thesis, Brigham Young University, Provo, Utah, USA (2004).

[62] H. K. Dunn and D. W. Farnsworth, "Exploration of Pressure Field Around the Human Head During Speech," J. Acoust. Soc. Am. **10**, 184–199 (1939).

[63] A. Moreno and J. Pfretzschner, "Human Head Directivity in Speech Emission : A New Approach," Acoustics Letter **1**, 78–84 (1978).

[64] J. L. Flanagan, "Analog Measurements of Sound Radiation from the Mouth", *J. Acoust. Soc. Am.* 32 (12), December, 1613-1620 (1960).

[65] W. T. Chu and A.C.C. Warnock, "Detailed Directivity of Sound Fields Around Human Talkers", IRC-RR-104, December, National Research Council Canada (2004).

[66] B. Day, "Acoustic Scale Model Materials," Auditorium Acoustics: the proceedings of an International Symposium on Architectural Acoustics, Heriot-Watt University, Edinburgh, Scotland (1974), pp. 87-99.

[67] R. G. Monk, "Thermal relaxation in humid air," J. Acoust. Soc. Am. **46**, 580–586 (1969).

[68] C. M. Harris and W. Tempest, "Absorption of Sound in Oxygen/Water Mixtures," J. Acoust. Soc. Am. **36**, 2416–2417 (1964).

[69] M. M. Boone and E. Braat-Eggen, "Room Acoustics Parameters in a Physical Scale Model of the New Music Center in Eindhoven: Measurement Method and Results," Applied Acoustics **42**, 13–28 (1994).

[70] ISO 9613-1-1996: Acoustics-attenuation of sound during propagation outdoors-Part 1: Calculation of the absorption of sound by the atmosphere.

APPENDIX A

All the MATLAB® codes in Appendix-A were used to generate the impulse responses and calculated the speech parameters (C50, % Alcons, and RASTI).

1. Function to Compute Batch Files of the Wave Files

```
function X=Namer(ON,NS,NF)

%  This function accept the name you want to use and automatically produces
%  an array that contains the name with a number incremented for use in
%  making names for variables in other prgrams.  Written by Ryan Chester, October, 2004)
Explanation:
%
%        X=Namer(ON,NS,NF)
%
%  ON is the overal name used in the naming process, NS is the first number
%  and NF is the last number of names to have a numerical ending added to
%  the name of the file.  Both are required imputs and would be entered like
%  this:
%
%     X=Namer('name',3,45);
%
%  to get an aray of names name003 to name045 stored in the aray X
%
%  NOTE: the bigest number this program works for is 999.  Feel free to
%  alter it to make it bigger, the code is pretty simple.
m=1;
for n=NS:NF
  if n<10
    X(m,:)=[ON '00' int2str(n)];
  elseif n<100
    X(m,:)=[ON '0' int2str(n)];
  elseif n<1000
    X(m,:)=[ON int2str(n)];
  end
  m=m+1;
end
```

2. Impulse Response Scaling

```
% This code is to scale the sampling frequency of the impulse responses from the scale model
measurements to the actual building measurement (1:12 scale model).
% written Jan 12, 2005.
clear;  close all;
dir=input('Enter The directory where the data can be found\n        ');
namfile=input('Enter the name of file\n          ');
```

```
q=input('Enter the first number you want for the names\n          ');
n=input('Enter the last number you want for the names\n          ');
namfolder=Namer([namfile],q,n);
namwav=input('Enter the name you would like your new wave file to have\n          ');
namwavF=Namer(namwav,q,n);
mkdir('Scaled\')
for      m=q:n
         [A,FS,NBITS]=wavread([dir namfile int2str(m) '.wav']);
         figure
         B=0:1/FS:length(A)/FS;
         plot(B(1:length(A)),A,'-r')
         FS=FS/12;
         NBITS=16
         figure
         C=0:1/FS:length(A)/FS;
         plot(C(1:length(A)),A,'b-')
         wavwrite(A,FS,NBITS,['Scaled\' namwavF(m,:) '.wav'])
end
```

3. Octave Band Filter and Air Absorption Compensation

This code is to filter the whole impulse responses into five octave bands of interest (250Hz, 500Hz, 1000Hz, 2000Hz, and 4000Hz octave bands). After they were filtered, applying the air absorption compensation for impulse responses in each octave bands modified the impulse responses.

```
function [B,A] = octdsgn(Fc,Fs,N); %found in the internet January, 2005.
% OCTDSGN  Design of an octave filter.
%    [B,A] = OCTDSGN(Fc,Fs,N) designs a digital octave filter with
%    center frequency Fc for sampling frequency Fs.
%    The filter are designed according to the Order-N specification
%    of the ANSI S1.1-1986 standard. Default value for N is 3.
%    Warning: for meaningful design results, center values used
%    should preferably be in range Fs/200 < Fc < Fs/5.
%    Usage of the filter: Y = FILTER(B,A,X).
% Author: Christophe Couvreur, Faculte Polytechnique de Mons (Belgium)
%         couvreur@thor.fpms.ac.be
% Last modification: Aug. 22, 1997, 9:00pm.
% References:
%    [1] ANSI S1.1-1986 (ASA 65-1986): Specifications for
%        Octave-Band and Fractional-Octave-Band Analog and
%        Digital Filters, 1993.

if (nargin > 3) | (nargin < 2)
  error('Invalide number of arguments.');
end
if (nargin == 2)
  N = 3;
end
if (Fc > 0.70*(Fs/2))
  error('Design not possible. Check frequencies.');
end
pi = 3.14159265358979;
beta = pi/2/N/sin(pi/2/N);
```

```
alpha = (1+sqrt(1+8*beta^2))/4/beta;
W1 = Fc/(Fs/2)*sqrt(1/2)/alpha;
W2 = Fc/(Fs/2)*sqrt(2)*alpha;
[B,A] = butter(N,[W1,W2]);


clear; close all;
%This is the same code as filteroctdsgn, only it is using the scaled impulse
%responses.  Author : Sentagi S. Utami, Jan 26,2005.
%last modified February 3, 2005.
dir=input('Enter the directory where the data can be found\n');
namfold=input('Enter the name of the old wave file without the numbers that distinguish them\n');
q=input('Enter the first number you want for the names\n');
n=input('Enter the last number you want for the names\n');
namwaver=Namer([namfold],q,n);
namwave=input ('Enter the filename for the filtered wave file\n   ');
namwaver1=Namer([namwave],q,n);
fprintf('Working, Lets just see how fast this goes\n');
mkdir ('filtercomp\');


% the air absorption compensation (see Pages 86-90) in this code was applied only for 500Hz,
1000Hz, and 2000Hz octave bands.
To=293.1;
TairC=[To,27+To];        %Temperature while running the measurement in the scale model
RH=[30,48];              % RH = Relative Humidity
IFreq=[500,1000,2000,6000,12000,24000];
airab5=air(RH(2),TairC(2),IFreq(4));
airab1=air(RH(2),TairC(2),IFreq(5));
airab2=air(RH(2),TairC(2),IFreq(6));
airref5=air(RH(1),TairC(1),IFreq(1));
airref1=air(RH(1),TairC(1),IFreq(2));
airref2=air(RH(1),TairC(1),IFreq(3));
cm=343.2*sqrt(TairC(2)/To);
cref=343.2;
comp5=airab5*cm-12*airref5*cref;
comp1=airab1*cm-12*airref1*cref;
comp2=airab2*cm-12*airref2*cref;
x=[2.51,13.31,17.92,24.11,26.93,12.26,4.72,8.38,14.26,11.11,8.69,7.71,15.53,13.9,22.4,20.53,19
.33,18.91,25.4,24.44];    % distance of the receivers to the source
for m=q:n
  [data,FS,NBITS]=wavread([dir namwaver(m,:) '.wav']);
  compensate5=12^(comp5*(x(m)/cm)/20);
  compensate1=12^(comp1*(x(m)/cm)/20);
  compensate2=12^(comp2*(x(m)/cm)/20);
  [B250,A250]=octdsgn(250,FS);
  [B500,A500]=octdsgn(500,FS);
  [B1000,A1000]=octdsgn(1000,FS);
  [B2000,A2000]=octdsgn(2000,FS);
  [B4000,A4000]=octdsgn(4000,FS);
%   for 250Hz octave band
  wavdata=filter(B250,A250,data);
  wavwrite(wavdata,FS,NBITS,['filtercomp\' namwaver1(m,:) '_250Hz' '.wav']);
%   for 500Hz octave band
  wavdata=filter(B500,A500,data);
  wavdata=wavdata*compensate5;
  wavwrite(wavdata,FS,NBITS,['filtercomp\' namwaver1(m,:) '_500Hz' '.wav']);
%   for 1000Hz octave band
```

```
    wavdata=filter(B1000,A1000,data);
    wavdata=wavdata*compensate1;
    wavwrite(wavdata,FS,NBITS,['filtercomp\' namwaver1(m,:) '_1000Hz' '.wav']);
%   for 2000Hz octave band
    wavdata=filter(B2000,A2000,data);
    wavdata=wavdata*compensate2;
    wavwrite(wavdata,FS,NBITS,['filtercomp\' namwaver1(m,:) '_2000Hz' '.wav']);
%   for 4000Hz octave band
    wavdata=filter(B4000,A4000,data);
    wavwrite(wavdata,FS,NBITS,['filtercomp\' namwaver1(m,:) '_4000Hz' '.wav']);

end
```

4. Impulse Response with Air Absorption Compensation

For auralization in the listening test, a new impulse responses was used, which covered five octave bands of interest as mentioned above.

```
clear; close all;
%The wave files were accessed using the same batch code as above. The wave files used in the
%code below were already compensated due to the air absorption. Author : Sentagi S. Utami,
%written : February 10, 2005.

for m=q:n
    [wavdata25,FS,NBITS]=wavread([dir namwaver(m-q+1,:) '_250Hz' '.wav']);
    [wavdata5,FS,NBITS]=wavread([dir namwaver(m-q+1,:) '_500Hz' '.wav']);
    [wavdata1,FS,NBITS]=wavread([dir namwaver(m-q+1,:) '_1000Hz' '.wav']);
    [wavdata2,FS,NBITS]=wavread([dir namwaver(m-q+1,:) '_2000Hz' '.wav']);
    [wavdata4,FS,NBITS]=wavread([dir namwaver(m-q+1,:) '_4000Hz' '.wav']);
    wavdataall=wavdata25+wavdata5+wavdata1+wavdata2+wavdata4;

    figure
    B=0:1/FS:length(wavdataall)/FS;
    plot(B(1:length(wavdataall)),wavdataall,'-r')
    wavwrite(wavdataall,FS,NBITS,['newimpulse\' namwaver(m-q+1,:) '.wav']);
end
```

5. Calculation for C_{50}, % Al_{cons}, and RASTI

```
% The wave files have already gone through a certain process in order to meet the needs.
function C_50=C50(wavdata,time)
num=0;      %num is numerator
denom=0;    %denom is denominator
for b=1:length(wavdata)
   if time(b)<=.05
      num=num+(wavdata(b))^2;
   end
   if time(b)>=.05
       denom=denom+(wavdata(b))^2;
   end
end
C_50=10*log10(num/denom);

clear;  close all;
```

```
% this is a batch code to plot the wavfile and calculate C50 at 1000Hz
% octave bands for a whole set measurement
global FS
dir=input('Enter the directory where the data can be found\n        ');
namwave=input('Enter the name of file\n        ');
q=input('Enter the first number you want for the names\n         ');
n=input('Enter the last number you want for the names\n         ');
namwaver=Namer([namwave],q,n);
fprintf('Sit back and wait, this could take a while\n');
for   m=q:n
   [wavdata1,FS,NBITS]=wavread([dir namwaver(m-q+1,:) '_1000Hz' '.wav']);
%    B=0:1/FS:length(wavdata1)/FS;
%    figure
%    plot(B(1:length(wavdata1)),wavdata1,'--b')

   time=(0:(length(wavdata1)-1))/FS;
   b=1:length(wavdata1);
   C_50(m)=C50(wavdata1,time(b));
   all=sprintf('C50=%.3g\n',C_50(m));
   fprintf(all);
end

clear;  close all;
% this is a batch code to calculate %AI_cons at 1000Hz and RASTI
% octave bands for a whole set measurement
global FS
dir=input('Enter the directory where the data can be found\n         ');
namwave=input('Enter the name of file\n        ');
q=input('Enter the first number you want for the names\n         ');
n=input('Enter the last number you want for the names\n         ');
namwaver=Namer([namwave],q,n);
fprintf('Sit back and wait, this could take a while\n');
x=[2.51,13.31,17.92,24.11,26.93,12.26,4.72,8.38,14.26,11.11,8.69,7.71,15.53,13.9,22.4,20.53,19
.33,18.91,25.4,24.44];
V=[6486.06, 6485.69, 6688.73];
for   m=q:n
   [wavdata1,FS,NBITS]=wavread([dir namwaver(m-q+1,:) '_1000Hz' '.wav']);
   RT601000=RT60calc(wavdata1);
   alcons=200*(x(m))^2*(RT601000/1000)^2/V(2);
   all=sprintf('alcons=%.3g\n',alcons);
   fprintf(all);
end
```

Function for Reverberation Time

```
function T30=RT60calc(data)

%Code for calculating RT60 using Schroeder integration
%Impulse responses are .wav files
%after many tries...finished July 21, 2004, by Sarah Rollins
%plot of integrated impulse response checked against
%plot from 't60.m', found on the Matlab website, by Micah Shepherd
%written by Christopher Brown, cbrown@phi.luc.edu
%modified as a function in the RASTI Jan 26, 2005.
global FS
```

```matlab
for n=1:length(data)
    if data(n) == 0
        data(n)=.0000001; %avoid 'log of zero' warning
    end
end
dt=1/FS/1000; %delta t in ms
endtime=length(data);
data=data(1:endtime);
impdata=data.^2;
tms=(1:endtime)/16;
schrint(endtime:-1:1)=cumsum(impdata(endtime:-1:1));
pschr=10*log10(schrint./max(abs(schrint)));%+.9*max(plsqimp);
last4th=round(.5*length(pschr));
dh=15;
%Determine an approximation for the end of the linear part of the Schroeder curve
for h=last4th:dh:length(pschr)
    temp(h)=abs(pschr(h)-pschr(h-dh));
    if temp(h) > abs(pschr(last4th)-(pschr(last4th-dh)))+.03
        ends=h;
        break;
    else
        ends=length(pschr);
    end
end
%Calculate the T60 from Schroeder curve between 5 dB down and 35 dB down
%unless the decay range is too small, then use 5 dB down to 25 dB down
%**REF: ISO 3382:1997(E), pp 9,14**
dBdown5=max(pschr)-5;
dBdown35=max(pschr)-35;
dBdown25=max(pschr)-25;
if pschr(ends)>dBdown35
    dBdown=dBdown25;
else
    dBdown=dBdown35;
end
%Find the 5 dB down point
for k=1:length(pschr)/10
    if pschr(k)==dBdown5
        fivedB=k;
        break;
    else
        dif5(k)=abs(pschr(k)-dBdown5);
    end
end
%Find the 35 or 25 dB down point
n=1;
dift5=10*ones(1,length(pschr));
% for m=1:length(pschr)
for m=round(.5*length(pschr)):length(pschr);
    if pschr(m)==dBdown
        tfivedB=m;
        break;
    else
        dift5(m)=abs(pschr(m)-dBdown);
    end
    n=n+1;
```

```
end
fivedB=find(dif5==min(dif5));
tfivedB=max(find(dift5==min(dift5)));
%Calculate T60 from Schroeder integration curve
%Find a and b for the least squares regression line
x=tms(fivedB:tfivedB);%(2400:4800);
y=pschr(fivedB:tfivedB);%(2400:4800);
% x=1:20;
% y=20:-1:1;
N=length(x);%different N from index 'n' above
a=(mean(y)*sum(x.^2)-mean(x)*sum(x.*y))/(sum(x.^2)-N*mean(x)^2);
b=(sum(x.*y)-N*mean(x)*mean(y))/(sum(x.^2)-N*mean(x)^2);
regline=a+b*x;
T30=(max(pschr)-60-a)/b;
```

Function for RASTI

```
function RASTI=RASTI2(RT60500,RT602000)

RT60500=RT60500/1000;
RT602000=RT602000/1000;
%code to compute the Rapid Speech Transmission Index (RASTI)
%from measured impulse responses in 2 octave bands, 500-Hz octave band, and
%2000-Hz octave band.
%Using equations from Houtgast '85(p1072) and Schroeder '81(p179-180)

omega1=2*pi*[ 1.0, 2.0, 4.0, 8.0 ];
%modulation freq for the 500-Hz octave band
omega2=2*pi*[ 0.7, 1.4, 2.8, 5.6, 11.2 ];
%modulation freq for the 2000-Hz octave band
S=input('Enter value for the signal output\n    ');
N=input('Enter value for ambient noise level modeled\n      ');
for k=1:4
    mtf5=(1/sqrt(1+(omega1(k)*RT60500/13.8).^2))*(1/(1+10^((-S/N)/10)));
    SNapp5(k)=10*log10(mtf5/(1-mtf5));
    if SNapp5(k) > 15
        SNapp5(k)=15;
    elseif SNapp5(k) < -15
        SNapp5(k)=-15;
    end
end
for j=1:5
    mtf2=(1/sqrt(1+(omega2(k)*RT602000/13.8)^2))*(1/(1+10^((-S/N)/10)));
    SNapp2(j)=10*log10(mtf2/(1-mtf2));
    if SNapp2(j) > 15
        SNapp2(j)=15;
    elseif SNapp2(j) < -15
        SNapp2(j)=-15;
    end
end
SNappmean=mean([SNapp5,SNapp2])
%Step 5: Conversion to STI
RASTI=(SNappmean+15)/30;
```

APPENDIX B

Questionnaire for Auralization Test in the Scale Model

Please listen to different male voices as pointed in each question in order to give the answer. Choose an appropriate answer (based on what you hear).

1. Please listen to male voice 1a and 1b, and compare these voices.
   Do you hear any difference between these voices?   □ Yes   □ No
   If yes, which one do you think sounds better?   □ 1a   □ 1b

2. Please listen to male voice 2a and 2b, and compare these voices.
   Do you hear any difference between these voices?   □ Yes   □ No
   If yes, which one do you think sounds better?   □ 2a   □ 2b

3. Please listen to male voice 3a and 3b, and compare these voices.
   Do you hear any difference between these voices?   □ Yes   □ No
   If yes, which one do you think sounds better?   □ 3a   □ 3b

4. Please listen to male voice 4a and 4b, and compare these voices.
   Do you hear any difference between these voices?   □ Yes   □ No
   If yes, which one do you think sounds better?   □ 4a   □ 4b

5. Please listen to male voice 6a and 6b, and compare these voices.
   Do you hear any difference between these voices?   □ Yes   □ No
   If yes, which one do you think sounds better?   □ 6a   □ 6b

6. Please listen to male voice 1a, 3a and 5, and compare these voices.
   Do you hear any difference between these voices?   □ Yes   □ No
   If yes, which one do you think has the best intelligibility?
   o   1a
   o   3a
   o   5

7. Please listen to male voice 2a, 4a and 6a, compare these voices.
   Do you hear any difference between these voices?   □ Yes   □ No
   If yes, which one do you think has the best intelligibility?
   o   2a
   o   4a
   o   6a

8. Please listen to male voice 1a and 7, compare these voices.
   Do you hear any difference between these voices?   □ Yes   □ No
   If yes, which one do you think sounds better?   □ 1a   □ 7

9. Please listen to male voice 2a and 8, compare these voices.
    Do you hear any difference between these voices?   □ Yes   □ No
    If yes, which one do you think sounds better?   □ 2a   □ 8

10. Please listen to male voice 5 and 9, compare these voices.
    Do you hear any difference between these voices?   □ Yes   □ No
    If yes, which one do you think sounds better?   □ 5   □ 9

11. Please listen to male voice 6a and 10, compare these voices.
    Do you hear any difference between these voices?   □ Yes   □ No
    If yes, which one do you think sounds better?   □ 6a   □ 10

12. Please listen to male voice 1a and 11, compare these voices.
    Do you hear any difference between these voices?   □ Yes   □ No
    If yes, which one do you think sounds better?   □ 1a   □ 11

13. Please listen to male voice 2a and 12, compare these voices.
    Do you hear any difference between these voices?   □ Yes   □ No
    If yes, which one do you think sounds better?   □ 2a   □ 12

Thankyou!!!